Thesis for the degree of Doctor of Philosophy

Auralisation of airplanes considering sound propagation in a turbulent atmosphere

Frederik Rietdijk

Department of Architecture and Civil Engineering
CHALMERS UNIVERSITY OF TECHNOLOGY
Göteborg, Sweden 2017

Auralisation of airplanes considering sound propagation in a turbulent atmosphere
Frederik Rietdijk
ISBN: 978-91-7597-620-4

Doktorsavhandlingar vid Chalmers tekniska högskola
Ny serie nr 4301
ISSN: 0346-718X

Department of Architecture and Civil Engineering
Chalmers University of Technology
SE–412 96 Göteborg, Sweden
Telephone + 46 (0) 31 – 772 1000

Printed by Chalmers Reproservice
Göteborg, Sweden 2017

Auralisation of airplanes considering sound propagation in a turbulent atmosphere

Frederik Rietdijk
Architecture and Civil Engineering
Chalmers University of Technology

Abstract

Aircraft noise is a major issue in urban areas. Due to a rising level of urbanisation and the continuing growth of air traffic more people are exposed to aircraft noise than ever. Methods currently used for assessing the impact of aircraft noise on humans consider mostly energetic quantities, and not the dynamic character of the sound. Therefore, in order to obtain a more accurate picture of the impact of aircraft sound it may be helpful to assess how the audible sound is perceived.

Auralisation is a method for rendering audible sound fields and may be used to create audible aircraft sound. A tool was developed to auralise the sound of jet airplanes and consists of an outdoor sound propagation model and an emission synthesiser. The emission synthesiser computes an emission signal consisting of tonal components and broadband noise. The spectral components vary over time and take into account directivity.

An inverse propagation model was developed to compute back from a receiver to source in time-domain. An automated procedure was developed to extract features from the resulting signal. These features were then used to directly synthesise the emission as function of time, and this signal was propagated to the original receiver resulting in an auralisation that should reproduce the recording it is based on.

To validate the auralisation tool, a listening test was conducted where participants were presented with recordings and auralisations and had to rate their similarity. Results indicate that differences exist between the auralisations and recordings. Improving the synthesis of the blade passing frequency is expected to improve the similarity between auralisations and recordings.

Finally, fluctuations can typically be noticed when listening to sound from a distant aircraft, and one cause of these fluctuations is atmospheric turbulence. A computationally fast algorithm was developed to take into account the amplitude and phase modulations that arise as the sound propagates through the turbulent atmosphere. According to the author the method results in improved plausibility of the auralisations.

Keywords: Aircraft noise, Auralisation, Outdoor sound propagation, Atmospheric turbulence

Acknowledgments

The research leading to these results has received funding from the People Programme (Marie Curie Actions) of the European Union's Seventh Framework Programme FP7/2007-2013 under REA grant agreement number 290110, SONORUS "Urban Sound Planner".

Four years ago I began to work on aircraft auralisation at Empa in Switzerland. Not yet fully grasping the importance of the aircraft noise issue I soon found out, enjoying aircraft sounds daily, both at work, and at home! So, thank you to everyone flying in and out of Zürich Airport during that period for the wonderful learning experience!

Thankfully, there was far more than just the annoyance and sleep disturance due to these aircraft. There were my colleagues at Empa, whom I thank for the discussions and the introduction to your secret language and its dialects, some of which were just impossible to understand. You tried hard and I appreciate the attempts, but I think its safe to say I'll never speak "Switzerdeutsch". What I will remember is the "li" at the end of words, since it does sound funny :)

Kurt H., I am glad I had you as a supervisor during these years at Empa. I've learned a lot from you and from our discussions. It was very nice being able to just walk in, discuss, and write down our ideas. We tried real hard getting to the bottom of that pile of old seminar abstracts! Reto, thank you also for the useful discussions, for contributing some decent music to the playlist, and for ensuring the music was on by the time I got in. Christoph, thank you for helping with the aircraft and airport "things", and for providing that mountain of data. It was good to be able to discuss and compare our approaches.

Then, there are my colleagues in the SONORUS project. Four years ago we embarked on an "Urban Sound Planning" journey and faced soundwalks, noise maps, discussions, presentations, and pubs. And, indeed, our research projects. Frustrating at times, I am still glad for the experience and our time together.

Time to fly to Sweden: Chalmers. Wolfgang, thank you for the supervision. We did not meet often, and mails occasionally ended up in a black hole, but the meetings we had, and the feedback I got, was very useful, thank you! Jens, I recall you said you "had an idea" on auralisation and turbulence. I don't think I could have imagined at the time what kind of literature would follow. Thank you for that initial idea, and thank you for the assistence along the way. Finally, I would like to say thank you to everyone at the division for the talks, discussions, fikor, puzzle tour(s) and the "gezellige" environment!

List of Publications

This thesis is based on the work contained in the following papers, referred to by roman numerals in the text:

I F. Rietdijk, J. Forssén, and K. Heutschi. "Generating sequences of acoustic scintillations". In: *Acta Acustica united with Acustica* 103.2 (2017)

II F. Rietdijk and K. Heutschi. "Auralisation of aircraft with a synthesised emission signal based on features determined from recordings". In: *To be submitted* ()

III F. Rietdijk and K. Heutschi. "Auralization of aircraft noise in an urban environment". In: *InterNoise 2016*. 2016, pp. 2877–2881. DOI: 10.5281/zenodo.12642

IV F. Rietdijk, K. Heutschi, and C. Zellmann. "Determining an empirical emission model for the auralization of jet aircraft". In: *Proceedings of EuroNoise 2015*. Maastricht, The Netherlands, 2015, pp. 781–784. DOI: 10.5281/zenodo.15702

V F. Rietdijk, K. Heutschi, and J. Forssén. "Modelling sound propagation in the presence of atmospheric turbulence for the auralisation of aircraft noise". In: *Forum Acusticum 2014*. Krakow, 2014

The following conference paper is not included due to an overlap with Paper V:

VI F. Rietdijk, K. Heutschi, and J. Forssén. "Modelling sound propagation in the presence of atmospheric turbulence for the auralization of aircraft noise". In: *The Journal of the Acoustical Society of America* 136.4 (Oct. 2014), pp. 2286–2286. ISSN: 0001-4966. DOI: 10.1121/1.4900268. URL: http://scitation.aip.org/content/asa/journal/jasa/136/4/10.1121/1.4900268

Contents

Chapter 1

Introduction

1.1 Background

1.1.1 History of aviation

On December 17th, 1903, the Wright brothers made the first sustained and controlled flight of a powered, heavier-than-air, airplane, and in the years after developed the first practical fixed-wing aircraft, the Flyer III. Their invention of aircraft controls was a fundamental breakthrough and marked the beginning of the Pioneer Era of aviation.

The Pioneer Era, lasting until the First World War in August 1914, saw flight becoming an established technology. Aircraft exhibitions were held, demonstrations given, and prizes with the intention of encouraging aviation were offered. Plenty of developments took place in construction, configuration, controls, propellers and engines. Centres were established for aeronautical research and flying schools were opened. In 1911 the first aircraft was used for military purposes by Italy in the Italian-Turkish war and soon after they were also deployed during the First World War.

In the period between the World Wars airplanes evolved from biplanes made from mostly wood and fabric to monoplanes made of aluminium. Power of the engines increased as well. Many aviation firsts occurred during this period, like the first transatlantic flight in 1919, and commercial airlines followed soon on routes like these.

Development and production continued at an even higher pace during the the Second World War and saw the development and deployment of jet aircraft as well as the first turboprop engine that went into mass-production.

After the Second World War commercial aviation grew rapidly, with the first purpose-built commercial jet airliner scheduled into service in 1952, and the first sustained and regular service airline operating only 4 years after. In 1947 a rocket-powered aircraft went through the sound-barrier and this quickly led to the development of supersonic interceptor aircraft as a countermeasure against long-range bombers. The development of intercontinental ballistic missiles and the successful launch of the Sputnik 1 began the Space Race increasing again the pace of aeronau-

tical developments.

In 1969 the Apollo 11 landed the first humans on the moon. It was also the year that both the iconic "Jumbo Jet" Boeing 747 and the Concorde supersonic passenger airliner had their first flights. Around this time, commercial airliners started using higher bypass-ratios, resulting in better fuel economy and less noise.

In the last quarter of the 20$^{\text{th}}$ century, the Digital Age, emphasis changed. Digital computers were used for design and modelling, and digital systems also started to appear inside the aircraft. Digital fly-by-wire systems improved manoeuvrability, stability and drag. In-flight management of the flight plan was being handled by the newly introduced flight management system, reducing the workload of the crew.

The beginning of the 21$^{\text{st}}$ century saw the application of autonomous unmanned aerial vehicles (UAVs), and the first entirely autonomous flight across the Atlantic became reality. Furthermore, the solar-powered airplane Solar Impulse 2 completed a circumnavigation of the Earth demonstrating the possibilities of using renewable energy in an aircraft.

1.1.2 Urbanisation, transportation and the impact of aviation

In 2014 54% of the world population was living in urban areas. The world population is growing rapidly and it is expected that the given percentage increases to 66% by 2050 [1], resulting in higher urban densities.

People not only live closer to each other than ever before, but also transport more than before. Transport allows the spreading of people as well as trade and is therefore an important aspect for economic growth. People typically commute to where they work or study, and transport themselves as well for leisure. Travelling for holidays requires passenger transport, and so does commerce, where people may need to meet to conduct business. Production and consumption of goods and products can occur at different locations, thus requiring transport.

While there is a demand for transport, transport also has a negative impact on our environment. Aviation contributes to climate change and air and noise pollution. Transport uses most of the world's petroleum creating air pollution and contributing to global warming and thereby climate change. Despite more fuel-efficient and less polluting turbofan and turboprop engines, the rapid growth of air travel contributes to an increase in total pollution attributable to aviation. In the European Union, greenhouse gas emissions from aviation increased by 87% between 1990 and 2006. By 2020, aviation emissions are likely to more than double from present levels [2].

Furthermore, these environmental issues have the potential to limit the operation and growth of airports. Indeed, aircraft noise is already a limiting factor for the capacity of regional and international airports throughout the world [3].

1.1.3 Aircraft noise and human response

Aircraft noise is noise associated with the operation of airports and in particular the noise that is caused by aircraft during take-off, flight, or landing [3]. Aircraft noise

is a major environmental constraint for aviation, and is likely to become even more important in the future considering the densification of cities worldwide.

In Europe, several millions of people are affected by aircraft noise [4]. In for example Switzerland, a country with just over 8 million inhabitants, 3% (225,000 persons) and 1.3% (95,000 persons) of the population are exposed to A-weighted noise levels of above 55 dB by day and above 50 dB by night, respectively [5, 6].

Aircraft noise produced during operations in the vicinity of airports represents a serious social, ecological, and economic problem. The noise has a negative impact on people's health, lowers their quality of life, and reduces their productivity at work [3]. Aircraft noise can impact land use planning [7], cause building restrictions, or result in additional measures taken like improved insulation of windows. Noise can affect real estate prices [8], which in turn can cause different forms of segregation [9].

Sound can have a large impact on people's well being. One aspect that has been extensively investigated is how noise affects noise annoyance. Annoyance is an unpleasant mental state, and is a term that is used in general for all negative feelings, such as nuisance, disturbance, unpleasantness and irritation [10]. Aircraft noise can have a major impact on noise annoyance, and there are findings suggesting that people's attitude towards aircraft noise has changed over the years, rating aircraft noisier than before [11].

Another consequence of aircraft noise that is being studied is sleep disturbance [12]. Adequate sleep is essential to one's well being, and aircraft noise-induced sleep disturbance is therefore often seen as a potential public health hazard. How noise affects sleep depends on many factors, the sound pressure level, duration of the noise, how many sources there are and where the sources are situated, character of the sound, and thereby also the intermittency of aircraft noise. Furthermore, there's individual differences such age, sex and noise sensitivity.

1.1.4 Aircraft noise mitigation and modelling

Aircraft noise became a public issue in the 1950s and 1960s. As a consequence governments enacted legislative controls. Noise regulations typically put a constraint on the amount of noise that can be produced as measured at certain locations. Such a constraint can limit the amount of flight operations that are permitted within a certain time window. As a result, airports may optimise their flight routes and schedules to reduce noise exposure. Furthermore, aircraft types may be banned if they're too noisy, providing an incentive for aircraft manufacturers to develop more quiet aircraft.

The Convention on International Civil Aviation established the International Civil Aviation Organization (ICAO) [13]. This organisation is a specialised agency of the United Nations and is charged with coordinating and regulating international air travel. The ICAO adopts standards and guidelines on matters like navigation, infrastructure and inspection. They also provide guidelines related to aircraft noise. For example, Doc 9501 describes procedures for noise emission certification of aircraft [14].

For the certification of aircraft several single-value noise metrics may be used []. These metrics are computed for a single fly-over. In case of light-weight propeller-driven aircraft the A-weighted maximum sound pressure level $L_{A,max}$ is used, and for lightweight helicopters the sound exposure level (SEL), $L_{A,E}$. The effective perceived noise level (EPNL) is used for the majority of aircraft types. EPNL is also a single-value metric and accounts for noisiness and tonality. Signal duration is taken into account as well as spectral content.

The European Civil Aviation Conference (ECAC), founded by ICAO and the Council of Europe, is an intergovernmental organisation and is tasked with "the promotion of the continued development of a safe, efficient and sustainable European air transport system" [15]. The ECAC provides Doc 29, which contains a standardised method for computing noise contours around civil airports [16] and is the recommended method for European Union member states [17].

As a counter-proposal to a people's initiative to limit the amount of flights from Zürich Airport, the Zürich cantonal government proposed to instead limit the amount of people that were allowed to be highly affected by the aircraft noise. This counter-proposal, the "Zürcher Fluglärm-Index" (ZFI) or Zürich Aircraft Noise Index was accepted [18]. The ZFI is a single number, representing the amount of persons that are affected by annoyance and/or sleep disturbance due to aircraft noise related to a single airport. Exposure-response relations are used for both annoyance during daytime and sleep disturbance during nighttime.

For the computation of indices like the ZFI it is necessary to obtain exposure-response relations as well as sound pressure levels that serve as input. Typically noise levels are predicted on the facades of houses, and a correction is made to obtain indoor levels. The ZFI considers as input for determining the amount of sleep disturbed people the A-weighted maximum sound pressure level $L_{A,max}$ per event and the A-weighted equivalent level $L_{A,eq}$ over the night period. For annoyance the $L_{A,eq}$ over the daytime period is used with an additional penalty of 5 dB for the first and last hour.

While exposure-response relations have been determined, the computation of the ZFI assumes that an event and environment can be entirely described by their noise levels. However, an assumption or simplification like this disregards the fact that other aspects than the average or maximum sound pressure level impact the human response as was mentioned before. Tonal components, for example, are known to significantly contribute to noise annoyance and therefore improved metrics may be needed [19, 20]. Especially with developments like NASA's X-57 Maxwell Electric Propulsion Airplane [21, 22] which features 14 propellers, each driven by its own electric engine, and quadcopters [23] that are now commonly used as drones. Some parameters that affect the sound field and what is perceived by a listener are the phase relation between propellers, unsteadiness of the sources, interferences, and fluctuations due to atmospheric turbulence. These parameters all affect the sound field and what is perceived by a listener. Simple models do not take into account these parameters, and are therefore insufficient for determining the impact of the sound on humans.

1.1.5 Auralisation

Auralisation is a method to render audible virtual sound fields created from numerical data [24, 25]. The method is commonly used in room acoustics to simulate the audible sound inside spaces. In recent years the method is also used for simulating exterior sound of cars [26–30], trains [31], wind turbines [32, 33], fans [34] and aircraft [35–37]. The Virtual Acoustic Simulation Technology for Community Noise Technical Working Group, or in short VASTCON TWG, is a technical working group dedicated to the auralisation of outdoor sources and environments [38].

The method, essentially a part of virtual reality, could be used as a communication tool, for example, when discussing urban development. Noise contours are typically computed and plotted to show the spatial distribution of noise. These figures are often hard to interpret for non-specialists, and they also give no insight in what the noise may sound like because they do not include the temporal structure of the sounds.

In 2015 Lelystad Airport in The Netherlands was expanding, extending its runway to facilitate aircraft models like the A320. Residents living nearby were initially presented with noise contours but struggled with interpreting them. The Netherlands Aerospace Centre (NLR) was asked to help residents understand the implications of the airport changes, and so they used auralisations at town hall meetings [39].

Sounds are typically created based on some underlying physical model. This allows the possibility of generating sounds that correspond to specific situations or conditions and is an important benefit over recordings where it is not possible to control every parameter. Auralisation is therefore an interesting tool for studying the impact of an acoustic soundscape on humans and the development of improved descriptors.

While the sounds are often entirely generated, this is not necessarily always the case. One could work with existing sounds and modify these instead. An example would be to take a recording made outside and in front of a building, and then simulate the sound indoors by applying a filter to account for the attenuation of walls and windows. As with noise prediction, emission synthesis and sound propagation are often separated. This is, not always possible however, e.g. when using a wave-based method [40–42].

Methods that are commonly used for emission synthesis are spectral modelling synthesis (SMS) and granular synthesis. With granular synthesis small parts of existing signals are considered, and a new signal is synthesised by combining these small parts called grains. Grains are often based on measurements, but that is not necessarily the case. A grain typically corresponds to specific conditions, for example the speed of the source. Granular synthesis is a computationally fast method. With spectral modelling synthesis a signal is created from a superposition of tone and noise components. An advantage of spectral modelling synthesis is that the synthesis strategy can be considered separate from the underlying model. Therefore, an emission synthesis model can be established that relates tonal and spectral components to the operational state of the source.

1.1.6 Aircraft noise auralisation

Auralisation is an interesting method and has been used to study future aircraft types [36, 37, 43] and flight procedures [19] through perception-influenced design. The method was also used to investigate the perceived unpleasantness of aircraft flyover noise as a function of certain temporal parameters [44]. An extensive introduction to aircraft auralisation is provided by Arntzen in his doctoral thesis [35].

Aspects to consider when simulating the sound of aircraft are the different noise sources on the aircraft, the state of the aircraft (e.g. thrust setting) and thereby the state of these sources (e.g. frequency engine shaft), as well as the condition of the environment. Main noise sources on an airplane with turbofan engines are the jet, fan, turbine, combustor and airframe. The significance of these sources depends on aircraft type, flight procedure, as well as the position of the source with respect to the receiver due to directivity of the sources [45].

The aircraft emission prediction tools found in the ANOPP-Source Functional Module of NASA's ANOPP2 [46, 47] and INSTANT [20], which is based on ANOPP, use established models for the noise prediction of the individual noise sources. The Heidmann model is for example used for fan noise and the Stone model for jet noise. The Heidmann model in ANOPP models five sources explicitly, of which three correspond to emission of tones and two to emission of broadband noise [35]. The model outputs for each of these five sources a spectrum in fractional-octaves. For broadband synthesis in the NASA Auralization Framework (NAF)[48], power of the tonal components in each band is divided by the amount of tones in that band. Nowadays the Heidmann model in ANOPP can output the frequencies and amplitudes of forward and aft radiated fan tones. Only Buzz-Saw noise is still output in $^1/_3$-octaves.

Other models do not describe the contributions from the individual noise sources or spectral components but merge them together into a single spectrum. The ECAC Doc29 method [16] uses the ICAO ANP database and provides 24 $^1/_3$-octave bands, and so does CNOSSOS-EU which has adopted the 3rd edition of Doc29 [49]. The Swiss sonAIR model [50, 51] computes an emission spectrum that is composed of two source spectra: an engine spectrum and an airframe spectrum. The current Swiss model, FLULA2, does not consider an emission spectrum but instead uses a database of immission spectra where propagation effects are already included [6, 52].

Aside from ANOPP2 and INSTANT, none of the mentioned models make a distinction between tonal and broadband noise contributions, thereby making them unfit for the use of aircraft auralisation which requires explicit knowledge about tonal and noise contributions.

1.1.7 Plausibility of aircraft auralisations and the influence of the atmosphere

In the last couple of years relatively many papers have been written about auralisation and aircraft auralisation. Initially basic propagation models were developed,

and then emphasis shifted to the development of emission models. A common issue with current auralisations is that they can still sound artificial or "perfect" [35].

One cause is that one typically models only the source of interest, neglecting any background sounds. Aside from impacting how plausible an auralisation sounds, the lack of such background sounds may also help listeners discriminate between recordings and auralisations. E.g., in a listening test where recordings and auralisations of wind turbines were compared, cow bells were audible in the recordings but missing in the auralisations [32].

Another issue is the (un)steadiness of the source and/or the medium through which the waves propagate. Consider for example a rotating fan. The fan radiates besides broadband noise also strong tonal components. Turbulent flow around the fan can cause additional motion of the fan. This motion will effect the sound that is radiated, causing modulations of the tonal components. Effects like these are typically not included in prediction models, and a similar effect was shown to be important for the assessment of noise annoyance caused by quadcopters [23].

In past work it was mentioned that auralisations of (distant) airplanes also lack a certain randomness or fluctuations in the sound [35]. Atmospheric turbulence can cause not only fluctuations of the emitted sound but can also scatter waves that propagate through the turbulent atmosphere. Temporal and spatial variations of temperature and wind velocity fields result in fluctuations of the refractive-index field. Multiple scattering in combination with these temporal and spatial variations results in log-amplitude and phase modulations.

The log-amplitude fluctuations can often be noticed when listening to distant aircraft. The phase fluctuations are not perceived by humans directly, but when considering multiple sources, e.g. the direct path contribution and (ground) reflected path contribution, they may have an impact on the interference causing coherence loss [53] which can be audible. Also, when modelling the different sound sources on a aircraft as separate sources, their contributions may be Doppler shifted differently, resulting in audible beating which may sound unrealistic [43]. Decorrelation can reduce the beating. A coherence factor was introduced in earlier work [35, 54, 55] to account for coherence loss due to atmospheric turbulence, resulting in less pronounced interference dips, as will be further explained in Chapter 5.

1.1.8 Measurements for sonAIR

Between 2012 and 2016 a new aircraft noise calculation model called sonAIR was developed at Empa [50, 51]. This semi-empirical model is based on data obtained from flights that occurred at Zürich airport in 2013 and 2014.

The main data set consists of sound recordings at various positions nearby the airport as well as at larger distances. Sound recordings were made at 44.1 kHz with microphones at a height of 4 meters above ground level and at several locations simultaneously. The position of the aircraft was recorded in several ways. Two special cameras were used to determine the aircraft their position when they were close to the strip. Radar information was available as well. Furthermore, for a subset of the events additional data was available from the Flight Data Recorder (FDR).

Some examples of data the FDR provides are the trajectory, engine shaft rotational frequency and configuration of the gear and flaps. All data was time-synchronised using GPS receivers. Finally, meteorological data was available.

This extensive data set was used for the development for an aircraft noise prediction model, but could also be interesting for the development of an aircraft emission model for auralisations.

1.2 Thesis

1.2.1 Aim

The aim of the thesis is to develop a tool to simulate the audible sound of airplanes in an urban environment, so that in the future aspects like annoyance and sleep disturbance due to aircraft noise can be investigated using auralisations as provided by the tool. Therefore, in order to investigate those aspects, the tool should provide auralisations that sound sufficiently plausible. That means an auralisation should sound like an aircraft and, more specifically, it should sound like the aircraft type and the situation that is modelled.

There is a large variety of different aircraft in use nowadays, that could each be perceived differently. In order to investigate the human response impact of each of these aircraft, an additional requirement is that the tool should be able to simulate the audible sound of of the current fleet of airplanes. Instead of simulating the emission of the aircraft based on (existing) emission models for the different radiating components, the goal of this work is to investigate whether plausible sounding auralisations can be made with its emission properties derived from recordings.

To improve the plausibility of auralisations of aircraft at especially larger distances, a second goal is to develop a method for incorporating amplitude and phase fluctuations due to atmospheric turbulence. The method should improve the plausibility of the auralisations while at the same time have a physical basis and preferably perform well enough for use in real-time simulators.

1.2.2 Outline

The thesis is structured as follows.

Chapter 2 provides an overview of theory required to understand the concepts that are used throughout the thesis. Discussed are the basics of sound, signal processing, and aircraft noise emission.

Chapter 3 describes the auralisation tool that was developed. The propagation model is explained, as well as an algorithm for extracting features from recordings that were then used to synthesise aircraft sounds.

Chapter 4 aims to answer the question whether the auralisation tool provides sufficiently plausible auralisations.

Chapter 5 gives an extensive overview on a novel algorithm for simulating fluctuations due to atmospheric turbulence and how to apply this algorithm in auralisations to improve their plausibility.

Finally, the work is summarised in Chapter 6 and future work is suggested.

Many of the figures in this thesis are based on audio files. These files can be found online [56]. Appendix A gives an overview of the files.

1.2.3 Scope

The goal is to develop a tool that can deliver auralisations of airplanes that sound plausible. Unless mentioned otherwise, the type of aircraft considered are commercial airliners that have jet engines.

Events that are considered are take-offs relatively close to the airport. In this case, the airport is Zürich Airport as that is where data was gathered. Take-offs are considered instead of landings because landings can contain relatively fast-varying frequency components due to thrust corrections made by the pilot.

The auralisation tool considers only source motion and not receiver motion or mean motion of the medium.

Chapter 2

Theory

As mentioned in the introduction, auralisation is a method to render a sound field audible. In order to create an auralisation of aircraft an understanding of sound, signal processing and aircraft is needed. This Chapter provides a brief introduction to each of these topics.

2.1 Sound

A repetitive variation about a central value of some quantity is called an oscillation. Oscillations of mechanical nature are vibrations. An oscillation travelling through a medium and transferring energy is a wave. Sound is then a mechanical wave travelling through a fluid medium. In certain fields sound may however refer only to those oscillations that can be perceived by the human brain. Being a small repetitive perturbation about the barometric mean pressure of the medium, the fluctuating or dynamic part of the pressure, denoted sound pressure, is typically many orders smaller than the mean pressure.

In the 17^{th} century Newton proposed a model for sound waves in elastic media in his Principia. Newton assumed an isothermal process for the wave motion and thereby computed incorrect values for the speed of sound. Laplace gave the correct derivation of the classical wave equation, describing the wave motion as an adiabatic process. In the 19^{th} century Kirchoff described the motion of a rigid body in an ideal fluid and Helmholtz gave a time-independent form of the wave equation. These were some of the important foundations for the classical theory of sound. This section and the next two sections give a brief overview of sound. Discussed are sound generation and sound propagation.

The wave equation is a differential equation for describing waves and is used throughout physics. In the 18^{th} century d'Alembert discovered the one-dimensional wave equation, and a couple of years later Euler presented the three-dimensional wave equation. The acoustic wave equation describes the motion of sound waves and can be derived from the fundamental laws of fluid dynamics.

In this section a brief overview is given of the wave equation and expressions that are relevant when considering sound emitted by aircraft. More details can be found in [57].

Mass and momentum conservation

The mass conservation or continuity equation is given by

$$\frac{\partial \rho}{\partial t} + \nabla \cdot (\rho \mathbf{u}) = m \tag{2.1}$$

with ρ the density of the medium, t the time, $\mathbf{u}$ the flow velocity vector, m the mass and $\nabla = \left(\frac{\partial}{\partial x_1}, \frac{\partial}{\partial x_2}, \frac{\partial}{\partial x_3}\right)$. The momentum conservation equation is

$$\frac{\partial}{\partial t}\rho \mathbf{u} + \nabla \cdot (\boldsymbol{P} + \rho \mathbf{u}\mathbf{u}) = \mathbf{f} + m\mathbf{u} \tag{2.2}$$

where $\mathbf{uu}$ is a dyadic product[1], $\mathbf{f}$ the external force density and $\boldsymbol{P}$ the fluid stress tensor. The fluid stress tensor relates the pressure p and the viscous stress tensor $\boldsymbol{\tau}$ by

$$\boldsymbol{P} = p\boldsymbol{I} - \boldsymbol{\tau} \tag{2.3}$$

where $\boldsymbol{I}$ is a unit tensor. Viscous stresses are small compared to inertial forces. Assuming an ideal fluid by ignoring the viscous stresses, and rewriting equation (2.2) using equation (2.1), we obtain the following form for the momentum conservation equation

$$\rho \left(\frac{\partial \mathbf{u}}{\partial t} + (\mathbf{u} \cdot \nabla)\, \mathbf{u} \right) + \nabla p = \mathbf{f} \tag{2.4}$$

Linearisation

Sound is a small perturbation of a steady state, and so we can apply linearisation to obtain a wave equation. Ignoring the source term at the right-hand side (thus considering the homogeneous solution), the linearised versions of the mass and momentum equations are given by

$$\frac{\partial \rho'}{\partial t} + \mathbf{u_0} \cdot \nabla \rho' + \rho_0 \nabla \cdot \mathbf{u}' = 0 \tag{2.5}$$

$$\rho_0 \left(\frac{\partial \mathbf{u}'}{\partial t} + (\mathbf{u_0} \cdot \nabla)\, \mathbf{u}' \right) + \nabla p' = 0 \tag{2.6}$$

with the fluctuating components of the variables denoted with a prime and the steady components subscripted with a zero.

Speed of sound

Viscosity is neglected and thereby also heat transfer. The fluid is considered to behave adiabatic and thus the following relation between pressure and density fluctuations can be used

$$p' = c^2 \rho' \tag{2.7}$$

[1] The dyadic product of the vectors $\mathbf{a}$ and $\mathbf{b}$ is the tensor $\mathbf{ab} = a_i b_j$

where c is the speed of sound

$$c = \sqrt{\left(\frac{\partial p}{\partial \rho}\right)_s} \tag{2.8}$$

The subscript s indicates an isentropic (constant entropy s) or adiabatic process. In general, the speed of sound is given by $c = \sqrt{\frac{K}{\rho}}$ where K is the bulk modulus of the medium. For ideal gases the bulk modulus is $K = \gamma p$ where $\gamma = C_p/C_v$ is the ratio of specific heat capacities at constant pressure C_p and constant volume C_V.

Classical wave equation

Taking the time derivative of the linearised mass conservation equation, subtracting the divergence of the linearised momentum conservation equation and assuming an adiabatic process results in the classical wave equation

$$\frac{1}{c^2}\frac{\partial^2 p'}{\partial t^2} - \nabla^2 p' = 0 \tag{2.9}$$

Harmonic wave

In acoustics harmonic waves in the following complex form are typically considered

$$p'(\mathbf{x}, t) = \hat{p}\,(\mathbf{x}) \exp\left(j\omega t\right) \tag{2.10}$$

where $\hat{p}\,(\mathbf{x})$ is the amplitude of the wave and $\omega = 2\pi f$ the angular frequency.

Helmholtz equation

Inserting (the derivatives of) a harmonic wave in the wave equation results in the Helmholtz equation

$$\left(\nabla^2 + k^2\right)\hat{p} = 0 \tag{2.11}$$

where $k = w/c$ is the wavenumber.

Plane wave solution

The solution to the wave equation in one dimension is

$$p'(x, t) = p'_+(t - x/c) + p'_-(t + x/c) \tag{2.12}$$

where p'_+ and p'_- are respectively a right and left travelling function.

Spherical wave solution

A solution in three dimensions assuming spherical symmetry is the spherical wave solution

$$p'(r, t) = \frac{1}{r}p'_+(t - r/c) + \frac{1}{r}p'_-(t + r/c) \tag{2.13}$$

and looks similar to the plane wave solution. In this expression r is the distance travelled by the wave. The spherical wave solution represents the sum of a wave propagating out from the origin and that of a wave propagating towards the origin. In acoustics only the outgoing wave is typically kept. Contrary to a plane wave the pressure of a spherical wave decreases with $1/r$.

Wave equation with source terms

The above solutions considered a homogeneous wave equation and therefore do not take into account any source terms. Linearisation of the mass and momentum equations would have resulted in a unsteady mass injection m' and unsteady external force $\mathbf{f}'$ that correspond to a vibrating solid boundary. The classical wave equation with these terms is

$$\frac{1}{c^2}\frac{\partial^2 p'}{\partial t^2} - \nabla^2 p' = \frac{\partial m'}{\partial t} - \nabla \cdot \mathbf{f}' \tag{2.14}$$

In general a source term can be written as a source s.

Green's function

The simplest possible source is a point source that is represented by a Dirac delta function $\delta(\mathbf{x} - \mathbf{x}_0)$ where $\mathbf{x}_0$ is the position of the point source. A Green's function is a solution or impulse response of an inhomogeneous linear differential equation. Therefore, the solution of the wave equation with such a point source excitation is a Green's function. For a harmonic point source the Green's function $\hat{G}$ should satisfy

$$\left(\nabla^2 + k^2\right)\hat{G} = -\delta\left(\mathbf{x} - \mathbf{x}_0\right) \tag{2.15}$$

Note that a Helmholtz equation is used because a harmonic point source is considered.

The solution of this inhomogeneous Helmholtz equation is again an ingoing and outgoing spherical wave. Because of causality we consider only the outgoing wave. In free field the Green's function of this outgoing wave is

$$\hat{G} = \frac{\exp\left(jkr\right)}{4\pi r} \tag{2.16}$$

with $r = |\mathbf{x} - \mathbf{x}_0|$ the distance from point source to receiver.

2.2 Generation of sound

Classical acoustics provides a method for modelling sound generation due to vibrating solid boundaries. Aerodynamic sources such as combustion or other unsteady fluid processes cannot be handled, however. With the development of jet-powered aircraft a description was needed to model such sources. This section provides a brief introduction to generation of aerodynamic sound. A more extensive discussion on generation of aerodynamic sound can be found in [57].

2.2.1 Aerodynamic sound sources

Lighthill provided the theory to take into account aerodynamic sources. The idea is that an unsteady flow will produce sound. A simple example is the sound that is generated when flow passes a string or antenna. The aero-acoustic analogy of Lighthill is the idea of representing a fluid mechanical process that acts as an acoustic source by an acoustically equivalent source term.

Taking the time derivative of the homogeneous version of the mass conservation equation and the divergence of the homogeneous version of the momentum conservation equation, then subtracting one from another, and finally subtracting from both sides of the equation $c^2\nabla^2\rho$, results in the Lighthill equation

$$\frac{\partial^2\rho}{\partial t^2} - c^2\nabla^2\rho = \nabla\cdot\nabla\cdot\boldsymbol{T} \tag{2.17}$$

where $\boldsymbol{T}$ is the Lighthill stress tensor

$$\boldsymbol{T} = \rho\mathbf{u}\mathbf{u} + \left(p - c^2\rho\right)\boldsymbol{I} - \boldsymbol{\tau} \tag{2.18}$$

The right-hand side of the Lighthill equation describes the non-homogeneous fluid in a finite volume V. This area is called the source region or source field. The left-hand side of the equation describes a homogeneous fluid. This region is called the sound field and is where the classical wave equation governs sound propagation.

The Lighthill stress tensor can be considered as a source term of a jet in an acoustic medium at rest, and consists of three aero-acoustic processes that are sources of sound [57]. The first are non-linear convective forces as described by the Reynold stress tensor $\rho\mathbf{u}\mathbf{u}$, the second viscous forces τ and the third deviations from isentropic behaviour $p - c^2\rho$.

Elementary sources

Deviations from the wave equation can be considered sources. Sources are typically classified as a multipole, e.g. a monopole or a dipole. The aerodynamic sound sources can also be classified as different multipoles, in case the sources are compact, i.e., the source is small compared to the wavelength. We will now consider the different aerodynamic sound sources.

The Lighthill equation is an exact reformulation of the fundamental equations. Equation (2.17) is the density-based variant of the Lighthill equation. Linearisation

of the pressure-based variant results in

$$\frac{1}{c_0^2}\frac{\partial^2 p'}{\partial t^2} - \frac{\partial^2 p'}{\partial x_i^2} = \frac{\partial}{\partial t}\left(m + \frac{1}{c_0^2}\frac{\partial}{\partial t}\left(p' - c_0^2\rho'\right)\right) - \frac{\partial f_i}{\partial x_i} + \frac{\partial^2}{\partial x_i x_j}\left(\rho u_i u_j - \tau_{ij}\right) \quad (2.19)$$

where Cartesian tensor notation is used. The source term can be split into the following three parts

$$s_1 = \frac{\partial}{\partial t}\left(m + \frac{1}{c_0^2}\frac{\partial}{\partial t}\left(p' - c_0^2\rho'\right)\right) \quad (2.20)$$

$$s_2 = -\frac{\partial f_i}{\partial x_i} \quad (2.21)$$

$$s_3 = \frac{\partial^2}{\partial x_i x_j}\left(\rho u_i u_j - \tau_{ij}\right) \quad (2.22)$$

which are respectively the monopole, dipole and quadrupole source terms. We will now look at these different terms, assuming they are compact non-moving sources. Considering the Green's function given in the previous section, the general solution is

$$p'(\mathbf{x}, t) = \int_V \frac{s(\mathbf{y}, t - r/c_0)}{4\pi r}\mathrm{d}V \quad (2.23)$$

Monopole

The source mechanisms of the monopole source are mass injection and deviations from adiabatic behaviour. The sound generated by a compact monopole source due to a mass injection is given by

$$p'(\mathbf{x}, t) = \frac{\rho_0 \dot{Q}(t - x/c_0)}{4\pi x} \quad (2.24)$$

where $\dot{Q}$ is the time-derivative of the total unsteady volume flow $Q(t) = \int_V q'(\mathbf{y}, t)\mathrm{d}V$. The sound power is given by

$$\overline{W_m} = \frac{\rho_0 \overline{\dot{Q}^2}}{4\pi c_0} \quad (2.25)$$

Dipole

The dipole source term represents an unsteady force acting on the fluid. An example is a propeller, where the rotating blade forces represent a time-varying force distribution on the fluid. The sound pressure due to a compact dipole source is given by

$$p'(\mathbf{x}, t) = -\frac{\partial}{\partial x_i}\frac{F_i(t - x/c)}{4\pi x} \quad (2.26)$$

where $F_i(t) = \int_V f_i(\mathbf{y}, t)\mathrm{d}V$ is the total unsteady force acting on the fluid. The sound power is given by

$$\overline{W_d} = \frac{\overline{\dot{F}^2}}{12\pi\rho_0 c_0^3} \quad (2.27)$$

Quadrupole

The quadrupole source term describes noise due to unsteady momentum transport, $\rho u_i u_j$. The viscous forces τ_{ij} can be neglected because they are typically much smaller than the momentum transportation term and therefore hardly contribute in case of high Reynolds numbers. The sound pressure due to a quadrupole point source is given by

$$p'(\mathbf{x},t) = \frac{\partial^2}{\partial x_i \partial x_j}\left(\frac{Q_{ij}(t-x/c_0)}{4\pi x}\right) \tag{2.28}$$

where $Q_{ij}(t) = \int_V T_{ij}(\mathbf{y},t)\mathrm{d}V$ is the total quadrupole strength and T_{ij} the Lighthill stress tensor. The sound power is given by

$$\overline{W_q} = \frac{\epsilon ij \overline{\ddot{Q}_{ij}^{\,2}}}{\rho_0 c_0^5} \tag{2.29}$$

In this expression ϵ_{ij} is $1/20\pi$ when $i = j$ and $1/60\pi$ otherwise. The quadrupole source term is the main noise source of a high-speed jet.

Jet noise

After the Second World War, jet engines began to be used in commercial airplanes, and their noise emission was a big issue. That eventually led to the development of Lighthill's theory. A jet is a stream of fluid that is projected into the surrounding medium Turbulent mixing of the two fluids causes what is called jet noise. Jet noise is broadband noise, and the sound power of a jet may scale under certain conditions with Lighthill's U^8-law

$$\overline{W_j} \propto \frac{\rho_0 U^8 D^2}{c_0^5} \tag{2.30}$$

where U is the jet speed, and where the characteristic size D would be the diameter of the pipe.

Source motion

Source motion affects sound emission and can result in a Doppler shift and convective amplification. The Doppler shift is a frequency-shift of the signal and is caused by a time-varying propagation time from source to receiver. The Doppler shift will be discussed further in 2.4.1.

The source terms that were discussed in this section each represent a multipole, which has a characteristic directivity. Motion of the source affects sound emission altering the directivity of the source. This effect is called convective amplification and is especially noticeable at high source speeds or, to be more precise, high Mach numbers $M = U/c_0$.

2.3 Aircraft noise sources

There are several noise sources on an airplane and their level of contribution depends on the operating conditions as well as airplane specifics, like for example what type of engines are used. The main noise sources on a jet airplane are the jet engine and aerodynamic noise from different parts of the airframe [3]. Noise contributions from the jet engine can be further divided into subsources. Relevant subsources are the fan, combustor, turbine and finally the jet of the exhaust flow that is projected out of the nozzle. For noise reduction acoustic liners are typically present. Some aircraft may also have sawtooth patterns on the nozzle known as chevrons.

Engine types

The engine is the component generating power and providing thrust. Several kinds of engines are used in airplanes.

A turbojet engine consists of a combustion turbine with a propelling nozzle. Air is taken by an inlet and compressed by a compressor that is driven by the turbine. The compressed air is heated in the combustion chamber, then passes through the turbine expanding and driving it, and finally expands further in the nozzle where it is accelerated to provide thrust. Because of low fuel-efficiency most aircraft use a different engine nowadays.

Smaller aircraft typically use a turboprop engine. A turboprop engine is similar to a turbojet engine. Thrust is generated not by the outgoing flow, but by a propeller which is driven by the turbine.

The turbofan engine is mostly used by larger aircraft and is quite similar to both turbojet and turboprop engines. A fan is placed in front of the inlet. Whereas with a turbojet all the air taken in by the inlet passes through the turbine, with a turbofan some of the air taken in by the fan bypasses the turbine. Thrust is provided not only through the nozzle but also by the fan. The bypass ratio is defined as the ratio between the mass-flow rate of the bypass stream to the mass-flow rate entering the turbine. Commercial airliners typically have “high-bypass” turbofan engines that provide more fan-thrust relative to jet-thrust. Turbofan engines proved for commercial airliners to not only be more fuel-efficient, but also reduced their noise emission.

Fan

In a turbofan engine a fan is used for generating thrust. The blades rotate at high angular frequency, with the tips of the blades moving at sub- or supersonic Mach numbers. Unsteady flow due to inflow turbulence and flow separation from the blades causes broadband noise. Steady and unsteady forces acting on the flow cause tonal components at the blade passing frequency of the fan and harmonics.

When the tips of the blades move at supersonic Mach numbers, shocks are created resulting in multiple pure tones. A shock is created by each blade. Due to blade-to-blade differences the waves coalesce. Tonal components will therefore exist at the

angular frequency of the engine shaft. These tonal components are called "Buzz-Saw" noise and its time-domain signal resembles a sawtooth. The "Buzz-Saw" noise is common during take-off.

Combustor

To drive a turbine compressed air is heated in the combustion chamber. Heat is provided by burning fuel. Noise is created due to the combustion process as well as due to turbulent airflows. Low-frequent noise can propagate through the turbine and exhaust, and this type of noise is known as core noise [3].

Airframe

Airframe noise is noise that is generated by aerodynamic flow around the airframe and is an important noise source at low engine power settings. Aerodynamic noise can be generated on the tail, wing, flaps, slats and landing gear. Furthermore, airframe noise includes the airfoil-tip vortex [3].

Jet noise

Jet noise was briefly discussed in section 2.2. The exhaust flow is projected in the ambient air and turbulent mixing of the two fluids causes jet noise.

2.4 Propagation of sound

This section gives an overview of sound propagation effects that are relevant when considering aircraft sound.

2.4.1 Doppler shift

A commonly known effect related to movement is the Doppler shift. Relative motion between source, receiver and medium can cause Doppler shifts. If we consider a moving harmonic point source, $S(t) = \hat{S}_0 \exp(j\omega_0 t)$, a homogeneous fluid at rest, and a non-moving receiver, then the sound field is given by

$$p'(\mathbf{x}, t) = \sum_{t_e} \frac{\hat{S}_0 \exp(j\omega_0 t_e)}{4\pi r(t_e) |1 - M_r(t_e)|} \tag{2.31}$$

and represents a summation of the sound pressure contributions at all emission times t_e. The Mach number $M_r = \mathbf{M} \cdot \mathbf{e}_r = M \cos\theta$ is the projection of the Mach number of the source in the direction towards the receiver. The Mach number of the source is $\mathbf{M} = \mathbf{v}/c$ and $\mathbf{e}_r = \mathbf{r}/r$ is the unit vector pointing towards the receiver. The instantaneous angular frequency is then given by

$$\omega = \frac{\omega_0}{1 - M_r(t_e)} \tag{2.32}$$

2.4.2 Atmospheric attenuation

As sound waves travel through an atmosphere the waves are attenuated through atmospheric attenuation. There are two effects causing attenuation. The first effect causing attenuation is classical heat conduction and shear viscosity. These effects were considered insignificant when deriving the wave equation. The second effect is on a molecular scale and is due to an energy exchange between translation and rotational or vibrational modes. Molecules collide and are excited when a wave passes resulting in energy transfer. The energy transfer is a function of the relaxation time of the molecules. Because the molecules need a certain time to reach equilibrium the heat capacity of the medium is time-dependent thus resulting in an irreversible process causing losses.

A model for atmospheric attenuation is given in Part 1 of ISO 9613-1:1993 [58]. The attenuation coefficient α, in dB/m, is given by

$$\begin{aligned}\alpha = 8.686 f^2 \Bigg(& \left[1.84 \times 10^{-11} \left(\frac{p_r}{p_a} \right)^{-1} \left(\frac{T}{T_0} \right)^{1/2} \right] + \left(\frac{T}{T_0} \right)^{-5/2} \\ & \times \Bigg\{ 0.01275 \left[\exp \frac{-2239.1}{T} \right] \left[f_{r,O} + \frac{f^2}{f_{r,O}} \right]^{-1} \\ & + 0.1068 \left[\exp \frac{-3352.0}{T} \right] \left[f_{r,N} + \frac{f^2}{f_{r,N}} \right]^{-1} \Bigg\} \Bigg)\end{aligned} \tag{2.33}$$

and is a function of the ambient temperature in kelvin T, the reference temperature $T_0 = 293.15$ K, the ambient pressure p_a in kilopascal, the reference pressure $p_r = 101.325$ kPa and the relaxation frequencies for oxygen $f_{r,O}$ and nitrogen $f_{r,N}$. The relaxation frequency of oxygen is given by

$$f_{r,O} = \frac{p_a}{p_r}\left(24 + 4.04 \cdot 10^4 h \frac{0.02 + h}{0.391 + h}\right) \tag{2.34}$$

and the relaxation frequency of nitrogen by

$$f_{r,N} = \frac{p_a}{p_r}\left(\frac{T}{T_0}\right)^{-1/2} \cdot \left(9 + 280h \exp\left\{-4.170\left[\left(\frac{T}{T_0}\right)^{-1/3} - 1\right]\right\}\right) \tag{2.35}$$

Both depend on the molar concentration of water vapour h, given by

$$h = h_r \frac{p_{sat}}{p_a} \tag{2.36}$$

The molar concentration of water vapour is a function of the saturation pressure

$$p_{sat} = 10^C \cdot p_r \tag{2.37}$$

where

$$C = -6.8346 \cdot \left(\frac{T_{01}}{T}\right)^{1.261} + 4.6151 \tag{2.38}$$

and where T_{01} is the triple-point isotherm temperature of 273.16 K. Figure 2.1 shows the atmospheric attenuation coefficient α as function of frequency, in case of a reference atmosphere. A reference atmosphere is an atmosphere where $p_a = p_r$ and $T = 293.15$ K.

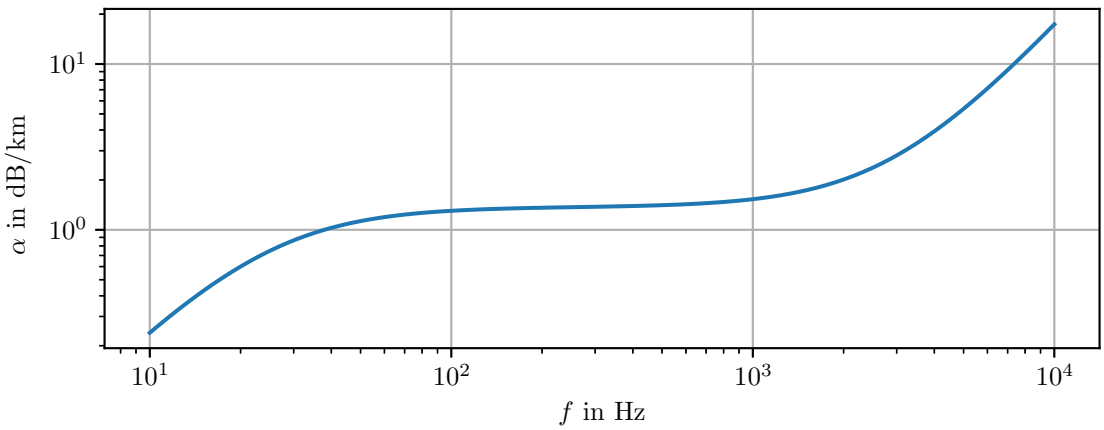

Figure 2.1: Atmospheric attenuation as function of frequency for a reference atmosphere.

2.4.3 Reflections

Sound hitting a boundary between materials of different impedance may be transmitted, reflected or absorbed. When sound is transmitted the incident wave is partially refracted. Sound reflected by a smooth surface results in a specular reflection, and sound reflected on a rough surface results in a diffuse reflection. In outdoor situations sound is typically reflected by the ground surface and other obstacles like buildings. The sound pressure at a receiver is then the sum of the direct contribution as well as indirect contributions from reflections. Due to this superposition strong interference effects may occur.

Impedance

An impedance is a complex ratio between two interdependent dynamic quantities and describes the resistance to a direct flow (resistance) and alternating flow (reactance). The specific acoustical impedance of a material is the ratio of the sound pressure to the particle velocity normal to the surface $Z_s = p/\mathbf{u}$. The specific acoustical impedance of a material or surface normalised by the impedance of air $Z_{s,air} = \rho c$ is called the normalised specific acoustic impedance. This impedance is typically used to characterise surfaces, and is what impedance in the following text refers to.

Multiple models are available for the prediction of the impedance of a surface. Attenborough et. al. made a comparison of impedance models and recommends the Delany and Bazley one-parameter model for predicting outdoor ground impedance [59]. The empirical one-parameter model by Delaney and Bazley is widely used and depends on the flow resistivity of the material σ and the frequency f

$$Z = 1 + 9.08\left(\frac{1000f}{\sigma}\right)^{-0.75} - 11.9j\left(\frac{1000f}{\sigma}\right)^{-0.73} \tag{2.39}$$

Flow resistivity describes how difficult it is for air to flow through a surface. Values for surfaces can vary significantly, with average values ranging from $29\,\mathrm{kPa\,s\,m^{-2}}$ for snow to $200\,000\,\mathrm{kPa\,s\,m^{-2}}$ for painted concrete. Grass has an average flow resistivity of $200\,\mathrm{kPa\,s\,m^{-2}}$ [60]. Furthermore, a surface is called locally reacting if at a certain point the particle velocity $\mathbf{u}$ depends only on the sound pressure p at that point. In case it does not, the surface has an extended reaction.

Reflection coefficient

The pressure reflection coefficient describes the ratio between the sound pressure of an incident wave p_i and the pressure of the reflected wave p_r and considers a wave incident on an infinite plane that is locally reacting and has impedance Z

$$R = \frac{p_r}{p_i} \tag{2.40}$$

The plane wave reflection coefficient gives the ratio of incident and reflected pressure assuming the incident wave is plane

$$R = \frac{Z\cos\theta - 1}{Z\cos\theta + 1} \tag{2.41}$$

and is a function of the angle of incidence θ of the incident wave. If the source is relatively close to the reflecting surface, then typically the wave front is not plane. In such case a spherical wave reflection factor is used that considers an incident spherical wave.

The impedance and reflection coefficient models together with their parameters determine in computations how much sound is reflected and how much is transmitted or absorbed. Because the reflection coefficient is complex-valued the reflected contribution may have not only a different magnitude than the direct contribution, but also an additional frequency-dependent phase shift or propagation delay. Surfaces that attenuate and phase shift the reflected wave are called acoustically soft surfaces. In case the normalised impedance approaches infinity, neither attenuation nor phase shift occur, and the surface is considered acoustically hard.

Ground effect

In outdoor situations the ground is typically providing the second-largest contribution. As mentioned before, impedances of surfaces can vary significantly, and this is especially the case for the ground surface. Spectrograms of recordings of aircraft often show a distinct interference pattern called the Lloyd's mirror effect. Figure 2.2 shows a spectrogram of a synthesised example of the Lloyd's mirror effect as caused by an elevated moving source. The upper spectrogram considers a hard reflecting surface and the lower spectrogram considers a soft reflecting surface, which results in decorrelation between the two propagation paths.

A spectrogram shows an estimate of the power spectral density as function of time and these type of figures are used throughout the thesis. In this case, the spectrogram shows two tonal components that are Doppler-shifted. Superposition of the direct and reflected path contributions result interference showing as bands in the spectrogram. Sound has a finite speed of sound, and the black section in the first couple of seconds represents the initial sound travel time from source to receiver.

Multiple reflections and shielding

In urban environments there are more reflecting surfaces besides the ground. Buildings can reflect sound and shield as well. In courtyards or street canyons multiple reflections and strong reverberance may occur.

Sound can be considered as a ray if the wavelength of the sound is much smaller than the characteristic lengths of the objects or geometries. Assuming sound can be described as a ray, a raytracer could be used to determine the immission at a receiver position, taking into account refractions and reflections. Raytracers are commonly used in room acoustics but also in environmental acoustics for noise prediction.

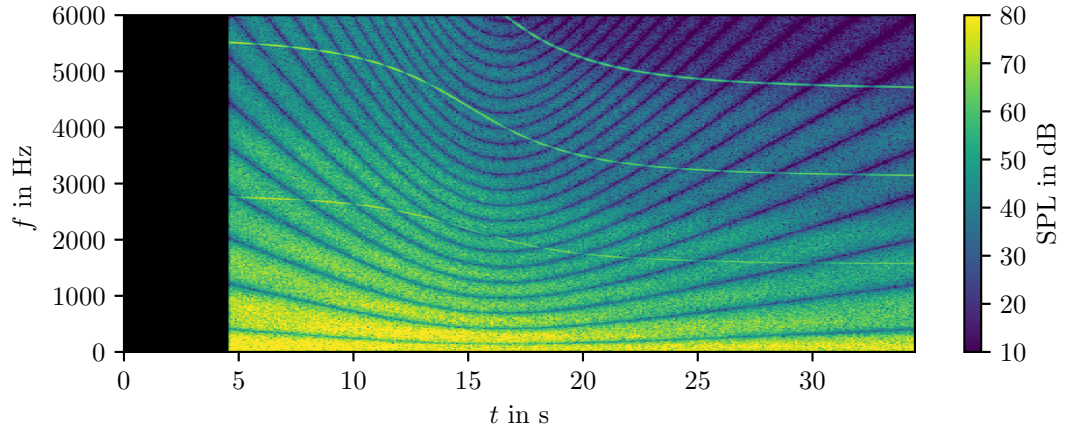

(a) Hard surface.

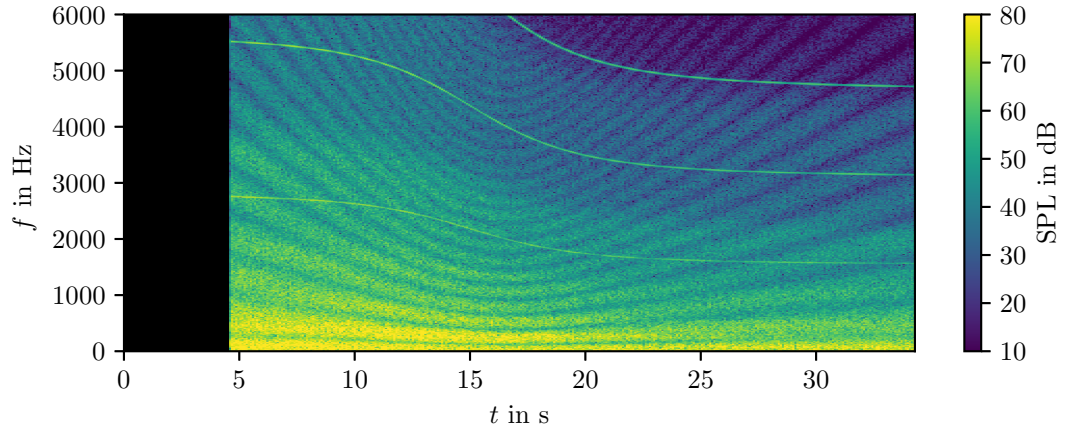

(b) Soft surface.

Figure 2.2: Superposition of the direct contribution and ground-reflected contribution results in an interference pattern known as the Lloyd's mirror effect.

The Image Source Method (ISM) is a computationally fast algorithm for taking into account reflections and uses the concept of mirror sources [61, 62]. Mirror sources are found by mirroring the original source with respect to the reflective surface that is considered. Higher-order mirror sources can be found by repeating the process, mirroring the previous order mirror source with respect to another surface. Care should be taken to determine whether there is in fact line-of-sight between a mirror-source and the receiver. Lack of line-of-sight may result in discontinuous behaviour.

When neither source nor receiver move, the image sources have to be determined only once, and their validity, that is, whether there is line-of-sight between image source and receiver, needs to be checked only once as well. If instead the receiver moves, line-of-sight will have to be checked as function of time. When both move, both the mirror source search as well as the line-of-sight validation has to be performed as function of time. An interesting question is how to connect image sources at one instance in time to the image sources the next instance, considering sources can appear and disappear over time. If only the source moves, it may be more interesting to consider mirror receivers instead of mirror sources.

2.4.4 Atmospheric turbulence

In an outdoor situation, spatial and temporal variations in temperature and wind velocity cause small changes in the refractive index. As waves pass through the atmosphere, the index-of-refraction variations in effect cause scintillations, i.e. fluctuations or modulations in the received intensity of the wave. Scintillations affect both sound and electromagnetic waves. They are a major limitation for astronomical observations using Earth-based telescopes and also reduce performance of wireless communication systems. Scintillations can also be noticed when hearing sound emitted by a source at a large distance, like for example by an aircraft or distant wind turbine [33]. Shown is in this section how weak fluctuations cause sound pressure perturbations. Weak turbulence fluctuations are non-linearities but they are assumed to be small.

Turbulent flow

In a laminar flow, fluid motion is smooth. Fluid "particles" move parallel to each other in the flow direction and viscous forces dominate. In a turbulent flow, inertial forces dominate, fluid motion is chaotic and fluid particles no longer follow a straight path. Instead, they may loop, forming instabilities such as eddies and vortices. The Reynolds number Re may be used to predict the transition from laminar to turbulent flow and is the dimensionless ratio between inertial and viscous forces.

The onset of turbulence and formation of eddies can be explained by considering a particle that moves faster than its neighbouring particles. As it encounters other particles it is forced to deviate from its straight course. The term eddy is used not only for loops or swirls. The region wherein velocity fluctuations exist is also called an eddy. Furthermore, an eddy corresponds not only to a velocity fluctuation, but also to a temperature fluctuation. The size of the eddies is limited by some

characteristic dimension. For example, the eddies that can occur in a turbulent flow in a pipe are smaller than the pipe diameter.

If advection[2] contributed by turbulent circulations is small compared to that of the mean flow, then the eddies can be considered as "frozen" fluctuations passing through the fluid. The size of the eddy L is then related to a characteristic time τ and mean flow velocity of the fluid u by $L = u\tau$. This assumption is referred to as Taylor's frozen turbulence hypothesis.

Atmospheric boundary layer

In the atmospheric boundary layer the height above the ground is the characteristic dimension and with increasing height larger eddies occur. These large eddies break down into smaller eddies forming a broad distribution or spectrum of eddy sizes and thus turbulent fluctuations. The time scale of variations or fluctuations in the atmosphere therefore varies wildly, with variations ranging on scales from seconds or minutes, to hours or days.

The temperature and velocity fluctuations cause variations in the refractive-index of the medium. As sound passes, it is scattered multiple times along its propagation path resulting in modulations of amplitude and phase.

Atmospheric turbulence is a stochastic process and therefore the resulting modulations are also random. A random process has a distribution and a power spectral density. The spectrum of atmospheric turbulence is strongly related to the sizes of the eddies. Several models are available for describing the spectrum of turbulence. Furthermore, the shape of the wavefront is relevant when considering sound propagation through a turbulent atmosphere.

Rytov approximation

Variations in temperature and wind in both position $\mathbf{r}$ and time t cause variations in the refractive index field $n(\mathbf{r}, t)$. Interested in how these variations affect wave propagation, a first-order Rytov approximation is done to obtain expressions for the fluctuating pressure. The following expressions are based on [63] and [64], but instead of electromagnetic waves, sound waves are considered. We consider for now spatial variations only, and as a starting point we use the following Helmholtz equation

$$\left(\nabla^2 + k^2 n^2(\mathbf{r})\right) p(\mathbf{r}) = 0 \tag{2.42}$$

with pressure p, wavenumber k, and refractive-index field

$$n(\mathbf{r}) = n_0 + n_1(\mathbf{r}) \tag{2.43}$$

with mean value $n_0 = E[n(\mathbf{r})] = 1$ and first-order perturbation $n_1(\mathbf{r}) \ll 1$. Merging equations (2.42) and (2.43) results in

$$\left(\nabla^2 + k^2 (n_0 + n_1(\mathbf{r}))^2\right) p(\mathbf{r}) = 0 \tag{2.44}$$

[2] Advection is the transport of a substance and its properties by bulk motion.

For weak fluctuations, an approximation to equation (2.44) for small n_1 is used. The Rytov solution to equation (2.44) is

$$p = \exp(\psi_0 + \psi_1 + \psi_2 + \dots) = \exp(\psi) \tag{2.45}$$

where ψ_0 is the complex phase of the unperturbed wave in free space, and ψ_1 and ψ_2 respectively first-order and second-order complex phase perturbations.

We are interested in the effect of first-order perturbations n_1, on the sound pressure, and therefore write $\psi = \psi_0 + \psi_1$. The refractive index n is written in terms of an average $\langle n \rangle$ and fluctuation n_1, with

$$\delta n = (1 + n_1)^2 - 1 = 2n_1 + n_1^2 \tag{2.46}$$

As derived in [63], ψ_1 satisfies the following integral equation

$$\psi_1(\mathbf{r}) = \frac{1}{p_0(\mathbf{r})} \int_{V'} G(\mathbf{r} - \mathbf{r}') \left[\nabla\psi_1 \cdot \nabla\psi_1 + k^2 \delta n \right] p_0(\mathbf{r}') dV' \tag{2.47}$$

where $G(\mathbf{r} - \mathbf{r}')$ is the free field Green's function. By iteration a series solution can be obtained. For the first iteration we set $\psi_1 = 0$ inside the integral and obtain the first Rytov solution

$$\psi_{10}(\mathbf{r}) = \frac{k^2}{p_0(\mathbf{r})} \int_{V'} G(\mathbf{r} - \mathbf{r}') \delta n(\mathbf{r}') p_0(\mathbf{r}') dV' \tag{2.48}$$

where $p_0(\mathbf{r})$ is the unperturbed sound pressure field. The sound pressure after the first iteration is then

$$p(\mathbf{r}) = e^{(\psi_0 + \psi_{10})} = p_0(\mathbf{r}) e^{(\psi_{10})} \tag{2.49}$$

The first-order complex phase perturbation ψ_1 can be understood as a sum of waves, generated at various points $\mathbf{r}'$ throughout the scattering volume V'. The strength of each of these waves is proportional to the product of the unperturbed field term p_0, and the refractive-index perturbation δn at a point $\mathbf{r}'$ [64].

Amplitude and phase fluctuations

We now want to find expressions for the log-amplitude and phase fluctuations, and will use Rytov's first solution. We approximate the refractive-index fluctuation as

$$\delta n = 2n_1 + n_1^2 \simeq 2n_1 \tag{2.50}$$

and write

$$p(\mathbf{r}) = A(\mathbf{r}) e^{jS(\mathbf{r})}, \quad p_0(\mathbf{r}) = A_0(\mathbf{r}) e^{jS_0(\mathbf{r})} \tag{2.51}$$

where A and S are respectively the amplitude and phase of the fluctuating field $p(\mathbf{r})$, and obtain for the first order perturbations

$$\psi_1(\mathbf{r}) = \chi + jS = \log(A/A_0) + j(S - S_0) \tag{2.52}$$

In this expression χ and S represent respectively the log-amplitude fluctuation and phase fluctuation.

By applying the central limit theorem to the first Rytov solution, it follows that the complex phase follows a normal probability distribution [64]. This is an important result to keep in mind when generating sequences of fluctuations.

Amplitude and phase covariance

The log-amplitude and phase fluctuations are considered to be the result of a random temperature fluctuation field. A characteristic of a random function or field is its correlation function [65]. The spatial correlation function of a random field $f(\mathbf{r})$, as function of distance $\mathbf{r} = \mathbf{r}_2 - \mathbf{r}_1$ between observation points $\mathbf{r}_1$ and $\mathbf{r}_2$, is defined as

$$C(\mathbf{r}_1, \mathbf{r}_2) = \langle f(\mathbf{r}_1) f(\mathbf{r}_2) \rangle \tag{2.53}$$

In a homogeneous and isotropic random field the correlation function $C(r)$ depends only on the distance $r = \|\mathbf{r}_2 - \mathbf{r}_1\|$ between the observation points and not the path $\mathbf{r} = \mathbf{r}_2 - \mathbf{r}_1$ [66]. Note that at this point, the atmosphere is assumed frozen in time, i.e., variations are only spatially, not temporal.

We would like to obtain expressions for the covariance functions of the log-amplitude and phase fluctuations. A specific part of the turbulence spectrum can be approximated with a Gaussian correlation function

$$C_\mu = \langle \mu(r_1)\mu(r_2) \rangle = \sigma_\mu^2 e^{-x^2/L^2} \tag{2.54}$$

where σ_μ^2 is the variance of the dynamic refractive index, $x = r_1 - r_2$ the distance between two points in space and L the correlation distance or length [63].

We shall now consider a line-of-sight situation where d is the distance between the source and a receiver pair along the wave propagation direction, and ρ the spatial separation of the receivers transverse to the wave propagation direction.

If the correlation length L is much smaller than the Fresnel zone size of the sound $\sqrt{\lambda d}$, then the log-amplitude and phase variance scale with $\sigma_\chi^2 = \sigma_S^2 \sim k^2 d$ [63] and the variances of the fluctuations are given by [67]

$$\sigma_\chi^2 = \sigma_S^2 = \frac{\sqrt{\pi}}{2} \sigma_\mu^2 k^2 dL \tag{2.55}$$

In case the correlation length is much larger than the Fresnel zone, the variances scale as $\sigma_\chi \sim d^3$ and $\sigma_S \sim 2k^2 d$ [63].

For spherical waves the covariances of the fluctuations, $B_\chi(\rho)$ and $B_S(\rho)$, normalised to their variances, are given by

$$\frac{B_\chi(\rho)}{\sigma_\chi^2} = \frac{B_S(\rho)}{\sigma_S^2} = \frac{\Phi\left(\rho/L\right)}{\rho/L} = C_{sp}(\rho) \tag{2.56}$$

where

$$\Phi\left(\rho/L\right) = \int_0^{\rho/L} \exp\left(-u^2\right) \mathrm{d}u \tag{2.57}$$

$$= \frac{1}{2}\sqrt{\pi}\,\mathrm{erf}\left(\rho/L\right) \tag{2.58}$$

and erf is the error function. The covariance functions of the fluctuations $B_\chi(\rho)$ and $B_S(\rho)$ are thus

$$B_\chi(\rho) = B_S(\rho) = \frac{\sqrt{\pi}}{2} \sigma_\mu^2 k^2 dL \frac{\Phi(\rho/L)}{\rho/L} \tag{2.59}$$

2.5 Signal processing

The previous sections discussed sound generation and propagation. Synthesising the sound of aircraft requires generating and modifying signals. This section discusses several signal processing techniques that are useful or required to create auralisations. An introduction to signal processing for auralisation is provided by Vörlander [25] In this chapter all operations are considered to be in time or frequency domain. Generally, these operations can also be used with other domain pairs, like for example the space-wavenumber pair.

2.5.1 Fourier transform

The Fourier transform decomposes a signal into complex exponentials with different frequencies that the signal. Essential for creating certain filters for auralisations, the transform is also used to implement fast convolutions as will be discussed in section 2.5.3. The forward Fourier transform can be defined as

$$X(f) = \int_{-\infty}^{\infty} x(t) e^{-j2\pi ft} \mathrm{d}t \tag{2.60}$$

where $x(t)$ is a signal in the time-domain, f the frequency of the complex exponential and $j^2 = -1$. Often the complex exponent $e^{-j2\pi ft}$ is written as $e^{-j\omega t}$ where ω is the angular frequency. Typically, $\mathcal{F}\{x(t)\}$ is used to denote the Fourier transform of the function $x(t)$. For operation on digital signals a discretised version of the Fourier transform is needed. The Discrete Fourier Transform (DFT) both operates on, and returns, finite discrete signals and is defined as

$$X[k] = \sum_{n=0}^{N-1} x[n] \cdot e^{-j2\pi kn/N} \tag{2.61}$$

where x_n is a discrete signal in time-domain, X_k the resulting signal in frequency domain, N the amount of complex numbers the input and output signal consists of, and k integer frequencies. The DFT can be expressed as a matrix and applied through matrix multiplication with the signal. The Fast Fourier Transform (FFT) is an algorithm that calculates the DFT by decomposing the DFT matrix into a product of sparse factors, thereby reducing the amount of computations necessary and obtaining a higher performance.

Hermitian symmetry

The Fourier transform and DFT both operate on a complex function and return a complex function as well where the negative frequencies can be different from the positive frequencies. If however the input function is real-valued, then the negative frequencies are identical to the positive frequencies, and we say the Fourier transform of the function is Hermitian. A Hermitian function is a complex function with the property that its complex conjugate is equal to the original function with the variable changed in sign

$$f(-x) = \overline{f(x)} \tag{2.62}$$

Similarly, when the input function is Hermitian, then its Fourier transform is real-valued. This property turns out to be useful, since when computing the DFT of a real-valued signal this property will half the amount of computations and storage required.

Sine and cosine transform

The Fourier transform takes a complex-valued function and returns complex exponentials. The sine and cosine transforms operate on real-valued data with respectively odd and even symmetry. A function f is even when $f(x) = f(-x)$ holds in which case the graph of the function is symmetric with respect to the y-axis or ordinate. When $-f(x) = f(-x)$ holds the function is odd and the graph remains unchanged after rotation of 180 degrees about the origin. Just as with Hermitian symmetry, the sine and cosine transform are computationally more efficient reducing again by a factor two the required computations and storage.

2.5.2 Transfer functions and filters

Consider a continuous-time system that has an input $x(t)$ and an output $y(t)$. Functions often exist that can describe the relation between an input $x(t)$ and an output $y(t)$. A relation is typically described in frequency-domain between the Fourier transforms of the signals, $X(e^{j\omega})$ and $Y(e^{j\omega})$. The system is linear when it satisfies the properties of superposition, additivity and homogeneity. When the output does not depend on the particular time the input is applied the system is called time-invariant. The transfer function of a continuous-time linear time-invariant system is then given by

$$H(e^{j\omega}) = \frac{Y(e^{j\omega})}{X(e^{j\omega})} \tag{2.63}$$

and describes in frequency-domain the relation between the input and output.

A sound propagation model describes the ratio or transfer function between the immission and the emission. Depending on the situation that is modelled, the whole model or certain parts of it can be considered as linear time-invariant systems.

Gain and delay

A gain G is an amplification factor that amplifies or attenuates a signal, independently of frequency

$$y[n] = G[n]x[n] \tag{2.64}$$

Similarly, a delay is an element that delays samples by one sample or multiple samples m

$$y[n] = x[n - m][n] \tag{2.65}$$

Finite and Infinite Impulse Response filters

We will now consider two types of filters. In the following expressions $x[n]$ is an input signal to a filter, and $y[n]$ the signal after filtering.

An Infinite Impulse Response (IIR) filter is a type of filter whose impulse response never exactly reaches zero. Analog electronic filters like fractional-octave bandpass filters in sound level meters are generally IIR filters. The output of a digital IIR filter can be obtained through the difference equation

$$y[n] = \frac{1}{a_0}(b_0 x[n] + b_1 x[n-1] + \dots b_P x[n-P] \\ - a_1 y[n-1] - a_2 y[n-2] - \cdots - a_Q y[n-Q]) \quad (2.66)$$

where P and Q are respectively the feedforward and feedback filter orders, and b_i and a_i respectively the feedforward and feedback filter coefficients. The expression can be written as

$$y[n] = \frac{1}{a_0}\left(\sum_{i=0}^{P} b_i x[n-i] - \sum_{j=1}^{Q} a_j y[n-j]\right) \quad (2.67)$$

and its transfer function in z-domain is

$$H(z) = \frac{\sum_{i=0}^{P} b_i z^{-i}}{\sum_{j=0}^{Q} a_j z^{-j}} \quad (2.68)$$

Because an IIR filter has feedback terms, it will have poles which can have a negative effect on the stability of the filter.

A Finite Impulse Response (FIR) filter is a filter whose impulse response is of finite duration before it settles to zero in finite time. In the case of a causal digital FIR filter the output $y[n]$ is given by

$$y[n] = b_0 x[n] + b_1 x[n-1] + \cdots + b_N x[n-N] \quad (2.69)$$

which can be written as

$$y[n] = \sum_{n=0}^{N} b_i \cdot x[n-i] \quad (2.70)$$

where N the filter order and b_i the value of the ith impulse. The transfer function in z-domain is

$$H(z) = \sum_{n=-\infty}^{\infty} h[n] z^{-n} \quad (2.71)$$

This type of filter does not have any feedback terms, therefore there cannot be any poles and thus this type of filter is inherently stable. Furthermore, they can be easily designed to have linear phase, which is an important requirement for auralisations.

Linear phase and zero phase

A filter is said to have linear phase when the phase response of the filter is a linear function of frequency. In case of linear phase, all frequency components are delayed in time by the same amount and consequently there is no phase distortion. This

phase distortion, which is basically dispersion, is highly undesired in auralisations. Therefore, linear phase is a must for filters used in auralisations.

However, while a filter with linear phase causes no phase distortion, it still does cause a group delay of the signal. The delay in samples is $(L-1)/2$ with L the length of the filter. The signal will experience a constant delay, assuming the filter length remains constant over time. This is a known problem with real-time systems; the filters cause a latency in the system and this can effect the experience, especially when it is possible to interact with the simulated environment.

A possible method to correct for the group delay is by filtering the signal twice, once forward and once backward. This method, known as zero-phase filtering, is however only possible for offline auralisations because the operation is non-causal.

2.5.3 Convolution

Auralisations are signals that represent the sound pressure at a receiver location as function of time. In order to apply a Finite Impulse Response filter a convolution is essentially performed.

Convolution definition

The convolution of the functions h and x is written $h \star x$ and is defined as the integral of the product of the two functions after one of the functions is reversed and shifted.

$$y(t) = (h \star x)(t) = \int_{-\infty}^{\infty} h(\tau)x(t-\tau)\mathrm{d}\tau \tag{2.72}$$

In practice discrete and finite signals are used. The discrete convolution of finite signals h and x is defined as

$$y[n] = (h \star x)[n] = \sum_{m=0}^{M-1} h[m]x[n-m] \tag{2.73}$$

An example of the discrete convolution can be seen in Figure 2.3. The discrete convolution operation can be written as a matrix-vector multiplication

$$y[n] = T \star x = \begin{bmatrix} h_1 & 0 & \dots & 0 & 0 \\ h_2 & h_1 & \dots & \vdots & \vdots \\ h_3 & h_2 & \dots & 0 & 0 \\ \vdots & h_3 & \dots & h_1 & 0 \\ h_{m-1} & \vdots & \dots & h_2 & h_1 \\ h_m & h_{m-1} & \vdots & \vdots & h_2 \\ 0 & h_m & \dots & h_{m-2} & \vdots \\ 0 & 0 & \dots & h_{m-1} & h_{m-2} \\ \vdots & \vdots & \vdots & h_m & h_{m-1} \\ 0 & 0 & 0 & \dots & h_m \end{bmatrix} \begin{bmatrix} x_1 \\ x_2 \\ x_3 \\ \vdots \\ x_n \end{bmatrix} \tag{2.74}$$

The matrix T is a Toeplitz matrix with each column a shifted copy of h. For relative long signals the matrix will be sparse.

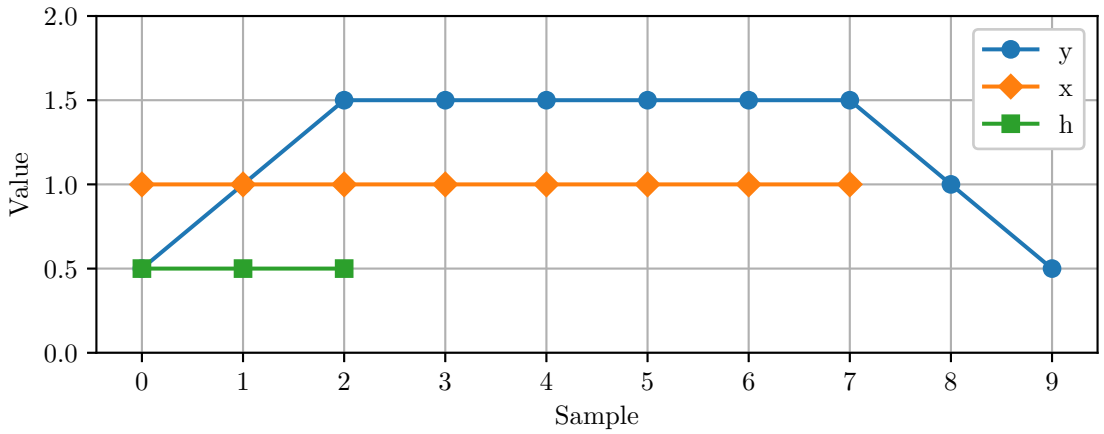

Figure 2.3: An example of a convolution. The signal x is convolved with impulse response h producing the output y. Both x and h are constant over time. Signal x has length N, h length M and the output y has length $N + M - 1$. It takes $M - 1$ samples before the signal and filter impulse response fully overlap. The length of the fully overlapped part is $N - M + 1$ samples.

The presented algorithms to calculate the convolution are straightforward to implement. However, there are better performing algorithms. According to the convolution theorem the Fourier transform of a convolution is the pointwise product of the Fourier transforms of the inputs

$$y = h \star x = \mathcal{F}^{-1}\Big\{\mathcal{F}\{h\} \cdot \mathcal{F}\{x\}\Big\} \tag{2.75}$$

This algorithm generally performs better for larger lengths of h and x.

Segmented convolution

If one of the sequences is much longer than the other, then it might be worth splitting up the long sequence into blocks and apply the convolution on each block. The overlap-add method is an example of such an algorithm. In the overlap-add method the signal $x[n]$ is divided into blocks of size L. We now define

$$x_k[n] = \begin{cases} x[n + kL], & n = 0, 1, \dots L \\ 0, & \text{otherwise,} \end{cases} \tag{2.76}$$

and rewrite $x[n]$ as

$$x[n] = \sum_k x_k[n - kL] \tag{2.77}$$

Equation (2.73) can then be written as a sum of short convolutions

$$y[n] = h[n] \star \left(\sum_k x_k[n - kL]\right) = \sum_k \left(h[n] \star x_k[n - kL]\right) \tag{2.78}$$

As shown in figure 2.3 it takes $M-1$ samples before the signal and filter fully overlap. We can divide the response into three parts; the left part we call the head, the fully overlapped part the body and the rightern part the tail. The fully overlapped part is $L-M+1$ samples long which is shorter than the blocksize L. Therefore, we need to keep the tail of each convolution and add it to the head of the next convolution.

For longer sequences the overlap-add method is much faster than the naive (direct-form) method, and especially when using the overlap-add method in combination with Fourier transformations (equation (2.75)) for the short convolutions. A disadvantage of overlap-add in a real-time simulation is that, as it operates on blocks, the simulation will incur a latency. A method similar to overlap-add is overlap-discard, known also as overlap-save.

Linear time-variant system

So far we considered linear time-invariant systems. In a linear time-variant system the impulse response can change over time. Consider again the Toeplitz matrix as shown in (2.74). In the time-invariant case each column is a time-shifted copy of the same impulse response. In the time-variant case, however, each column can be an entirely different impulse response.

The matrix-vector multiplication is a straightforward method to apply a time-variant filter. However, performance is generally bad because of the large amounts of multiplications and additions that have to be performed. As a consequence, it typically cannot be used in real-time simulations.

If we assume time-invariance during a short amount of time, then we can reuse the overlap-add overlap-discard method and perform each of the small convolutions with a possibly different impulse response. A requirement is that the filter changes sufficiently slow compared to the update rate of the impulse response.

Switching from one impulse response to the next can still cause discontinuities which may appear as audible clicks. A solution to this problem is to convolve a block with both impulse responses and crossfade the resulting sequences.

2.5.4 Amplitude envelope and instantaneous frequency

In some cases it is possible to directly extract the amplitude envelope $A(t)$ and instantaneous frequency $\phi(t)$ of a signal. An example of such a case would be a signal $s(t)$ consisting of a single sinusoidal. A sinusoidal is an analytic signal, and an analytic signal $s_a(t)$ is a complex-valued function that has no negative frequency components. Both real and imaginary parts of the analytic signal are real-valued functions, and they're related to each other by the Hilbert transform.

The amplitude envelope of an analytic signal is given by

$$A(t) = |s_a(t)| \tag{2.79}$$

and the wrapped instantaneous phase by

$$\phi(t) = \arg\left[s_a(t)\right] \tag{2.80}$$

The instantaneous angular frequency can be obtained by differentiating the unwrapped phase with respect to time

$$\omega(t) = \frac{\mathrm{d}\phi}{\mathrm{d}t} \tag{2.81}$$

and thus the instantaneous frequency is

$$f(t) = \frac{1}{2\pi}\frac{\mathrm{d}\phi}{\mathrm{d}t} \tag{2.82}$$

2.5.5 Resampling and interpolation

Generally a single, fixed, sample frequency is used in a chain of signal processing operations. However, sometimes it is necessary to resample a signal.

Resampling

Upsampling a signal with an integer factor can be done by inserting zeros between the actual samples and low-pass filtering the result to smooth out discontinuities, thereby replacing the zeros. Downsampling, also known as decimation, is done by first low-pass filtering the signal and then keeping every F sample where F is the integer downsampling factor.

If the resampling factor is not an integer, it is necessary to combine upsampling and downsampling. When upsampling with a rational fraction it is necessary to upsample first, and then downsample. Both operations require low-pass filtering, but because of the order of operations it is sufficient to low-pass filter only once and using the lower of the two cut-off frequencies.

Similarly, when downsampling with a rational fraction, the downsampling with an integer factor is done first, followed by upsampling. Again, because of the order of operations it is sufficient to low-pass filter only once with the lower of the two cut-off frequencies.

Interpolation

The low-pass filters used in resampling are basically interpolation filters. Interpolation filters can be used when applying for example a delay to a system in case the delay is not exactly an integer of the sample time, or when the delay changes as function of time. The latter is called a Variable Delay Line (VDL).

A simple interpolator is a linear interpolator. A linear interpolator works by basically drawing a straight line between two neighbouring samples and returning the requested value along that line. Consider a discrete signal $y[n]$, and let η be a number between 0 and 1 that represents by how much we want to interpolate the signal y between samples n and $n+1$. The interpolate

$$y_{\mathrm{lin}}(n+\eta) = (1-\eta)\cdot y[n] + \eta \cdot y[n+1] \tag{2.83}$$

returns then the value at non-integer sample $n+\eta$. Rewriting this expression to

$$y_{\mathrm{lin}}(n+\eta) = y[n] + \eta \cdot (y[n+1] - y[n]) \tag{2.84}$$

shows that the operation needs only one multiplication and two additions.

An interpolation filter acts as a low-pass filter and therefore introduces amplitude errors at higher frequencies. Furthermore, sampling the interpolated values results in aliasing. There are methods to reduce these artefacts. For example, upsampling the signal before resampling decreases the prominence of the artefacts. Another possibility is the application of a different interpolation scheme.

Theoretically, the optimal reconstruction filter is a sinc filter. In practice, only approximations of this filter can be used, and these approximations are generally achieved by windowing and truncating the sinc function. One of these approximations is the Lanczos filter or kernel, which is the sinc function windowed by another sinc function.

The Lanczos kernel is given by

$$L(z) = \begin{cases} \text{sinc}(z)\text{sinc}(z/a), & \text{if} -a < z < a \\ 0, & \text{otherwise} \end{cases} \tag{2.85}$$

where a is the size of the kernel and z a non-integer sample. The interpolator performs a convolution of the signal $x[n]$ with the kernel

$$y_{\text{lanc}}(z) = \sum_{\lfloor z \rfloor - a + 1}^{\lfloor z \rfloor + a} x[n] L(z - n) \tag{2.86}$$

Figure 2.4 compares the two interpolators. The figure shows spectrograms of a Doppler-shifted tone for the two explained interpolation algorithms and two values of the kernelsize a. Aside from the Doppler-shifted tones artefacts are clearly present and indeed also audible. The artefacts are clearly less pronounced when using a larger kernelsize. However, a larger kernelsize does come at a cost of performance.

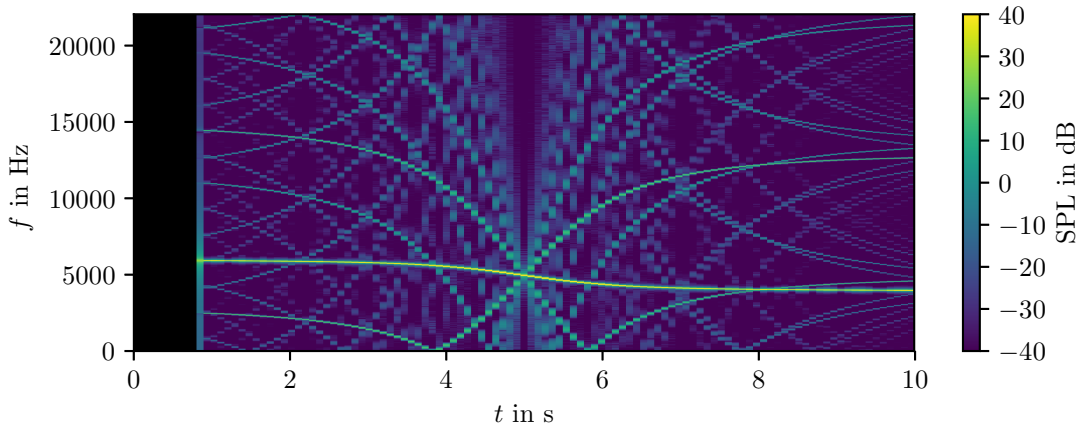

(a) Linear interpolation

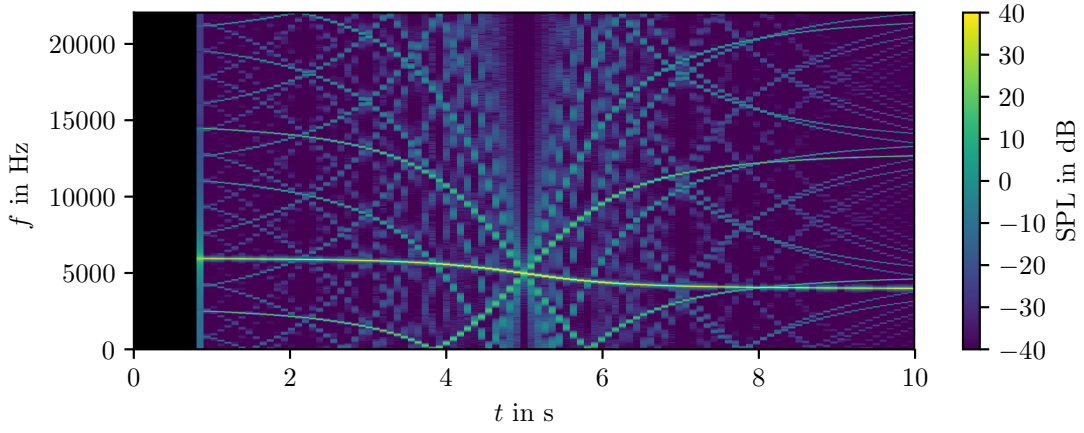

(b) Lanczos interpolation with $a = 2$

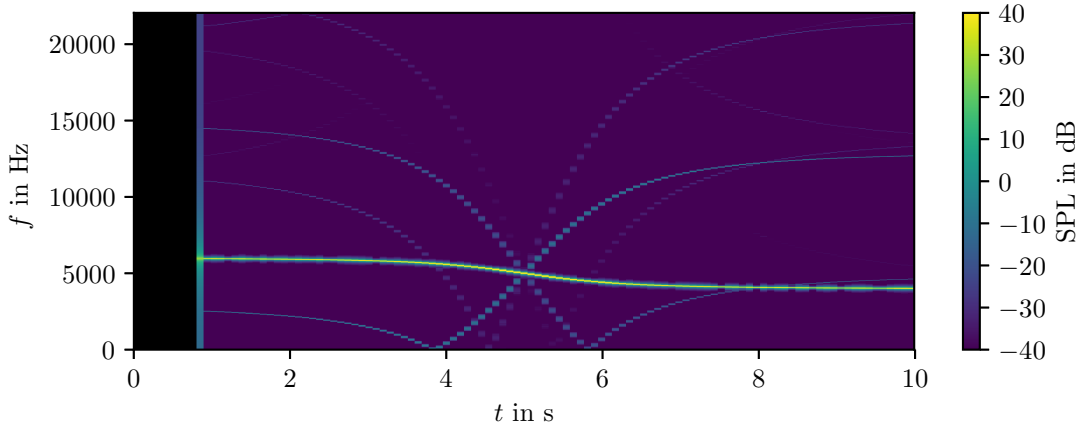

(c) Lanczos interpolation with $a = 10$

Figure 2.4: A comparison between linear interpolation (top) and Lanczos interpolation with different kernelsizes. The artefacts are weaker for Lanczos interpolation, especially with larger kernelsize a.

2.6 Synthesis software

Eventually software is needed for synthesis and auralisation. What software or tools to use depends on the requirements. What is the purpose of the software? Who is going to use it? Under what conditions is it going to be used? Is it going to be used online or only offline? How should it perform? How usable and learnable should it be? And is it supposed to interoperate with other tooling? Questions like these may determine what tooling to choose. What follows is a brief, though incomplete, overview of software that may be used for (real-time) synthesis and auralisation.

Max is a proprietary visual programming language for multimedia originally written in the 1980s [68]. With the Max Signal Processing (MSP) add-on package real-time signal processing is possible. Pure Data is written by the original author of Max and is a free and open-source alternative [69]. Both are data flow programming languages where programs are made by linking objects or blocks together into a block diagram.

SuperCollider is an environment and programming language for real-time audio synthesis [70] . The SuperCollider language (`sclang`) combines features from object-oriented languages with those from functional languages. SuperCollider uses a server (`scsynth`) that can be controlled by external programs. External programs that interpret the `sclang` language control what is being synthesised on the `scsynth` server through Open Sound Control (OSC), which is a protocol for connecting sound synthesisers, computers and other hardware that can be used for performances.

Simulink is a proprietary graphical programming environment for modelling and simulating dynamic systems [71]. Like with the previous mentioned languages, programs are composed through the graphical user interface and consist of a set of blocks forming a block diagram. While not specifically targeting sound synthesis, the provided blocks, its integration with MATLAB, and its possibility to deploy programs on external DSPs, can make Simulink a convenient and interesting environment for synthesis and auralisation.

FAUST is a functional programming language for real-time signal processing and sound synthesis [72]. The FAUST compiler translates FAUST code into C++, no runtime is needed. Digital signals are modelled as discrete functions of time, signal processors are functions that operate on the signals, and composition operators are used to combine signal processing functions. This allows one to take a block diagram approach when writing programs, and eventually allows a C++ compiler to heavily optimise the generated C++ code.

Finally, plenty of libraries and tools for signal processing are available natively or as bindings for higher-level languages.

Chapter 3

Auralisation tool

3.1 Introduction

The aim was to develop a tool for the auralisation of airplanes that can cover a wide range of aircraft that are currently in use. Aircraft are complex noise sources, with multiple components causing sound emission. The long-term goal is to develop a generic emission model and the idea is to use measured data from the sonAIR project for its development. Sound recordings include propagation effects, and these effects are undesirable when developing an emission model. This Chapter, which is based on Papers II, III and IV, describes the tool that was developed.

Removing the propagation effects requires a propagation model, and therefore the next section discusses first the basic propagation model. The section after describes the emission synthesis along with a method for determining the spectral information from airplane recordings. The plausibility of these auralisations is then compared to that of the recordings in the next chapter by means of a listening test. Note that parameters that are given in this section correspond to those that were used for that test.

Tool overview

The auralisation tool consists roughly of three parts as shown also in Figure 3.1:

- The first part covers emission synthesis and generates as function of time and emission angle a signal. Sources are considered to be point sources and the generated values correspond to their emission at 1 meter from the point source. Spectral modelling synthesis is chosen as synthesis strategy.
- The second part describes sound propagation in the far field through a, for now, isotropic and homogeneous atmosphere. The assumption is made that sound can be considered a ray.
- The third part deals with sound immission and more specifically sound immission encoding. For each source an immission of sound pressure is recorded along with the angle of incidence as a unit vector. With this data the emission

can be encoded into various formats, for example, as an Ambisonics format using spherical harmonics, or as monaural by adding the pressure contributions ignoring the angles of incidence.

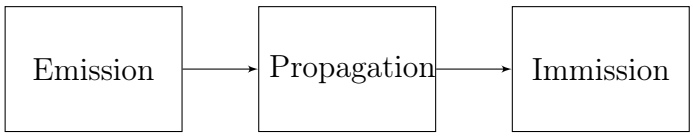

Figure 3.1: The three separate parts the auralisation tool consists of.

The tools mentioned in section 2.6, as well as other general-purpose languages, were considered for the implementation. Eventually the Python general-purpose language was chosen because of its flexibility, well-tested libraries for computing and signal processing as well as sufficiently good performance. The auralisation tool was implemented in Python 3.5 [73]. Certain computationally intensive routines were implemented in Cython [74, 75]. Extensive use was made of the Numpy [76, 77], Scipy [78] and Pandas [79] libraries. A full implementation of the tool can be found at [80].

3.2 Propagation model

3.2.1 Introduction

The propagation model covers sound propagation in the far field through a homogeneous and isotropic atmosphere and takes into account geometrical spreading, Doppler shift, atmospheric attenuation and the ground reflection. Sound is modelled as rays and the propagation effects are implemented as signal processing operations. The following sections will describe each of the implemented propagation effects in detail. To also demonstrate the different propagation effects, a fixed situation is considered and propagation effects are added sequentially.

Figure 3.2 shows a block diagram of the steps that are taken. Because of source motion all propagation effects are time-variant. The order of the operation matters although some could be exchanged. For operations that are distance-dependent and thus propagation-delay dependent care should be taken to consider the distances at the emission or retarded times. Divergence is computed first. The Doppler-shift, a result of a change in propagation delay as function of time, occurs between the source and the medium. The shifted frequencies are then attenuated in the atmosphere. A reflection is modelled as a parallel path with a filter representing the reflection coefficient. In case there is no movement this filter may be considered part of the mirror source, however, as movement is considered it needs to be placed after the Doppler-shift has been applied. The same applies for the turbulence filter.

Paper I describes a model that was developed to include scintillations, that is, fluctuations in the sound due to atmospheric turbulence. That part is discussed in detail in Chapter 5 and therefore not included in this Chapter.

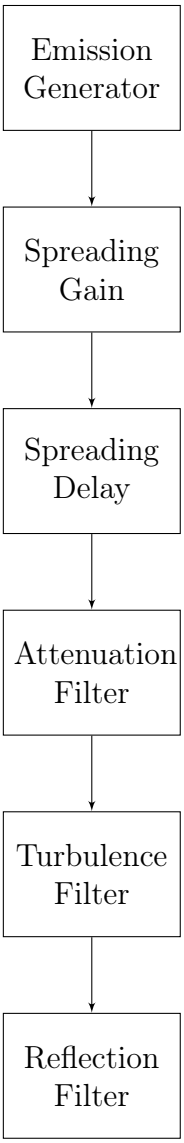

Figure 3.2: Block diagram of the propagation model. These steps are performed for each propagation path and the resulting signals are summed.

3.2.2 Emission signal and scenario

A simple emission signal is considered consisting of pink noise and several harmonic tones with a fundamental frequency of 2000 Hz, both modelled as a monopole point source at the same position. The broadband noise is the sum of 1/1-octave band-pass filtered noise. The band-pass filters are 8^{th} order Butterworth filters implemented

as second-order sections[1]. Directivity is not included, and there are no other signal strength variations either.

The "aircraft" moves at a height of 200 m and with a speed of 100 m s^{-1} at a transverse distance of about 500 m. The receiver is at a height of 1.7 meters. Figure 3.3 shows a spectrogram of the signal. In the next sections propagation effects will be added sequentially resulting in clear changes to the immission.

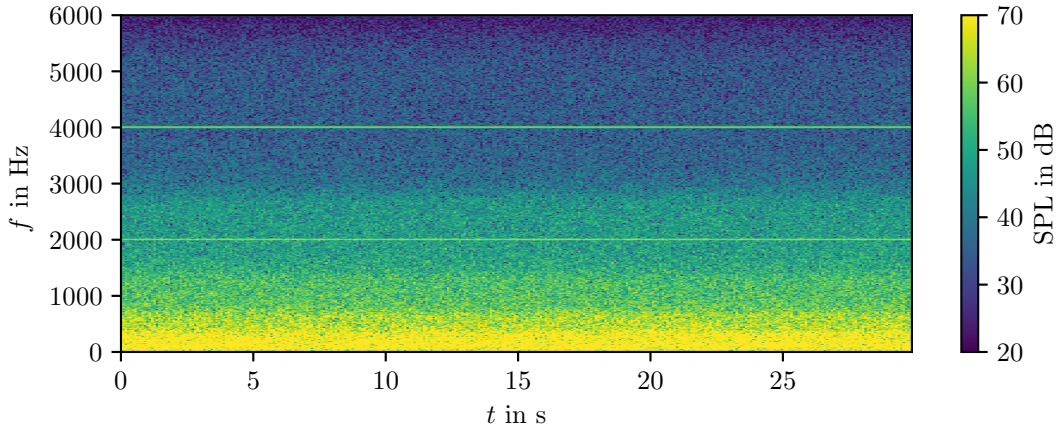

Figure 3.3: Spectrogram of the emission. The immission is stationary because an omni-directional source is considered and no other emission variations are modelled.

[1] Higher-order IIR filters can easily become unstable. A solution is to implement the filter as a serial cascade of biquad or second-order sections, i.e., filters with two poles and two zeros.

3.2.3 Geometrical spreading

Geometrical spreading causes a decrease in amplitude with distance due to divergence and increase in propagation delay with distance due to the finite speed of sound. Far field is assumed in which case the sound pressure at the receiver p_{rcv} is given by the Green's function given in equation (2.16). The emission signal p_{src} is computed at a fixed distance from the source r_{src}. The sound pressure at a receiver at distance r_{rcv} can be obtained by rescaling the magnitude of the sound pressure of the emission signal with the ratio of the distances

$$p_{\mathrm{rcv}} = p_{\mathrm{src}} \frac{r_{\mathrm{src}}}{r_{\mathrm{rcv}}} \tag{3.1}$$

This operation is implemented as a simple gain. Figure 3.4 shows a spectrogram of the immission when geometrical spreading is taken into account and applied to the signal showed in Figure 3.3. Due to the applied gain the sound pressure level is lower when the aircraft is farther away, which is here at the start and the end of the sample.

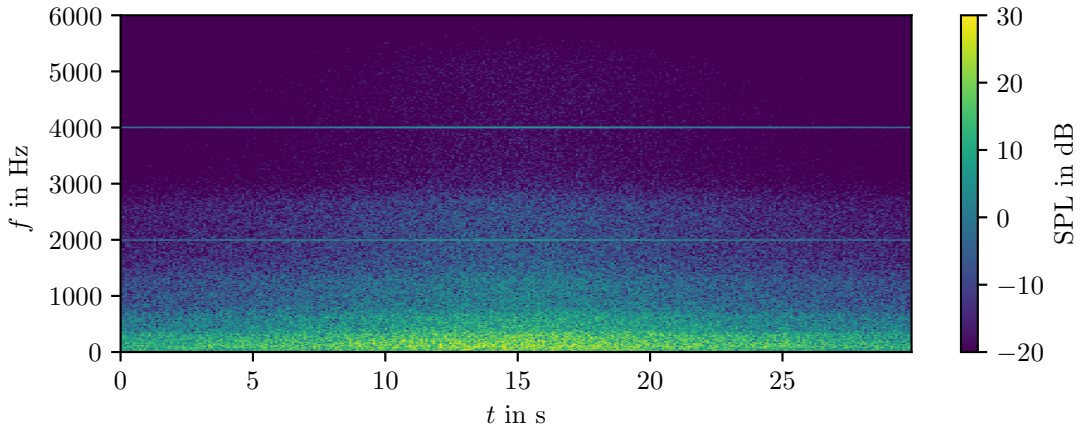

Figure 3.4: Spectrogram of the immission when the amplitude decrease due to geometrical spreading is included.

Doppler shift

The time-dependent propagation delay, which is relevant for the Doppler shift, is taken into account by resampling the discretised sound pressure signal with a Variable Delay Line. Since the signal is discrete and the delay is generally not an integer multiple of the sample time, an interpolation scheme is required.

As explained in section 2.5.5, multiple interpolation schemes exist, including Lanczos interpolation that was used for auralisation as well [28, 81]. In this case a linear interpolation scheme was chosen due to its simplicity and computational performance [33]. While linear interpolation can cause audible artefacts, these are in the case of a broadband signal less pronounced than if solely a tonal component is considered as was demonstrated in Figure 2.4.

For a given sound travel time $\Delta t(t)$ from source to receiver, the non-integer sample index n_e of the signal $y[n_e]$ at the source time-axis is given as

$$n_e = n_r - \Delta t(t) \cdot f_s \tag{3.2}$$

where f_s is the fixed sampling frequency and n_r the integer sample index of the signal at the receiver time-axis. Equation (2.84) can then be used for applying the Doppler shift when using $n = \lfloor n_e \rfloor$ and $\eta = n_e - \lfloor n_e \rfloor$ where $\lfloor n_e \rfloor$ corresponds to the floor function of n_e. Furthermore, an emission time should exist and therefore there is the requirement $\lfloor n_e \rfloor >= 0$.

The sound travel time was computed with the speed of sound $c = 343.2\sqrt{\frac{T}{T_0}}$ where T is the temperature during the event and $T_0 = 293.15$ K the reference temperature. Figure 3.5 shows a spectrogram of the immission when the propagation delay is also considered. The Doppler shift is clearly visible, especially when considering the tonal components. The black part in the first couple of seconds represents zero signal and is due to the initial propagation delay.

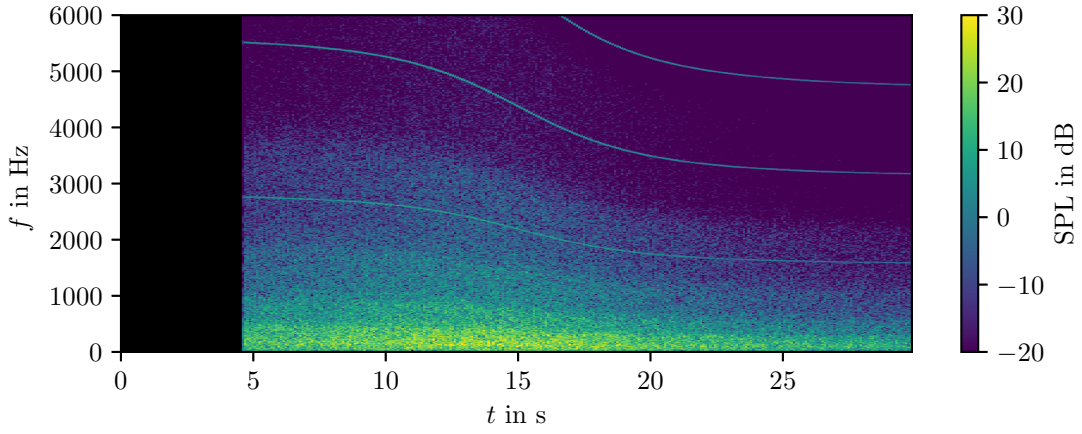

Figure 3.5: Spectrogram of the immission when the propagation delay, and thus the Doppler shift, is included as well.

3.2.4 Atmospheric attenuation

Atmospheric attenuation is accounted for by creating a time-variant filter of length N_{aa}. A single-sided magnitude spectrum is calculated as

$$|H_{aa}| = 10^{-d(t)\alpha(f)/20} \tag{3.3}$$

where d is the source-receiver distance in meter and $\alpha(f)$ the frequency-dependent attenuation coefficient in $\mathrm{dB\,m^{-1}}$ computed using equation (2.33).

The impulse response of a magnitude-only or zero-phase filter is non-causal and therefore in order to create a causal filter a linear-phase filter corresponding to a 90 degrees rotation is added. The spectrum is real and even, and therefore the impulse response is real and even as well. After convolution of the signal with the designed filter the first $N_{aa}/2$ samples were dropped to account for the delay caused by the linear-phase factor.

Convolution was performed using a segmented convolution as explained in section 2.5.3. The filter length was 4096 samples and the hop size 256 samples. Transitioning to the next impulse response was done without smoothing because the difference in the impulse responses is relatively small.

Figure 3.6 shows a spectrogram of the immission when atmospheric attenuation is included. A reference atmosphere was considered. The difference with the previous figure is small. That is because the distances considered are relatively small. Attenuation is especially strong at higher frequencies, however, the source spectrum that is considered is relatively weak at higher frequencies. Furthermore, the spectrograms only show up to 6 kHz.

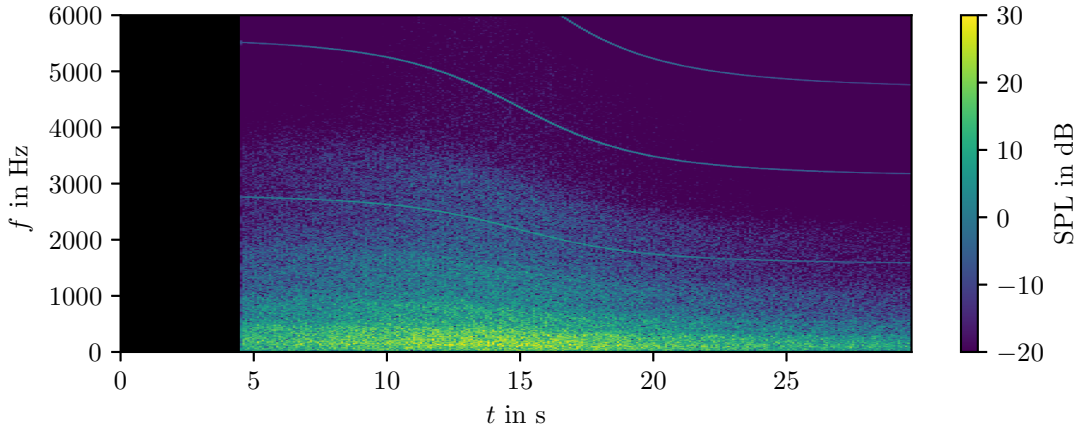

Figure 3.6: Spectrogram of the immission when atmospheric attenuation is included as well.

3.2.5 Ground reflection

While the Image Source Method was implemented with image receivers instead of image sources, only one additional path, a ground reflection, was considered. Therefore, the implementation of the ISM will not be treated any further.

The ground reflection is considered as a second propagation path using a mirror receiver. For the ground reflected path the same emission signal was used as for the direct path, thereby ignoring directivity of the sources. The reason why the directivity of the source is ignored will become clear in the following sections.

A filter was included to take into account the transfer funtion of the ground. For the ground reflection the plane wave reflection coefficient was used (eq. (2.41)) and the impedance Z was calculated using Delany and Bazley's one-parameter model (eq. (2.39)).

Because aircraft are mostly overhead and at larger distances, using the plane wave reflection coefficient should typically be sufficient. However, when simulating noise sources at low elevation angles, the plane-wave assumption is no longer valid and must be replaced by a model that takes into account the reflection of spherical waves from a ground surface of finite impedance [82].

The area around the airport consists mostly of grass and therefore a flow resistivity of $2 \times 10^5\,\mathrm{Pa\,s\,m^{-2}}$ was chosen. The filter length was 4096 samples and the hop size 256 samples.

Figure 3.7 shows a spectrogram of the immission when a reflection on a hard ground was added. The additional path clearly causes interference as can be seen from the bands in the Figure. The effect of a hard and soft ground was demonstrated before in Figure 2.2.

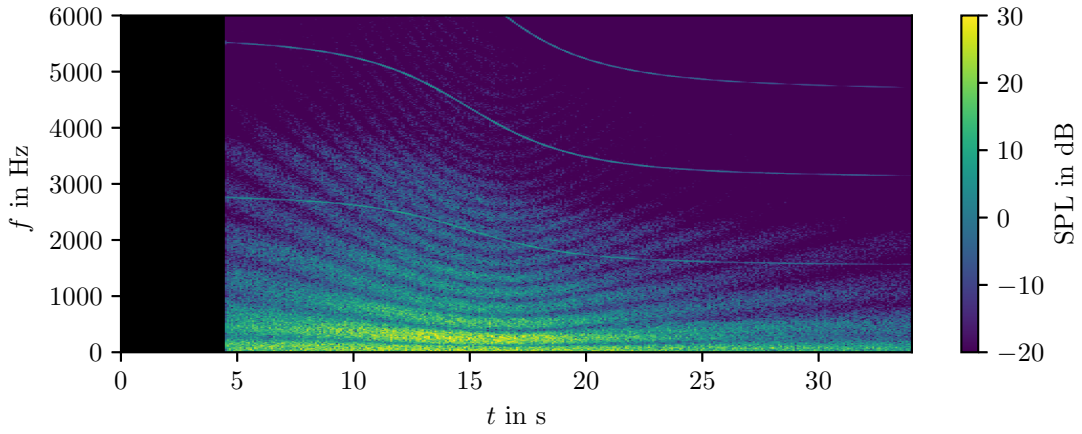

Figure 3.7: Spectrogram of the immission when a ground reflection is present. The Lloyd's mirror effect is clearly visible.

3.2.6 Concluding remarks

This section gave an overview of the propagation model that was implemented in the auralisation tool. The propagation effects that were considered were implemented as signal processing operations. The model that was implemented could now be used to investigate how properties of the atmosphere, boundaries and the geometry, affect sound propagation.

After taking into account sound propagation an immission signal is obtained that already starts to sound like an aircraft. However, thus far a simple emission signal consisting of some noise and several harmonics was considered. The next section presents a method to obtain a more accurate airplane emission signal.

3.3 Backpropagation and emission synthesis

3.3.1 Introduction

The previous section treated the propagation model of the tool. In order to simulate the audible sound of aircraft an emission signal is needed. This section describes a method to create an emission signal from features derived from recordings. An auralisation or pseudo-recording at a receiver position can then be created by propagating the signal using the propagation model. Figure 3.8 shows a block diagram of the steps that are treated in this section.

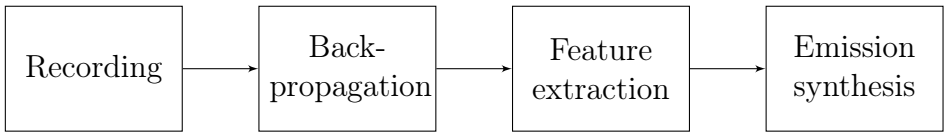

Figure 3.8: Block diagram of the backpropagation, synthesis and auralisation method.

For the emission synthesis a signal is generated that is based on measurements that were made for the sonAIR project as described in section 1.1.8. Figure 3.9 shows an overview of the airport, the trajectory and the receiver of the events considered. Aircraft took off and their height steadily increased from 30 to 260 meters.

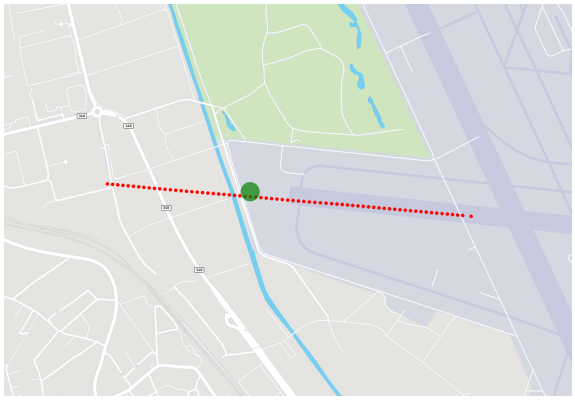

Figure 3.9: Overview of the airport, trajectory and the receiver. The receiver considered (green dot) is situated slightly north of the trajectory, almost straight underneath the trajectory.

3.3.2 Backpropagation

An automated procedure was developed to backpropagate from receiver to source in time-domain. The procedure assumes there is only one propagation path, the direct path, and that the aircraft can be considered a point source. As shown in Figure 3.10, the backpropagation algorithm undoes atmospheric attenuation, the Doppler shift, and geometrical spreading (magnitude) in that specific order, and using the methods as described in the previous section. Because only the direct path was

considered all parameters that were used in the backpropagation were based on values corresponding to that path.

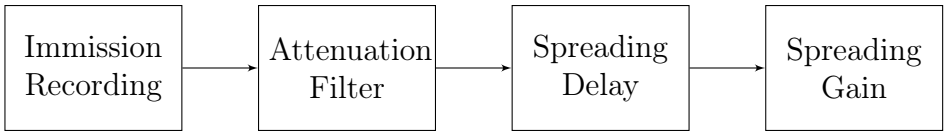

Figure 3.10: Block diagram of the backpropagation model. These steps are applied sequentially to a recording in order to obtain a signal in time-domain that corresponds to the emission of the aircraft.

Application of the backpropagation algorithm results in a time-domain signal that corresponds to the emission of the aircraft. The emission includes the effect of convective amplification, i.e., the directivity effects due to source motion.

The influence of the ground reflection is non-negligible. The backpropagation model does not undo the ground reflection because it was not expected that this would result in improved results due to the approximations that would have to be made. For example, let us assume two clear propagation paths exist. The immission consists of the contributions from each path. The propagation delays of each contribution are different. The contributions are therefore Doppler-shifted differently, and the contributions are generated at different emission times. Minor differences in emission may exist also due to the directivity. Furthermore, the reflection coefficient plays a large role and is only roughly known.

In order to account for the extra contribution, a correction is applied. A soft ground is still relatively hard and therefore a -3 dB correction was applied to the power of the features obtained in the next section. Ideally, a microphone on the ground was used, but the data set that was available consisted of recordings at a height of 4 meters.

Figure 3.11 shows a spectrogram of a recording. Clearly visible are the Doppler-shifted tones and the peaks due to atmospheric turbulence. The most powerful tone corresponds to the blade passing frequency of the fan. The other tones are Buzz-Saw tones.

Figure 3.12 shows a spectrogram of the recording after backpropagation. The signal after backpropagation is shorter than the recording due to lack of aircraft position information during the initial propagation delay. The Doppler-shift has mostly been removed. Aside from small variations, the tonal components remain constant in frequency over time. The variations are caused by uncertainties in the measured position of the aircraft and thus the estimated propagation delay. Artefacts like the mirror-effect and amplitude modulations due to atmospheric turbulence remain.

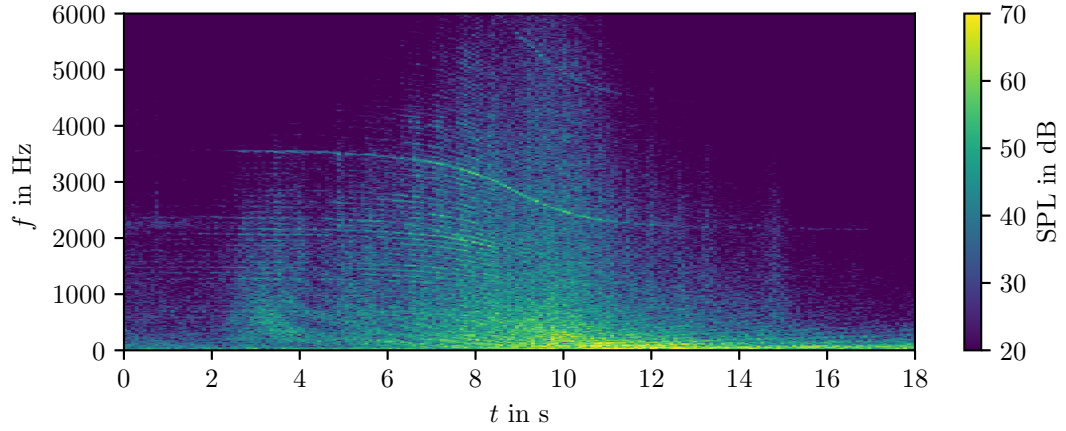

Figure 3.11: Spectrogram of a recording of an A320.

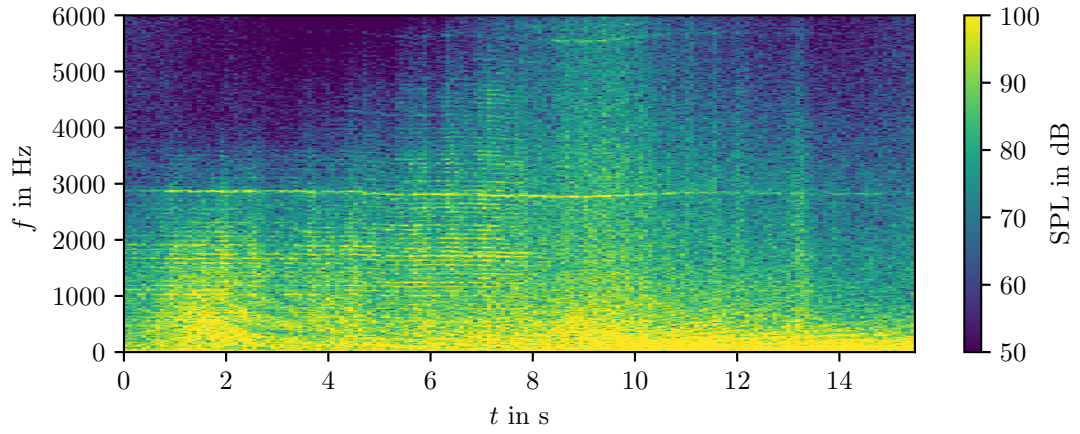

Figure 3.12: Spectrogram of the recording shown in Figure 3.11 after backpropagation to the source.

3.3.3 Feature extraction

Spectral modelling synthesis was chosen as emission synthesis strategy. With spectral modelling synthesis a signal is generated as a superposition of tones and bandpass-filtered noise. Therefore, a method is needed to extract from the backpropagated recordings the frequency, phase, and level of the tones, as well as the level of the noise as function of frequency. This section presents a method that was developed for extracting these features.

The situations considered are take-offs, and therefore the tonal components in the spectra are not only the blade passing frequency of the fan and its harmonics, but also “Buzz-Saw” tones. The common denominator of the frequencies of these components is the frequency at which the engine shaft rotates.

Motivation for method

The events considered are short, typically less than 30 seconds, and their spectra vary considerably over time due to directivity of the source. Thus, in order to get a sufficiently good directivity resolution, a high temporal resolution is needed, and that limits the possibility to average over time. The frequency resolution, however, also matters. The emission may contain Buzz-Saw harmonics with a fundamental frequency below 100 Hz. While that gives some freedom for using a lower frequency resolution, first the actual tonal components need to be detected and thus distinguished from the broadband noise.

While already corrected for in the backpropagation, the Doppler shift may make it difficult connecting obtained frequency-components at one step to those obtained the step later. Therefore, frequency-tracking algorithms were considered [83], notably Hidden Markov Models. Due to their complexity such solutions were not pursued further.

Tone-detection in the frequency-domain is in its simplest form a matter of peak detection for which a range of algorithms is known. However, a robust algorithm is needed that can distinguish between the tonal components and broadband noise peaks.

Initially, the complex cepstrum[2] was used to determine the fundamental frequency of the Buzz-Saw harmonics (Paper IV). The method was reliable for determining the fundamental frequency. Because all the tonal components considered are multiples of this fundamental frequency, all their frequencies would then be known as well. Unfortunately, the frequency-resolution, or more precisely the quefrency-resolution, was not high enough to reliably predict the frequency of the high-frequent components.

Tone-seeking algorithm

Annex C of ISO 1996-2:2007 [84] describes an objective method for assessing the audibility of tones in noise and a significant part of the method describes a tone-seeking algorithm. The tone-seeking algorithm works in frequency-domain on a narrowband power spectrum. An estimate of the narrowband spectrum is obtained using Welch's method. The time signal is split in chunks, a Hanning window is applied to each chunk, and a modified periodogram is determined for each chunk. Finally, linear averaging over the chunks results in Welch's estimate of the power spectral density.

In frequency-domain, the tone-seeking algorithm first determines noise pauses, which are local maxima with a probability of a tone. Noise pauses span multiple frequency lines, and their starts and ends can be found when the difference between two adjacent lines is larger than Δ dB, where Δ is the tone-seeking criterion. The next step is to assess whether tones exist in these noise pauses. Each frequency bin or line is assigned a label indicating whether it is part of a tone or whether it is masking noise.

[2]The complex cepstrum is defined as $c[n] = F^{-1}\left\{\log_{10}\left(F\left\{x[n]\right\}\right)\right\}$.

The power of the lines that are part of a tone are integrated. A correction is made for the masking noise contributions to those lines by estimating their contribution from a regression through the lines marked as noise within a portion of the critical band[3] around the centerfrequency of the tone. Furthermore, a 1.8 dB correction is applied as correction for the Hanning window.

Extension and modifications

The tone-seeking algorithm is capable of detecting many of the tonal components but not all of them. Therefore, the algorithm is modified and extended (Paper III). Because the tones of interest are all multiples of a fundamental frequency, the goal is to determine this fundamental frequency sufficiently accurate. The assumption was therefore made that all tones found by the tone-seeking algorithm from the standard were harmonics and that the fundamental frequency was within a specified range. The fundamental frequency is then given

$$f_0 = \gcd\left(f_1, f_2, \ldots, f_n\right) \tag{3.4}$$

where gcd is the *greatest common divisor*. Implementations of the gcd operator attempt to find an exact solution. Due to errors in the estimation of the frequency of the tones and because some tones are not harmonics, an exact solution does not exist. Given an initial estimate of the fundamental frequency, one could define an error as the sum of the squared deviation between the target order of the harmonics and the actual estimated order

$$e = \sum_{i=0}^{n} \left(\frac{f_i}{f_0} - \text{round}\left(\frac{f_i}{f_0}\right)\right)^2 \tag{3.5}$$

An estimate of the fundamental frequency is obtained by minimising this error.

According to the standard an A-weighted signal should be used. Because the frequencies of the tonal components are of interest, and not their audibleness, an unweighted signal is considered instead. Because at the start and the end of the signal the signal-to-noise is relatively low, the backpropagation algorithm may cause unwanted amplification of the background noise. Therefore, the signal was low-pass filtered with a 4^{th} order Butterworth low-pass filter with a cut-off frequency at 10 kHz. Furthermore, in order to obtain an accurate estimation an averaging-time of one minute is required, however, this could not be done as explained. Instead, two-second windows without overlap were used, and these windows were divided into 10 chunks in order to estimate a power spectrum with a resolution of about 5 Hz. A two-second window proved to be a good balance between temporal resolution and frequency resolution.

The tone-seeking algorithm is first ran with a tone-seeking criterion of 1 dB to detect tonal components and obtain their centerfrequencies. A fundamental frequency estimation is then done by minimising the error in equation (3.5). The next

[3] A critical band is the bandwidth of a filter created by the cochlea, the auditory part of the inner ear.

step is to determine the power of all harmonics. That was done by explicitly setting noise pauses for each of the harmonics, forcing the tone-seeking algorithm to determine tones. The noise-pause bandwidth was set to a value that was a function of the fundamental frequency f_0 in order to automatically scale. Because adjacent noise pauses should not overlap the bandwidth should be smaller than f_0. The noise pause bandwidth was set to $0.2f_0$ as this value appeared to work well for estimating the power of the "Buzz-Saw" harmonics. The level of the tones are then estimated as described by the standard.

The broadband noise or "masking noise" was integrated in $^1/_6$-octaves and a Hanning-window correction of 1.8 dB was applied. The -3dB bandwidth of the tones was recorded as well, although these values may be inaccurate due to the 5 Hz frequency-resolution. The bandwidth of the tonal components depends on various aspects, like frequency or phase modulations at the source or during propagation, e.g. due to atmospheric turbulence. The direct and reflected contribution are Doppler-shifted slightly differently and that causes either double peaks or a single broader peak. But also averaging time and window shape play a role.

3.3.4 Emission and immission synthesis

With the extracted features, which were obtained as function of time and at several receiver positions, it is possible to develop an emission model that takes into account directivity of the spectral components. Such emission model would then output input for the SMS synthesiser, and the created emission signal would be propagated to a receiver location.

An important question to ask is whether the described methodology of extracting features, synthesising an emission signal and propagating it would result in plausible auralisations. For example, it could be possible that the chosen synthesis strategy and features cannot reproduce certain characteristics in the sound. Therefore, the next chapter describes a comparison between auralisations and recordings with the auralisations based on recordings.

For a specific event and receiver, the immission was backpropagated and features were extracted. These features were used to re-synthesise the emission. The emission signal was propagated to the receiver, and a direct path and a single reflection were considered. The assumption was made that the emission is identical for the emission angles corresponding to direct and reflected path.

The feature extraction method provided frequencies and levels of tonal components as function of time. Variations in the frequencies as function of time could be observed, but with a two second window that would result in only few data points. Variations in frequency were therefore ignored and computed was an average value for the fundamental and each of the harmonics.

As mentioned in the previous section, values for the phase of the tones could not be obtained, and therefore values had to be chosen. Because the harmonics are "Buzz-Saw" noise, a phase corresponding to a sawtooth signal was initially assumed. Participants in a preliminary test found the simulations sound metallic compared to the recordings (Paper III). Therefore, the assumption was made that the initial

phase relation between the Buzz-Saw tones was entirely lost and could therefore be chosen randomly, in which case the probability distribution would likely be uniform as otherwise a certain initial phase would still be preferred.

Figure 3.13 shows a spectrogram of the emission synthesis. The level of the tonal components and the broadband noise varies over time. The blade passing frequency is not clearly visible. The feature extraction algorithm underestimated the levels of the blade passing frequency and its harmonics. As explained in 3.3.3 tones were searched for in noise pauses. These noise pauses were "created" after the fundamental frequency was determined. The bandwidth of these noise pauses was relatively small because they were tuned for the "Buzz-Saw" tones. An improvement would be to look in a larger noise pause bandwidth or bandwidth for these tonal components, however, that requires explicit knowledge of the amount of blades.

Figure 3.14 shows a spectrogram of the auralisation at the receiver. The Doppler-shifted tones and the mirror-effect are clearly visible. The Doppler-shifted tones are not very smooth. This is due to fluctuations in the measured aircraft position and a smoothing filter could reduce impact of these uncertainties.

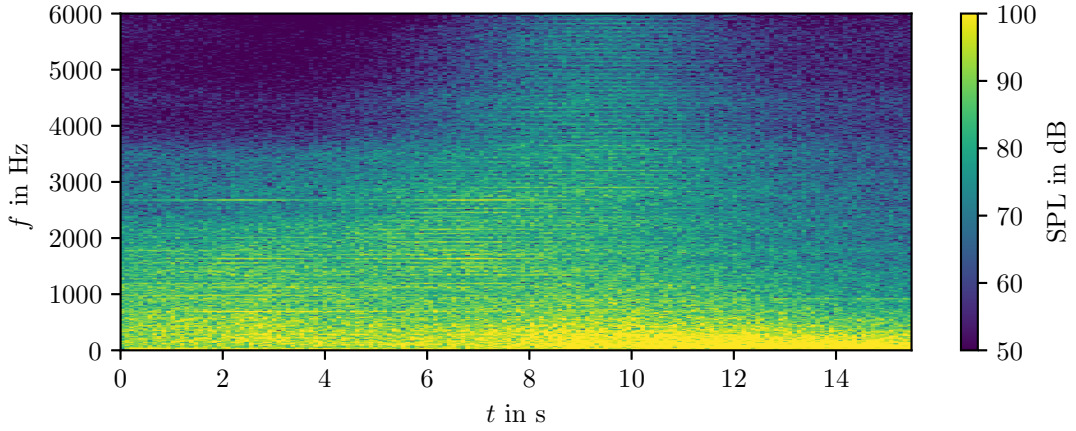

Figure 3.13: Emission synthesis of the aircraft. Inputs to the emission synthesiser were obtained by applying the feature-extraction algorithm to the signal shown in Figure 3.12.

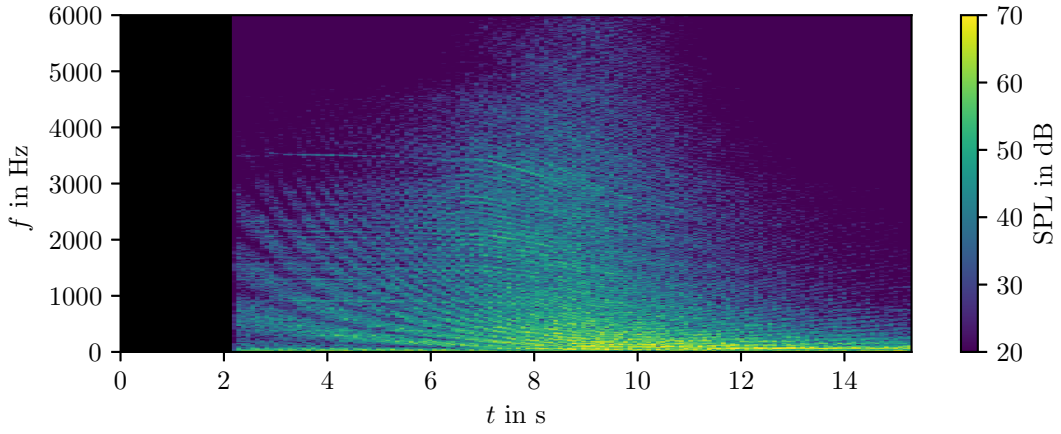

Figure 3.14: Auralisation of the event shown in Figure 3.11 .

Chapter 4

Subjective validation of auralisation method

4.1 Introduction

In the previous chapter an overview was given of the auralisation tool. A propagation model for aircraft sound was developed, as well as a method for obtaining features from recordings and creating auralisations using them. The purpose of determining the features is to use those features for the development of an emission model. The next step is to determine whether auralisations based on features obtained from the described approach actually sound plausible.

The purpose is to check whether the auralisations sound like an aircraft, and whether they sound like the aircraft model and event that is being simulated. The assumption is made that the propagation model represents the actual sound propagation sufficiently good that inaccuracies in sound propagation are negligible and the resulting differences are entirely due to the emission synthesis.

Perceptual validation

The question is then how to validate the plausibility of the auralisations. Comparing the overall and spectral sound pressure level as function of time could be a first simple test to determine whether the signal power is approximately correct. Signals with the same power may however still sound very different, and how they sound may depend on a multitude of factors. Factors can be properties of the sound, but also of the listener, or the environment.

Psychoacoustic measures describe how a sound is perceived by most listeners and can therefore be used to characterise a sound. Many measures exist, but not all measures are applicable to all sounds and care should therefore be taken when choosing measures. Examples of common measures are loudness, roughness and sharpness. Instead of using measures, participants could be asked to rate whether an auralisation sounds plausible. That would likely require a reference sound, e.g. a recording.

Regardless of the method a variability exists in events that are considered alike.

For example, consider events that are all landings of a certain aircraft type and with certain engines, and under meteorological conditions within a narrowly defined range. In one event the pilot may vary the thrust differently than in another event and that could already lead to audible differences. Clearly, the variance across events should be accounted for.

Past work

Several validations of auralisations have been done in the past. Maillard conducted a quantitative and perceptual validation of road traffic auralisations that were created using granular synthesis [85]. Pieren and Heutschi conducted a listening test to validate auralisations of wind turbines. Participants were presented with recordings and auralisations and had to choose for each stimuli whether they thought it was a recording, an auralisation, or whether they could not tell. Hoffmann combined a tyre-noise prediction model with a car auralisation tool, and tested the perceptual validity of the produced auralisations [29, 30]. Tests were done with semantic differentials using a categorical scale, and another test done was a paired comparison test.

A semantic differential is a set of semantic scales. Each scale is typically defined by a bipolar combination of adjectives, e.g. "loud-silent", and divided into steps. A categorical scale is similar, however, instead of a bipolar combination of adjectives with steps a single adjective is used with steps. An example is "agree-disagree", where each word is placed at opposite ends of the scale. A paired comparison test is a type of test that can be used to rank the items that are tested with respect to the attribute that is investigated.

Another interesting type of test is MUSHRA, short for MUltiple Stimuli with Hidden Reference and Anchor. The method is typically used to evaluate the perceived quality of the output from lossy audio compression algorithms, but was used by Southern to rate the plausibility of auralisations of car pass-by's [86].

Test overview

This chapter describes a listening test that was conducted. The purpose of the listening test was to check the plausibility or perceptual validity of the auralisations and a comparison was therefore made between recordings and auralisations.

The hypothesis is that *recordings and auralisations of aircraft of the same type and under similar conditions are samples of the same group.* Audible differences are likely to occur and are also acceptable, because even among recordings of the same aircraft type there are audible differences.

Psychoacoustic measures were not measured. Instead, an overall similarity between stimuli was determined by letting participants rate how similar they found two sounds to be, where similar is defined as entities that are alike or have characteristics in common.

Recordings were compared not only with auralisations, but also with other recordings, and similarly, auralisations with other auralisations. Each of these comparisons can be considered a group. If the hypothesis is valid, then the distribution

of the group with comparisons between recordings and auralisations, should be the same as the other two distributions.

4.2 Method

The goal of the listening test was to determine whether the auralisations sound similar to the recordings they were based on. Participants were presented with pairs of stimuli and asked to rate how similar they sounded, overall.

Eight different sounds were considered and they were each 12 seconds long. The sounds include the approach of an aircraft, its fly-over and its distancing. Because the character of the sounds varies considerably over time, they were each split into parts of four seconds, corresponding to the approach, fly-over and distancing. The listening test was also divided in these three parts. First, participants were presented to all approach stimuli, then all fly-over stimuli and finally all distancing stimuli. In each test part all stimuli combinations were considered. Therefore, each part consisted of 28 pairs of stimuli of four seconds.

Of the eight sounds four were recordings, and four were auralisations. The recordings were randomly chosen from the sonAIR data set. Each auralisation was based on one of the recordings. Two aircraft types were considered, an A320 and a RJ1H, as well as two events per aircraft type. Fade in and fade out was applied to the stimuli. The signals were mono and presented with headphones. Head-related transfer functions were not included.

Similarity is relative, and therefore an anchor is typically used. For each part, participants were first given the set of stimuli, in order to become familiar with the type of sounds and the spread in the sounds of that part, and then continued with rating the pairs. The rating was done on an eleven point Likert scale. The left side of the scale said “not so much” and the right side “very much”. The scale was not numbered. The order of the stimuli was randomised for each test and each part.

Figures 4.1 and 4.2 show spectrograms of some of the stimuli that were used. The blade passing frequency and harmonics are not as prominent in the auralisation as they are in the recording. The approach-part of the auralisation spectrogram shows a part where the signal was zero and this is due to the initial propagation delay. This was supposedly accounted for by creating longer auralisations and then selecting the part where there was signal, but judging from the spectrogram and inspection of the audio files, an error was made. This was noticed only after the listening tests. The errors are 0.15 and 0.35 seconds in the case of the RJ1H samples, and 0.65 and 0.75 seconds in case of the A320 samples.

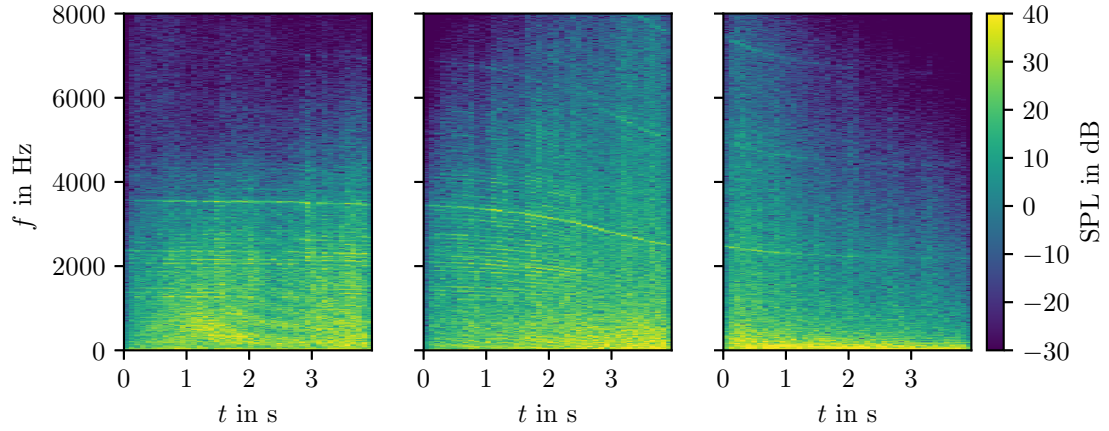

Figure 4.1: Spectrograms of the approach, fly-over and distancing parts of a recording of an A320.

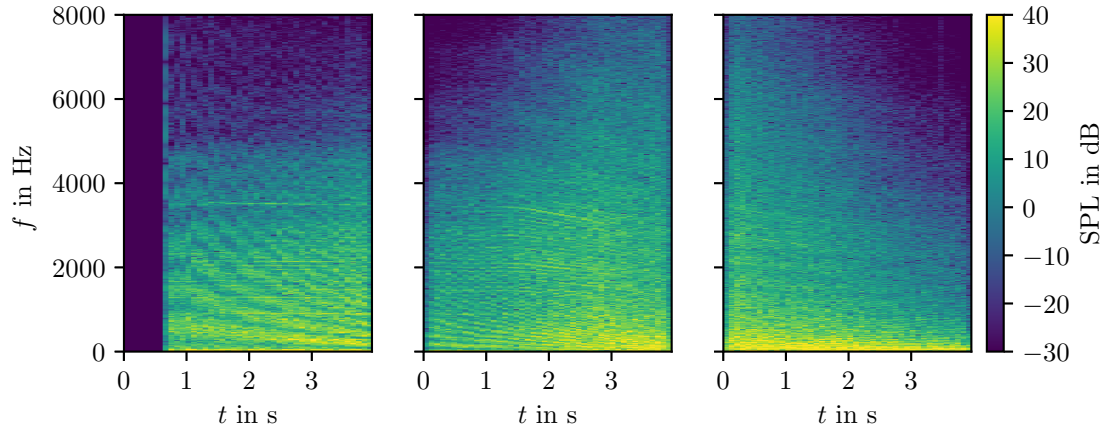

Figure 4.2: Spectrograms of the approach, fly-over and distancing parts of an auralisation of an A320.

4.3 Results

The results of the participants were scaled linearly from 0 to 1 with 0 corresponding to "not so much" and 1 corresponding to "very much". There were 17 participants, all graduate students, and of which the majority studied acoustics. The results that are shown are obtained after joining the data of all participants. The listening test data can be found at [87] and the raw results along with a brief analysis at [88].

Table 4.3 shows the sample mean μ, sample standard deviation σ and amount of samples n per group. Averaging was done over participants. Table 4.1 is similar, with averaging done over the three test parts as well. Table 4.2 is like Table 4.1, however, with all approach parts excluded. Because participants are a sample of the actual population, $n-1$ degrees of freedom were considered for the computation of the standard deviation and the standard error of the mean $\sigma/\sqrt{n}$.

The following figures show per group a normalised histogram and a kernel density estimation[1]. A Gaussian kernel was used. In Figure 4.3 averaging is done over all participants and all parts. In Figure 4.4 averaging is done over all participants, as well as the the fly-over and distancing parts. Figures 4.5, 4.6 and 4.7 consider the approach, fly-over and distancing separately. In these figures averaging is done only over participants.

Participants mentioned they noted larger differences at especially the approach of the events and the distancing. A common answer to the question how many different aircraft they heard was "two or three". Occasionally, the answer would start at "two" but go to "two or more" after they were told they were listening to not only recordings but also simulations. Some participants were surprised when told that simulations were included, others said they had thought so, and a few of the participants were already aware the test was possibly going to contain simulations.

[1] A kernel density estimation can be seen as a continuous version of a histogram. Each sample is replaced by a kernel function centred at the value of the sample. The curves are then summed to obtain a density and finally normalised so that the area under the resulting curve is 1.

Table 4.1: The mean value μ, standard deviation σ and amount of samples n per aircraft type combination, and stimuli type combination. Averaging was done over participants and parts.

kind	aircraft	μ	σ	n	SE
rec, rec	A320, A320	0.75	0.25	51	0.03
	A320, RJ1H	0.43	0.24	204	0.01
	RJ1H, RJ1H	0.68	0.23	51	0.02
rec, sim	A320, A320	0.50	0.26	203	0.01
	A320, RJ1H	0.33	0.23	407	0.01
	RJ1H, RJ1H	0.48	0.25	204	0.01
sim, sim	A320, A320	0.69	0.24	51	0.03
	A320, RJ1H	0.55	0.26	204	0.01
	RJ1H, RJ1H	0.73	0.24	51	0.03

Table 4.2: The mean value μ, standard deviation σ and amount of samples n per aircraft type combination, and stimuli type combination. Averaging was done over participants and parts, *excluding the approach parts.*

kind	aircraft	μ	σ	n	SE
rec, rec	A320, A320	0.80	0.21	34	0.03
	A320, RJ1H	0.43	0.24	136	0.02
	RJ1H, RJ1H	0.69	0.24	34	0.03
rec, sim	A320, A320	0.54	0.25	135	0.02
	A320, RJ1H	0.36	0.23	272	0.01
	RJ1H, RJ1H	0.52	0.26	136	0.02
sim, sim	A320, A320	0.71	0.24	34	0.03
	A320, RJ1H	0.54	0.26	136	0.02
	RJ1H, RJ1H	0.74	0.25	34	0.03

Table 4.3: The mean value μ, standard deviation σ and amount of samples n per test part, aircraft type combination, and stimuli type combination. Averaging was done over participants.

part	kind	aircraft	μ	σ	n	SE
approach	rec, rec	A320, A320	0.66	0.28	17	0.05
		A320, RJ1H	0.44	0.26	68	0.02
		RJ1H, RJ1H	0.64	0.22	17	0.04
	rec, sim	A320, A320	0.42	0.28	68	0.03
		A320, RJ1H	0.29	0.24	135	0.02
		RJ1H, RJ1H	0.41	0.23	68	0.02
	sim, sim	A320, A320	0.65	0.26	17	0.05
		A320, RJ1H	0.58	0.27	68	0.02
		RJ1H, RJ1H	0.72	0.22	17	0.04
distancing	rec, rec	A320, A320	0.89	0.09	17	0.02
		A320, RJ1H	0.40	0.23	68	0.02
		RJ1H, RJ1H	0.71	0.20	17	0.04
	rec, sim	A320, A320	0.54	0.24	67	0.02
		A320, RJ1H	0.35	0.22	136	0.01
		RJ1H, RJ1H	0.60	0.24	68	0.02
	sim, sim	A320, A320	0.68	0.27	17	0.05
		A320, RJ1H	0.52	0.25	68	0.02
		RJ1H, RJ1H	0.74	0.27	17	0.05
fly-over	rec, rec	A320, A320	0.72	0.27	17	0.05
		A320, RJ1H	0.45	0.24	68	0.02
		RJ1H, RJ1H	0.68	0.28	17	0.05
	rec, sim	A320, A320	0.53	0.26	68	0.02
		A320, RJ1H	0.36	0.24	136	0.02
		RJ1H, RJ1H	0.43	0.25	68	0.02
	sim, sim	A320, A320	0.73	0.21	17	0.04
		A320, RJ1H	0.56	0.27	68	0.02
		RJ1H, RJ1H	0.73	0.24	17	0.04

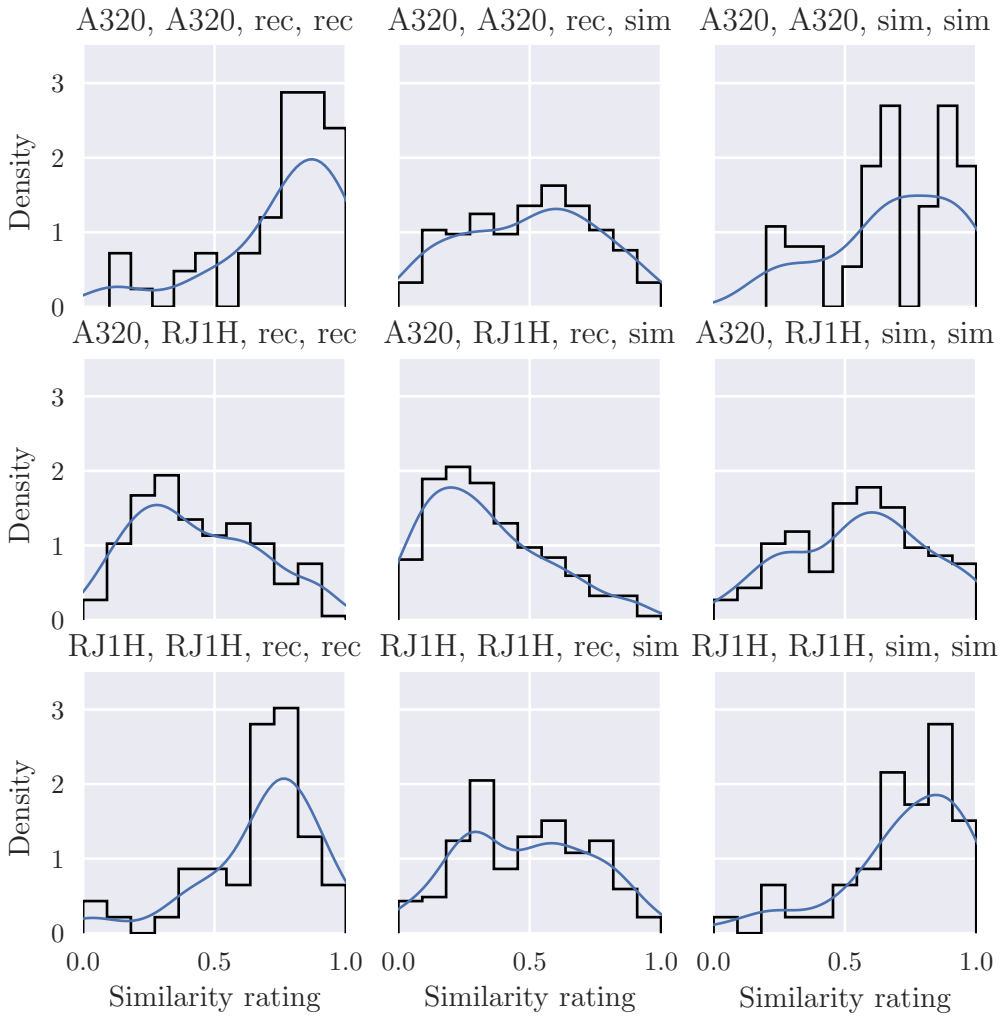

Figure 4.3: Normalised histogram and kernel density estimate per group. Averaging was done over all participants, and all parts.

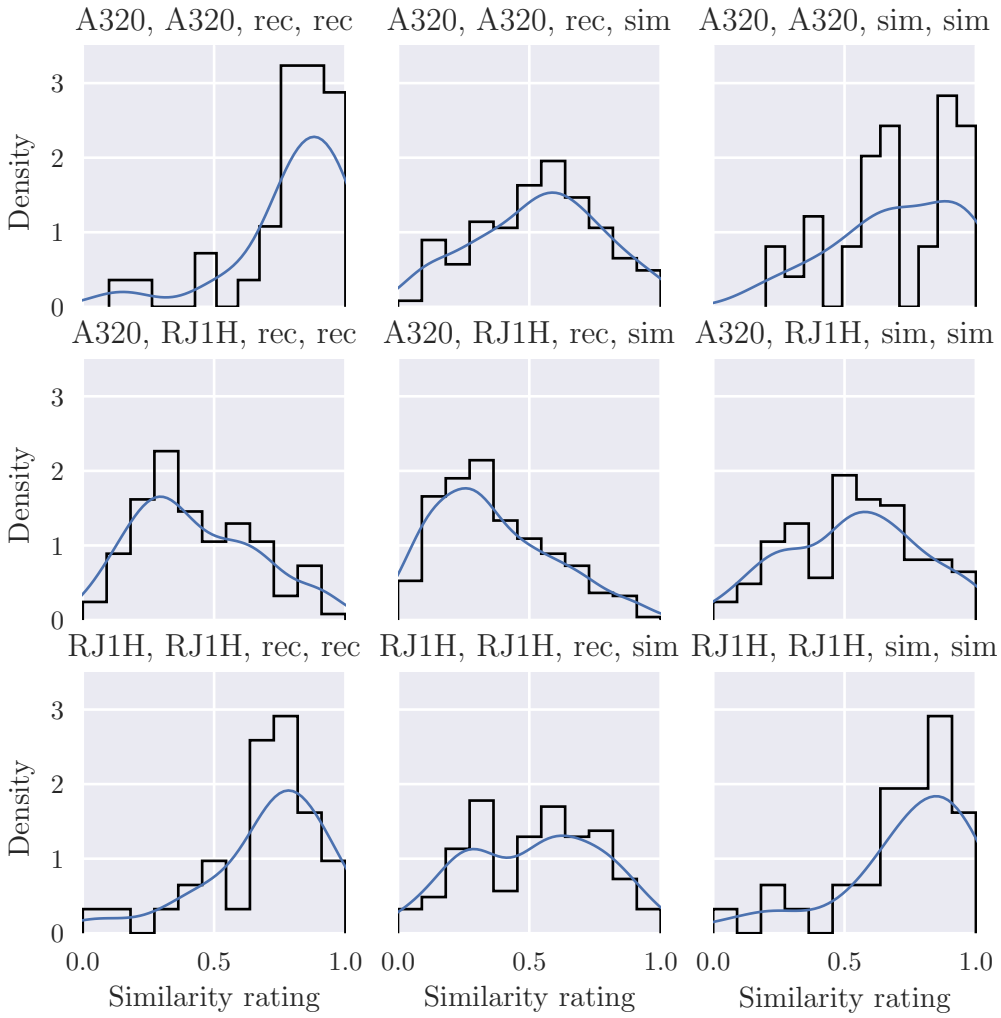

Figure 4.4: Normalised histogram and kernel density estimate per group. Averaging was done over all participants, and the fly-over and distancing parts.

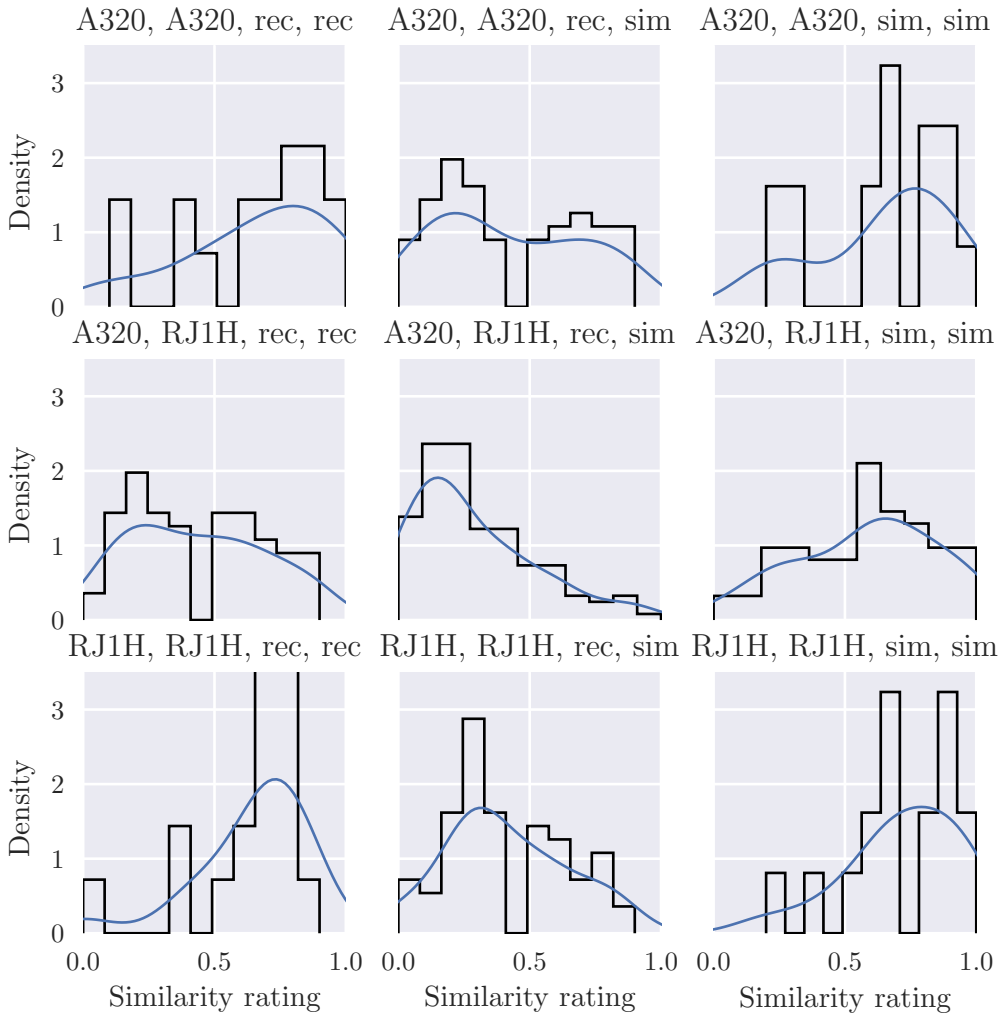

Figure 4.5: Normalised histogram and kernel density estimate per group for the approach part. Averaging was done over all participants.

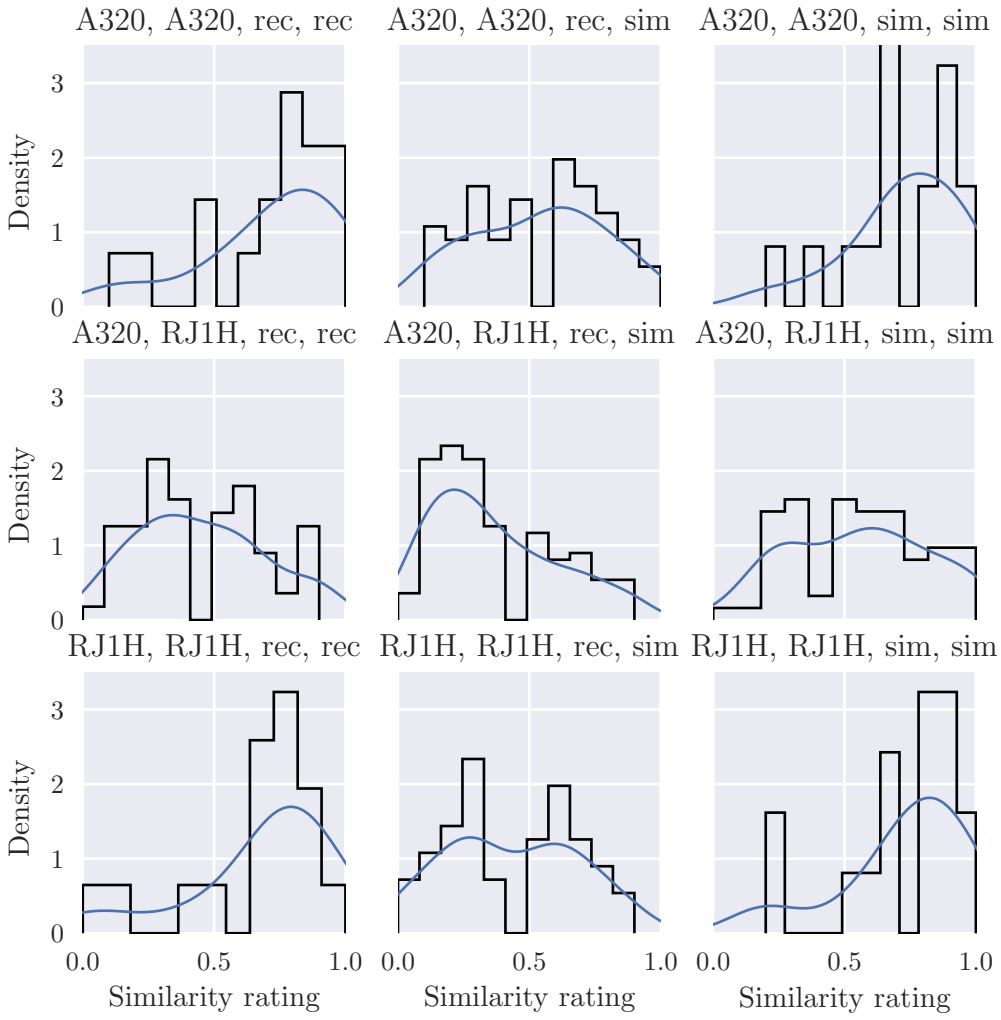

Figure 4.6: Normalised histogram and kernel density estimate per group for the fly-over part. Averaging was done over all participants.

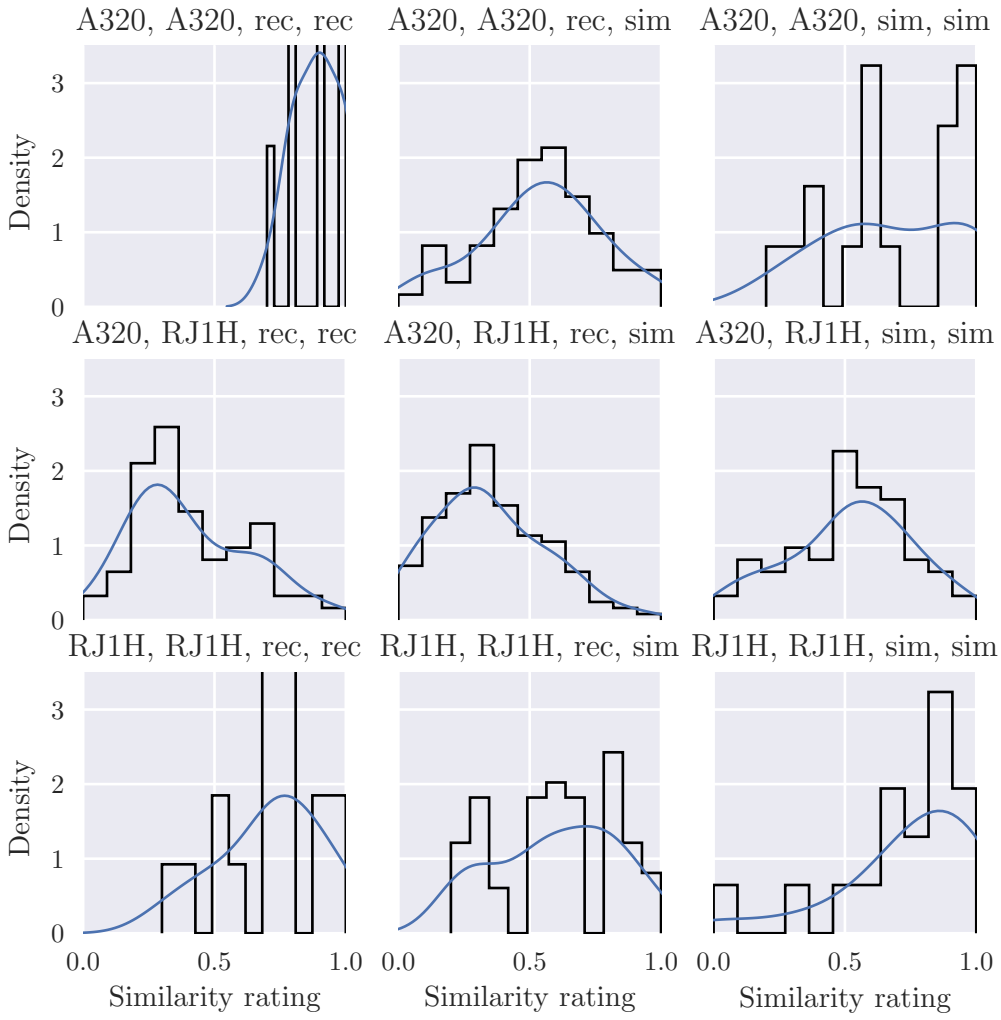

Figure 4.7: Normalised histogram and kernel density estimate per group for the distancing part. Averaging was done over all participants.

4.4 Discussion

Consider tables 4.1 and 4.2. In both tables the sample standard deviations are around 0.25. The spread in the mean within the tables is large, but the difference in mean values between the two tables is small. While the largest difference is 0.05, which is about two standard errors, for the majority of groups the difference is about one standard error.

Table 4.3 does not average over the three parts. Again, the standard deviation of the groups is mostly around 0.25, although a notable exception is the group in which two recordings of A320's were compared. The standard deviation is only 0.09 and the mean 0.89. Comparing that with the other groups, implies the two recordings this group consists of are relatively closer to each other than those in other groups. The standard deviation of the approach groups with the faulty auralisations is similar as that of the other groups.

The highest mean values are achieved when comparing similar aircraft types, regardless of whether the stimuli were recordings or auralisations. However, when comparing a recording with an auralisation the mean value is lower. The mean values of the groups comparing recordings and auralisations are systematically below those of the groups comparing recordings or auralisations. That would imply the hypothesis that "recordings and auralisations of aircraft of the same type and under similar conditions are samples of the same group" is not true.

Figures 4.3 and 4.4 show normalised histograms and kernel density estimates. The difference between the two figures is that the latter does not include approach samples. No notable differences can be observed in the figures, implying the approach samples are "average".

The similarity rating is a value given by participants after performing a comparison of two items, and comparing them on whichever aspects they choose to consider. Therefore, it is likely that the distributions are Gaussian. However, the ratings could only be given on a limited range and that may skew the distributions. In most cases the distributions do not appear to follow a Gaussian curve.

The recordings of the A320's (top-left) are judged to be very similar to each other, and the recordings of the RJ1H's (bottom-left) as quite similar to each other as well although slightly less. The A320's are not rated as very similar to the RJ1H's (centre-left) and therefore it appears that the participants can discriminate between the two aircraft types. For the auralisations, the results are similar in case of the A320's (top-right) and the RJ1H's (bottom-right), although less convincing. Furthermore, in this case the dissimilarity between the A320's and the RJ1H's isn't as large (centre-right). In fact, this distribution is relatively closer to the other two distributions than is the case with the recordings, implying the auralisations, regardless of aircraft type, all sound more alike. That is, they all sound more like another aircraft type.

Were the hypothesis valid, then the curves in the top would have to overlap, and the curves in the bottom as well. While the distributions of the groups that compare auralisations are quite similar to the distributions comparing recordings, they are not similar to the groups comparing auralisations with recordings. That

would again imply the hypothesis is not true and that the auralisations may appear to be different types of aircraft.

Figures 4.5, 4.6 and 4.7 show similar curves but per test part. Aside from the A320 distancing recordings that were mentioned before, there do not appear to be significant differences between the parts. In case of the RJ1H the distancing stimuli seem to be relatively close to each other.

The participants mentioned relatively larger differences in the stimuli that correspond to the approach of the aircraft (approach stimuli). During the approach the tonal components are clearly audible compared to other parts of the events due to the directivity. The feature-extraction algorithm was known to underestimate the power and bandwidth of the blade passing frequency and its harmonics because the algorithm was tuned for the Buzz-Saw tones. Therefore, a likely explanation is that this underestimation of power and bandwidth is causing audible differences between recordings and auralisations. Another cause could be the initial delay error.

The author noticed after the listening test that the initial phase of the tones was Gaussian distributed instead of uniform (see section 3.3.4) resulting in a most probable zero degrees initial phase for all tonal components. That may affect how the sound is perceived.

The listening test considered only two events per aircraft type. In order to correctly represent the spread that exists in recordings of a certain group, in this case, an aircraft type. Future tests should therefore consider more events and investigate the spread that already exists in the similarity between recordings. Increasing the test size would, however, significantly increase the test size, which is the reason only two events per aircraft type were considered.

Chapter 5

Propagation in a turbulent atmosphere

5.1 Introduction

Spatial and temporal variations in the atmosphere affect sound propagation and can cause audible modulations. Because they can be clearly audible it is presumed that including scintillations in auralisations increases their perceived realism. The multiple scattering affects the phase of the signal as well as the log-amplitude. In previous work a coherence factor was introduced that would account for coherence loss due to phase modulations [35, 54, 55]. Fluctuations due to turbulence have also been included in auralisations by simulating the amplitude modulations that were observed in measurements [33, 89].

This chapter describes a method, published in Paper I, for generating sequences of scintillations and including them in auralisations. The method considers line-of-sight propagation through a weakly turbulent atmosphere. Novel in this field, the method includes both log-amplitude and phase fluctuations. The presented method is based on [64] where it was used to predict the performance of wireless communication links, and [90] where it was used to determine the influence of turbulence on the performance of a barrier. An early version of the method was discussed in Papers V and VI. Furthermore, the method was implemented in the NAF[91].

5.2 Coherence loss factor

Before presenting the new method let us consider an existing method that was mentioned in the introduction. Arntzen developed a method to include coherence loss [35, 55], and the method considers a coherence factor T_c, first described by Clifford and Lataitis [92], as well as a reciprocal filter R_c. Consider a typically scenario of a direct path and ground-reflected path. The sound pressure at the receiver is given by

$$p = \frac{A_d}{r_d} e^{jkr_d} + Q \frac{A_r}{r_r} e^{jkr_r} \tag{5.1}$$

where A is an amplitude, r a path length, $Q = |Q| \exp(j\phi)$ a reflection factor (in the referred work the spherical reflection factor), and the indices d and r are used to represent respectively the direct and reflected paths. Note the amplitude can be different for each path to account for source directivity. The effective pressure squared, as used for computing a sound pressure level, is

$$p_e^2 = \frac{A_d^2}{2r_d^2} + |Q|^2 \frac{A_r^2}{2r_r^2} + 2|Q| \frac{A_d A_r}{r_d r_r} \cos\left(k\left(r_r - r_d\right) + \phi\right) \tag{5.2}$$

The sum of the first and second term is an incoherent addition of the direct and ground-reflected contributions. The third term on the right-hand side considers the interference between the direct and reflected paths.

Clifford and Lataitis considered atmospheric turbulence in a line-of-sight propagation situation and accounted for complex phase perturbations, i.e. log-amplitude and phase, for each propagation path. They introduced a coherence factor T_c in the third term to include additional coherence loss due to atmospheric turbulence in line-of-sight propagation

$$p_e^2 = \frac{A_d^2}{2r_d^2} + |Q|^2 \frac{A_r^2}{2r_r^2} + 2|Q| T_c \frac{A_d A_r}{r_d r_r} \cos\left(k\left(r_r - r_d\right) + \phi\right) \tag{5.3}$$

The factor ranges from zero to one and can nullify interference. Assuming a spherical wave front and a Gaussian turbulence spectrum, the coherence factor is given by

$$T_c = e^{-\sigma_S^2 (1 - C_{sp})} \tag{5.4}$$

where C_{sp} is the correlation function of the fluctuations (equation (2.56), and σ^2 the variance of the fluctuations. According to Clifford the variance is the sum of the direct and reflected path wave variances and accounts for both log-amplitude and phase fluctuations [92]. This value is then twice the variance given by equation 2.55. Arntzen considered only phase variances and took half this value. The correlation is a function of the spatial separation ρ perpendicular to the wave propagation direction which in this case was derived as

$$\frac{1}{\rho} = \frac{1}{2}\left(\frac{1}{h_s} + \frac{1}{h_r}\right) \tag{5.5}$$

where h_d and h_r are respectively the source and receiver height.

The interference term is implicitly included in auralisations. Therefore, Arntzen included T_c as a filter for the ground-reflected path and introduced another reciprocal filter R_c.

$$p = R_c \frac{A_d}{r_d} e^{j(kr_d)} + Q T_c \frac{A_r}{r_r} e^{j(kr_r)} \tag{5.6}$$

The magnitude-response of the reciprocal filter is given by

$$R_c = -|Q| T_c + \sqrt{|Q|^2 + 2|Q| T_c + 1} \tag{5.7}$$

and is needed because the ground-reflected wave would be lost in case T_c approached zero, which will happen with strong turbulence, i.e., high values of σ_S^2.

A qualitative validation showed that the model indeed results in audible and predictable coherence loss, reducing the rasping sound due to interference that was otherwise clearly audible, and thereby increasing the perceptual validity.

5.3 Generating sequences of scintillations

Atmospheric turbulence is known to result in not only coherence loss but also in audible amplitude modulations. We shall therefore now explore a new method that also includes audible amplitude modulations. Whereas the method from the previous section modified the magnitude of the coherent part to increase coherence loss, the method proposed in this section generates sequences of log-amplitude and phase fluctuations and applies these to each propagation path.

5.3.1 Space-to-time conversion

Consider again a line-of-sight situation where d is the distance between a source and a receiver pair along the wave propagation direction, and ρ the spatial separation of the receivers transverse to the wave propagation direction. Still assuming Taylor's hypothesis regarding frozen turbulence, we can perform a space-to-time conversion of the correlation and covariance functions to obtain $C(\tau)$ and $B(\tau)$ respectively. The turbulence correlation time is given by

$$\tau_0 = \frac{L}{v_\perp} \tag{5.8}$$

and the transverse time lag by

$$\tau = \frac{\rho}{v_\perp} \tag{5.9}$$

where $v_\perp$ is the transverse speed, corresponding to e.g. the mean speed at which the field is carried by the wind transverse to the wave propagation direction.

In this chapter the covariance for spherical waves and a Gaussian spectrum is considered for the same reason it was used in the other method: the Gaussian spectrum is the simplest model to work with and computationally least demanding. The method can also be used with covariance functions that describe other turbulence spectra, like e.g. the Von Karman spectrum [93].

5.3.2 Propagation in the turbulent atmosphere as a multichannel

The fluctuations in the atmosphere are temporal and/or spatial. Therefore, to model sound propagation of a signal $x(t)$ through such an atmosphere a time-varying channel is necessary. The received signal $y(t)$ consists of a line-of-sight contribution and additional contributions from scattering, together forming a multichannel [64]. Ignoring beam spreading, this can be written as

$$y(t) = \sum_n \alpha_{sc_n}(t) x(t - \tau_n(t)) \tag{5.10}$$

where $\alpha_{sc_n}(t)$ is the time-varying scintillation sequence representing the effect of the pressure fluctuations on the nth-multipath component, and τ_n the propagation delay of the nth component relative to the propagation delay in an undisturbed

atmosphere. Assuming the spread in propagation delay over the channels is small compared to the inverse of the signal bandwidth, so that $x(t-\tau_n) \approx x(t-\tau(t))$, then

$$y(t) = x(t-\tau(t)) \sum_n \alpha_{sc_n}(t) \tag{5.11}$$

Because the attenuation is very similar for the different multipaths, we can write that

$$y(t) = x(t-\tau(t))\alpha_{sc}(t) \tag{5.12}$$

Therefore, the received signal is obtained by shifting the emitted signal $x(t)$ with a time-varying propagation delay $\tau(t)$, and multiplying the result with a time-varying gain $\alpha_{sc}(t)$.

5.3.3 Design of scintillation sequence

We will now design a sequence of scintillations and for that we need to know the statistical distribution and power spectral density $|H_B(f)|^2$ of the desired sequence. As mentioned before the fluctuations are Gaussian-distributed. We can therefore generate a sequence with the correct distribution and power spectral density by convolving a random unit variance Gaussian signal $z(t)$ with the impulse response $h_B(t)$ of the designed filter.

$$\chi(t) = S(t) = (h_B * z)(t) \tag{5.13}$$

The power spectral density $|H_B(f)|^2$ of a random sequence forms a Fourier pair with its autocorrelation function $R(\tau)$ through the Wiener-Khinchin theorem[1]. Assuming $R(\tau) \cong B_\chi(\tau) = B_S(\tau)$, the power spectral density of χ and S is

$$|H_B(f)|^2 = \int_{-\infty}^{\infty} B(\tau) \exp(-j\omega\tau) \mathrm{d}\tau \tag{5.14}$$

This filter has zero phase and is non-causal. To create a causal filter with constant group delay α we can shift the peak in the impulse response by adding a linear-phase factor corresponding to 90 degrees

$$H_B(f) = |H_B(f)| \cdot \exp(-j2\pi f\alpha) \tag{5.15}$$

The impulse response of the filter is finally obtained through the Inverse Fourier Transform

$$h_B(t) = \int_{-\infty}^{\infty} H_B(f) \exp(+j\omega\tau) \mathrm{d}\tau \tag{5.16}$$

[1]The Wiener-Khinchin theorem states that the autocorrelation function of a wide-sense-stationary random process has a spectral decomposition given by the power spectrum of that process.

5.3.4 Discrete time

We now convert from continuous to discrete time

$$H_B[k] = H_B(e^{j\omega}), \quad 0 \leq k \leq N-1, \quad \omega = \frac{2\pi k}{N} \tag{5.17}$$

The linear-phase factor $\exp(-j2\pi f\alpha)$ is then given by

$$\exp\left\{-j2\pi k \frac{M_1}{2}\frac{f_s}{N}\right\} \tag{5.18}$$

where M_1 is the length of the desired impulse response. The frequency response of the filter is

$$H_B[k] = \sqrt{F\{B[n]\}}\exp\left\{-j2\pi k \frac{M_1}{2}\frac{f_s}{N}\right\}, \quad 0 \leq k \leq N/2 \tag{5.19}$$

where $F\{\}$ is the Discrete Fourier Transform (DFT). The desired impulse response is real-valued. Therefore, we have because of Hermitian symmetry

$$\begin{aligned} H_B[k] &= H_B(e^{j\omega}), && 0 \leq k \leq N/2, \quad \omega = \frac{2\pi k}{N} \\ H_B[N-k] &= H_B^*[k], && 1 \leq k \leq N/2 - 1 \end{aligned} \tag{5.20}$$

In fact, because both $B[n]$ and $|H_B[k]|$ are real and even, one can use the type-1 Discrete Cosine Transform (DCT) instead of the DFT in equation (5.19). The impulse response of the filter is obtained by taking the Inverse Discrete Fourier Transform (IDFT)

$$\begin{aligned} h_B[n] &= F^{-1}\{H_B[k]\} \\ &= F^{-1}\left\{\sqrt{F\{B[n]\}}\exp\left\{-j2\pi \frac{M_1}{2}k\frac{f_s}{N}\right\}\right\} \end{aligned} \tag{5.21}$$

Scintillations are finally obtained through the convolution of the impulse response $h_B[n]$ with Gaussian white noise $z[n]$

$$\chi[n] = S[n] = (z * h_B)[n] \tag{5.22}$$

The first $M_1/2$ samples would have to be dropped because of the filter delay. A block diagram of the steps is shown in Figure 5.1.

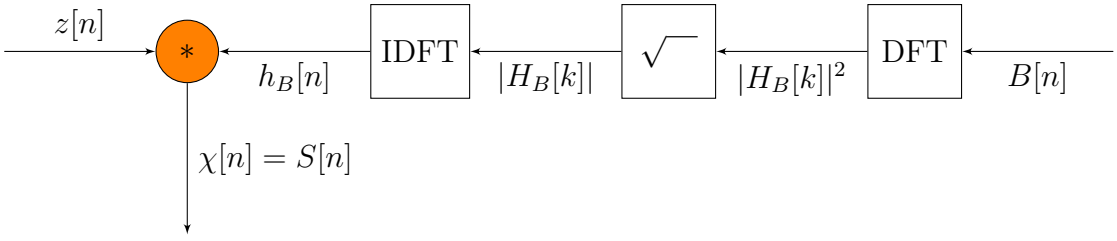

Figure 5.1: Block diagram of signal processing steps for generating scintillations. Gaussian white noise $z[n]$ is convolved with an impulse response $h_B[n]$ which is based on the covariance $B[n]$ of the turbulence spectrum.

5.3.5 Apply scintillations to signal

Now that we can generate sequences of fluctuations, we need to apply these to a carrier signal $x(t)$ or $x[n]$. According to equation (5.12) the log-amplitude fluctuations can be applied in a multiplicative manner, which is indeed the case of a signal with a sufficiently small bandwidth, like for example a monochromatic signal. However, the variance of the fluctuations is frequency-dependent, and since in practice broadband signals are commonly used, a method is sought for applying the fluctuations to a broadband signal.

One possible method would be to decompose the input signal in complex exponentials with the Inverse Discrete Fourier Transform, and apply per complex exponential the log-amplitude and phase fluctuations which, when combined, can be written as a complex exponential ψ as shown in equations (2.51) and (2.52).

A computationally less demanding method is to instead filter the carrier signal with multiple band-pass filters, and proceed with applying fluctuations to each of the band-pass filtered signals and combining the resulting signals. Scintillations would be computed for the center frequencies of the bands. The amplitude fluctuations could be applied through multiplication and the phase fluctuations could be converted to time-delay fluctuations (see equation (5.25)) and applied with a Variable Delay Line.

5.3.6 Scintillations as time-variant filter

A more efficient method to take into account the frequency-dependence of the scintillations, would be to instead convolve the carrier signal with a time-variant filter that is updated fast enough to represent the fluctuations.

The fluctuations χ and S, at each time step computed for M_2 frequencies, can be merged into a complex phase (see equation (2.52))

$$\psi[n] = \exp\left(\chi[n] + jS[n]\right) \tag{5.23}$$

Adding a linear-phase factor as was done with $h_B[n]$ and taking the Inverse Discrete Fourier Transform will result in an impulse response for every instance in time n. Convolution of the carrier signal $x[n]$ with this time-variant filter will result in a log-amplitude and phase modulated signal. The first $M_2/2$ samples will have to be dropped to correct for the filter delay.

Because the fluctuations are relatively low-frequent they can be sampled at a much lower sample frequency than the carrier signal. For a correlation length L of 10 meters and a transverse speed $v_\perp$ of 2 meters per second the correlation time would be 5 seconds. If we would sample the sequence of fluctuations at 5 times the maximum bandwidth of the filter, which is proportional to the inverse of the correlation time τ_0,

$$f_s = 5/\tau_0 \tag{5.24}$$

the required sample frequency would be 1 hertz.

In practice one might want to interpolate the impulse response as it changes over time, but because the phase also changes with time this can be problematic. Aside

from converting to a minimum-phase representation[2] we can also create a linear-phase filter for which the magnitude changes with time but the phase does not. If the phase fluctuations are linear-phase, then they can be applied to the carrier signal $x[n]$ with a Variable Delay Line. In the Gaussian model the phase fluctuations scale as $\sigma_S^2 \sim f^2$. A scatterer affects all frequencies, and therefore the fluctuations of different frequencies move together, resulting in a linear-phase. We therefore write the phase fluctuation $\mathrm{d}S(t)$ as a propagation delay fluctuation

$$\mathrm{d}t(t) = \mathrm{d}S(t)/(2\pi f) \tag{5.25}$$

or in discrete time

$$\mathrm{d}[n] = \mathrm{d}S[n]/(2\pi k f_s) \tag{5.26}$$

With the Gaussian turbulence spectrum it is straightforward to separate the covariance $B(\tau)$ into the correlation $C(\tau)$ and variance σ as defined in respectively equations (2.57) and (2.55). That way we can compute a filter $h_C[n]$ that depends solely on the correlation $C(\tau)$, and scale this afterwards with the correct variances σ_χ and σ_S. The advantage is having to compute only one sequence of fluctuations, which is determined entirely by the covariance and $z[n]$, and can then be scaled with the (frequency-dependent) variances σ_χ and S.

5.3.7 Moving source

Thus far it was assumed neither the source nor the receiver were moving, and that the fluctuations arise due to sampling a turbulent field that is moving by with constant speed at a fixed receiver position.

If the field is transported faster, the spatial fluctuations are sampled faster, and therefore the scintillations $\chi[n] = S[n]$ are compressed in time corresponding to fluctuations with relatively higher frequencies.

In case the turbulent field is transported by wind and neither source nor receiver are moving, the source-receiver distance remains constant. If we instead consider a moving source of which the emitted sound samples the turbulent field, then the source-receiver distance d generally changes and thus also the variances σ_χ and σ_S.

We will now consider a moving source. The transverse velocity is in this case the velocity component of the moving source, perpendicular to the wave propagation direction. This is the vector *rejection* of the source velocity vector $\mathbf{v_s}$ from the unit vector $\hat{\mathbf{o}}$ that represents the orientation from source to receiver. The transverse speed is the norm of this vector

$$v_\perp = \|\mathbf{v_s} - (\mathbf{v_s} \cdot \hat{\mathbf{o}}) \cdot \hat{\mathbf{o}}\| \tag{5.27}$$

The vector *projection* of the source velocity on the wave propagation direction is the component that is relevant for the Doppler shift. Therefore, as the Doppler shift is

[2] A system is minimum-phase when it and its inverse are both causal and stable, which would require both the poles and zeros to be inside the unit circle. The group delay is minimal and thus its energy is concentrated at the start of an impulse response.

maximum the modulations are relatively low-frequent, whereas if the Doppler shift is zero, the modulations are relatively high-frequent.

When computing two sequences of scintillations, but for different transverse speeds, one does not obtain a compressed version of the other using the method as described thus far in this section, even when using the same seed for the Pseudo-Random Number Generator. This is because, by adjusting $v_\perp$, we effectively applied the compression on the filter $h_C[n]$ before convolution with $z[n]$. Therefore, the two resulting sequences will not look compressed in time, but instead just filtered differently. Even so, the generated sequence will have the desired statistical properties.

We can obtain the desired compression, i.e., scaling in time, if we instead perform the convolution between $z[n]$ and a time-invariant $h_C[n]$ computed for a fixed τ_0, τ_{ref}, and then resample the values of $\chi[n]$ and $S[n]$ at different times to take into account the change in correlation. Instead of having a constant sample timestep

$$t_k = \frac{k}{f_s} = \sum_{i=0}^{k} \frac{1}{f_s}, \quad k = 0, 1, \ldots, \quad i = 0, 1, \ldots \tag{5.28}$$

the sample time varies with correlation time

$$t_k = \sum_{i=0}^{k} \frac{\tau_{\text{ref}}}{\tau_{0,i}} \frac{1}{f_s}, \quad k = 0, 1, \ldots, \quad i = 0, 1, \ldots \tag{5.29}$$

Figure 5.2 shows the full block diagram of the signal processing steps for generating scintillations and including them in an auralisation.

5.3.8 Saturation of the log-amplitude fluctuations

According to equation (2.55) the fluctuations increase with distance and frequency indefinitely. For longer path lengths or stronger turbulence, the amplitude fluctuations gradually level off. Saturation of the amplitude fluctuations can be observed when measuring aircraft noise at distances of over a few kilometres. The standard deviation of the fluctuating sound pressure levels is in such cases limited to approximately 6 dB [67].

Saturation of the log-amplitude fluctuations can be included based on an analysis by Wenzel [94]. In Wenzel's approach the soundwave is split up in a coherent and incoherent wave. The amplitude of the coherent wave decreases over distance while the incoherent wave obtains the energy from the coherent wave. The coherent wave p is written as

$$\langle p\ p^* \rangle = \left(A_m^2/4\pi r^2\right) \exp\left(-2\sigma_\mu k^2 r L\right) \tag{5.30}$$

Wenzel defines the distance to saturation r_s as the distance at which the coherent wave is reduced to e^{-1} of its original strength

$$r_s = \frac{1}{2\sigma_\mu^2 k^2 L} \tag{5.31}$$

Saturation of the log-amplitude fluctuations can now be included by multiplying the log-amplitude with a correction factor. The variance of log-amplitude fluctuations that includes saturation σ_χ, is given by

$$\sigma_{\chi,sat} = \sigma_\chi \frac{1}{1 + r/r_s} \tag{5.32}$$

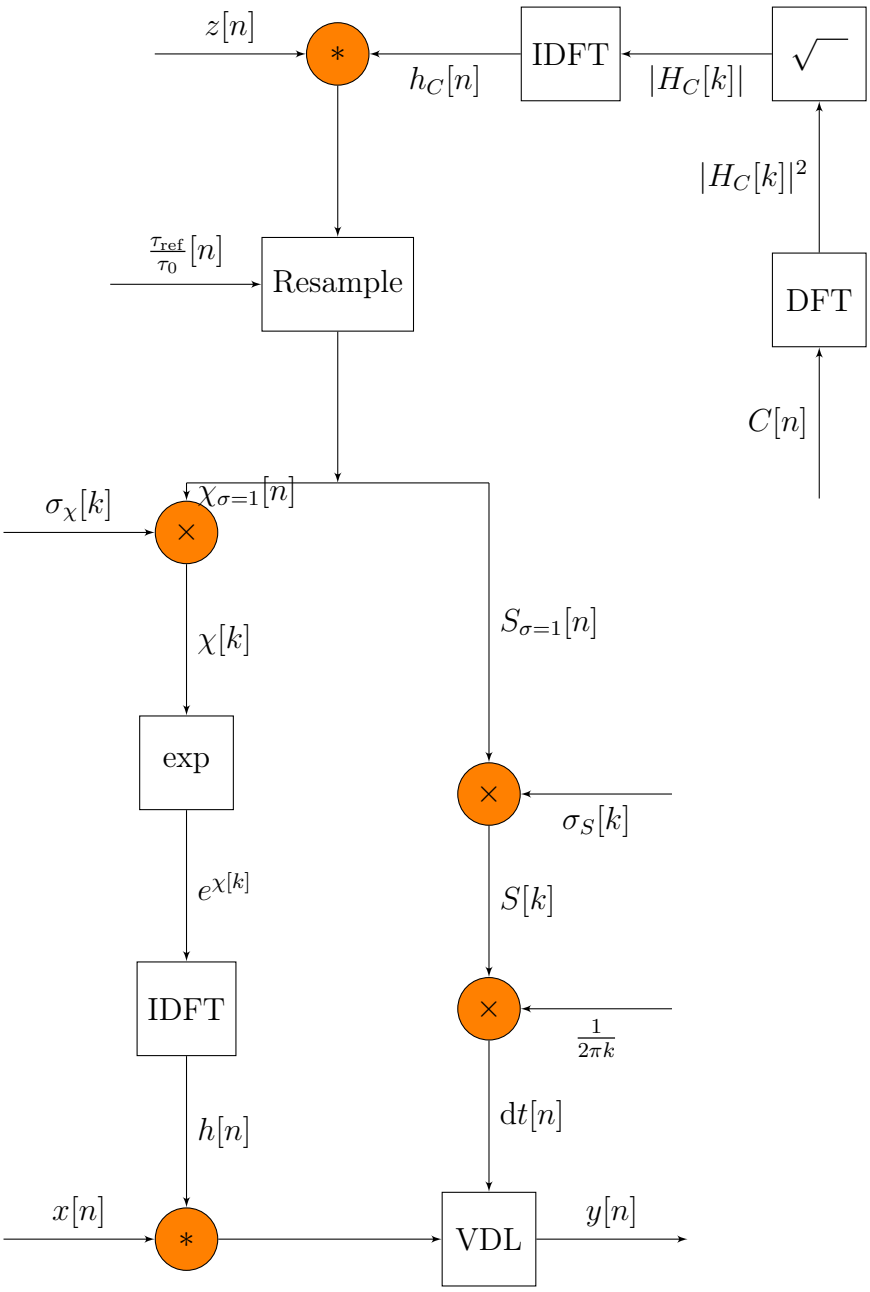

Figure 5.2: Block diagram of signal processing steps.

5.4 Results

5.4.1 A single tone

To demonstrate the model we shall now consider a tone of 1000 Hz and apply modulations to the tone. The following parameters are used: $c = 343.2$ m/s, $\sigma_\mu^2 = 3 \cdot 10^{-6}$, $L = 1.1$ m, $v_\perp = 2.0$ m/s and $d = 500$ m. Saturation according to equation (5.32) is also included. The filter h_c is designed to have 8192 taps. The correlation time is then $\tau = L/v_\perp = 0.55$ s and the sample frequency at which the modulations are generated $5/\tau = 9.1$ Hz.

Figure 5.3 shows the time series of amplitude and phase fluctuations that were generated. Figure 5.4 shows the tone along with a modulated version of the tone. The tone was sampled at 8000 Hz. In order to extract the log-amplitude and phase modulations from this tone, or for example from one measured outdoors, one could use the Hilbert transform as explained in section 2.5.4.

The log-amplitude and phase move in-phase. The value for the log-amplitude is slightly lower than that of the phase because of saturation. As expected the phase fluctuations cause spectral broadening of the tone as can be seen in Figure 5.5 [95].

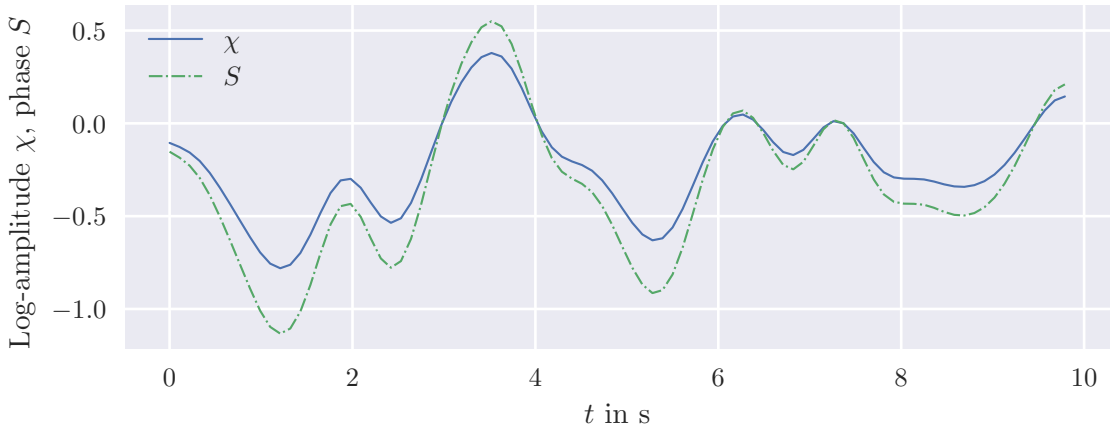

Figure 5.3: Amplitude and phase fluctuations as function of time. The fluctuations are less strong for the amplitude fluctuations due to saturation.

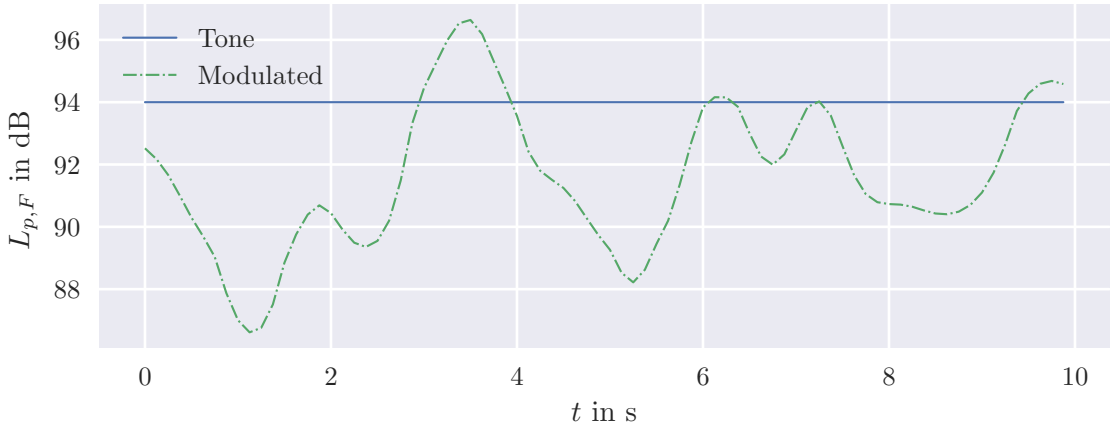

Figure 5.4: Sound pressure level of the tone as function of time, with and without fluctuations.

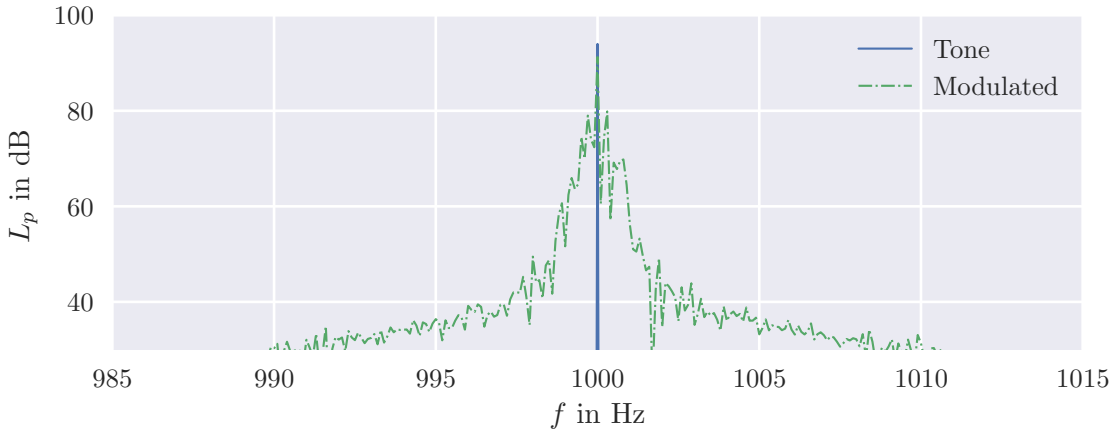

Figure 5.5: The power spectrum of the tone shows the broadening due to the phase fluctuations although the bandwidth at -3 dB from the maximum is still small.

5.4.2 Scintillations as function of transverse speed

By changing the transverse speed the refractive-index field is sampled at a different speed. This effectively changes the correlation length and shifts the frequency range that is covered by our applied filter [96].

Figure 5.6 shows the correlation function for different transverse speeds.

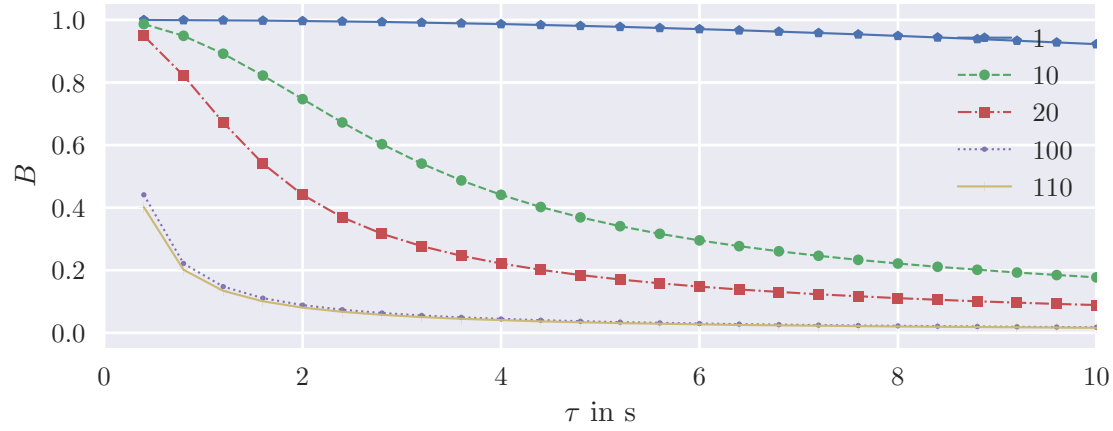

Figure 5.6: Correlation as function of time for different transverse speeds given in meters per second.

With a high transverse speed the correlation drops faster, and this will result in relatively more high-frequency fluctuations, as is shown in Figure 5.7.

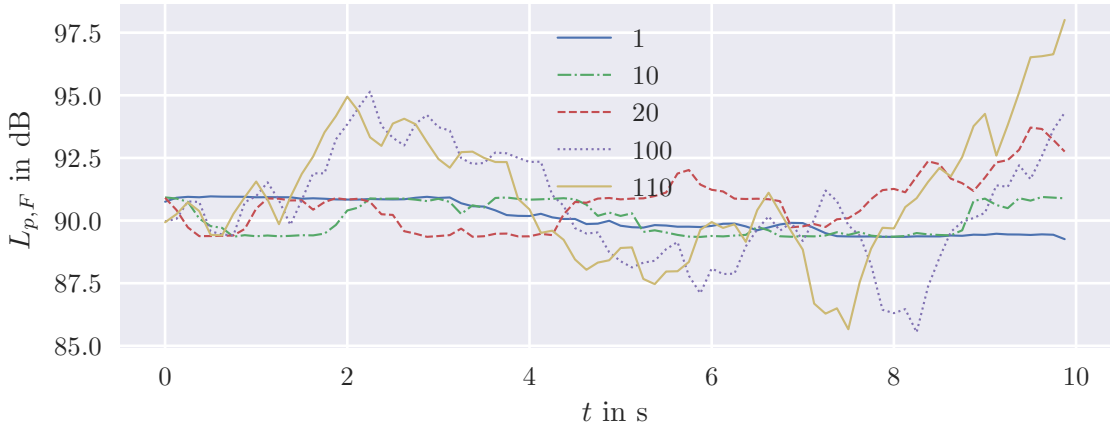

Figure 5.7: Sound pressure level as function of time for scintillations corresponding to different transverse speeds given in meters per second. The same $z[n]$ were used for each case. A compression in time of the modulations with increasing velocity can be observed.

5.4.3 Application in auralisation of aircraft

The method was developed in order to create more plausible sounding auralisations of aircraft. An aircraft moves at high speed through the atmosphere. A transverse speed is computed for each propagation path separately. Because the correlation time, distance and propagation varies between the two paths, decorrelation occurs. Figures 5.8 and 5.9 show spectrograms, respectively without and with turbulence. The vertical lines that can be seen are the amplitude modulations.

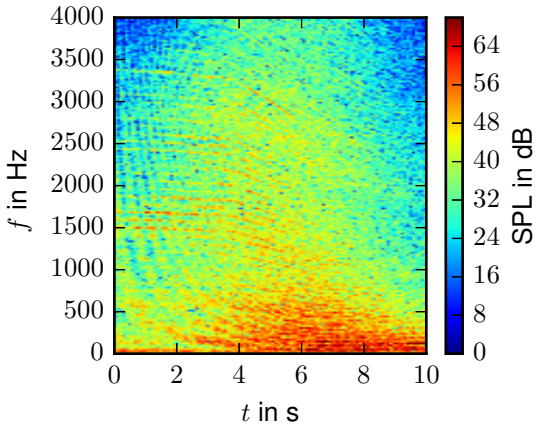

Figure 5.8: Spectrogram of an auralisation of an aircraft taking off. Scintillations were not included. Visible are the ground effect and the Doppler shift. In the initial seconds a high amount of tonal components are visible.

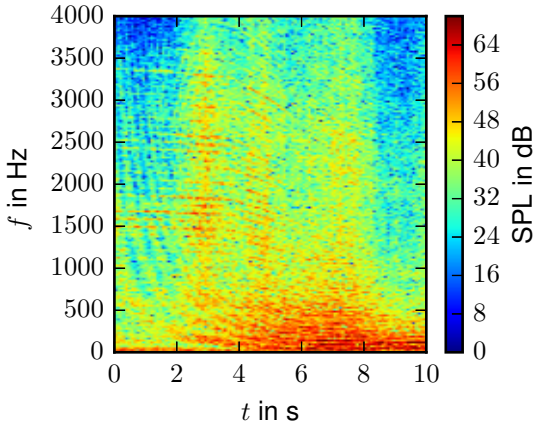

Figure 5.9: Spectrogram of the same event as in Figure 5.8, however, this time with scintillations included. Because of the high speed at which the aircraft samples the refractive-index field the scintillations are relatively high-frequent, resulting in vertical lines.

Earlier it was assumed that the correlation length was much smaller than the Fresnel zone size. In this auralisation the aircraft is moving close to the receiver. When the aircraft is closest, the distance is almost entirely given by the height which was approximately 100 meters. The correlation length was set at 20 meters. In that case the Fresnel zone is larger than the correlation length for the lower frequencies, and equation (2.55) is not valid. Instead, the log-amplitude and phase variances should scale with respectively d^3 and $2k^2d$ instead of k^2d.

5.4.4 Influence of parameters

The two main parameters of the Gaussian model are the variance of refractive-index fluctuations σ_μ^2 and the correlation length L. Figures 5.10 and 5.11 show examples of the effect of each of these parameters on an auralisation of an "aircraft".

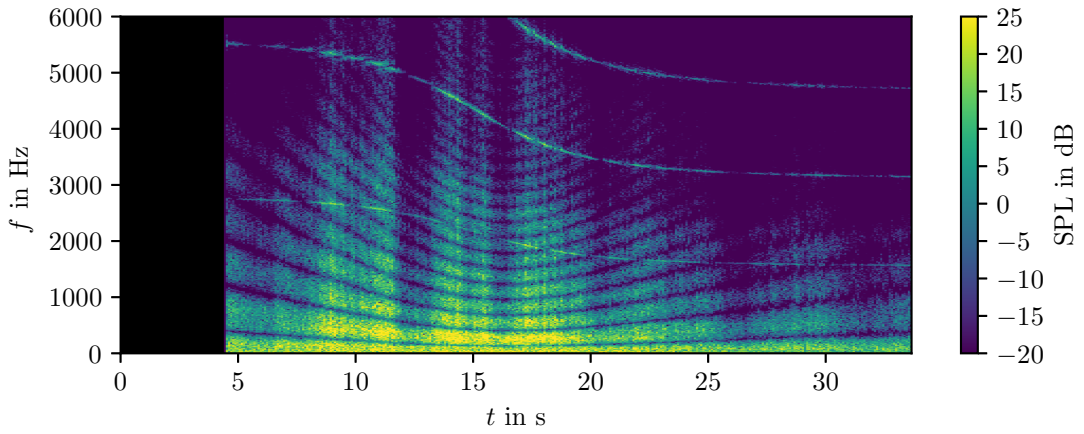

(a) 1 m

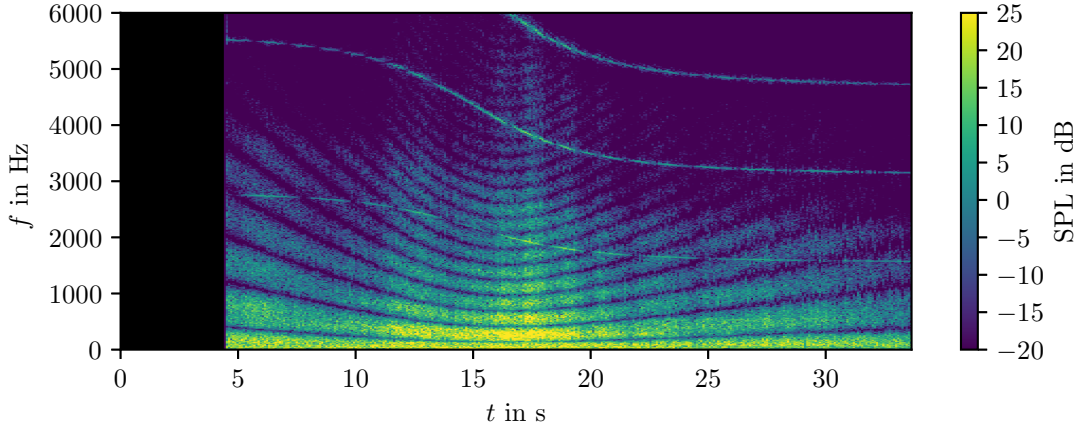

(b) 4 m

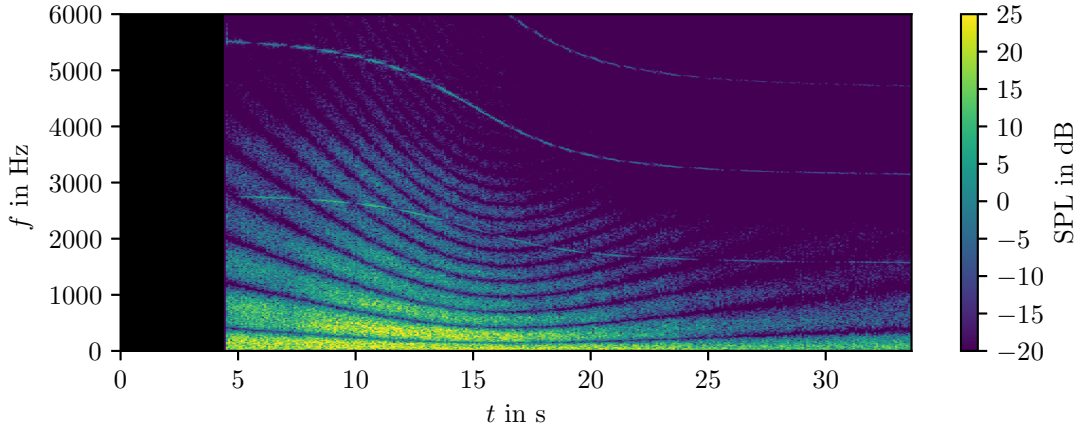

(c) 16 m

Figure 5.10: The influence of the correlation length L. The variance of the dynamic refractive-index is fixed at 1×10^{-5}. A higher correlation length results in slower fluctuations.

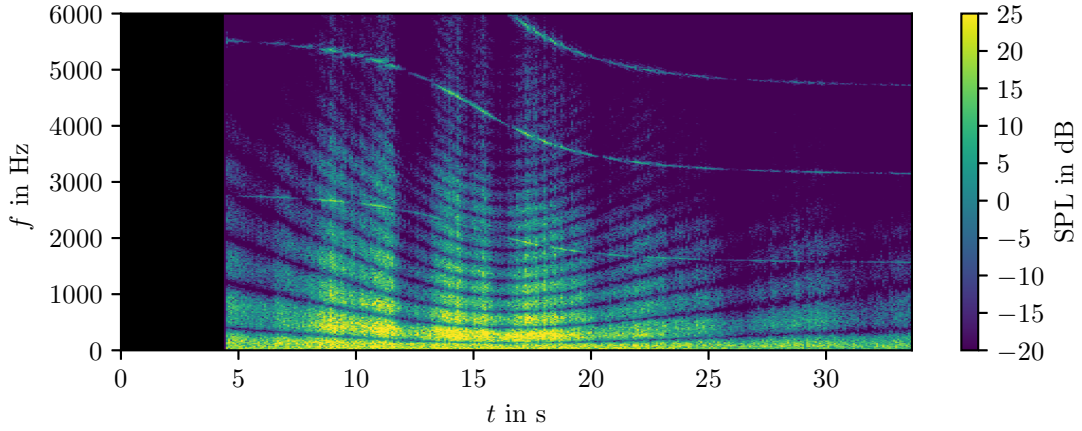

(a) 1×10^{-5}

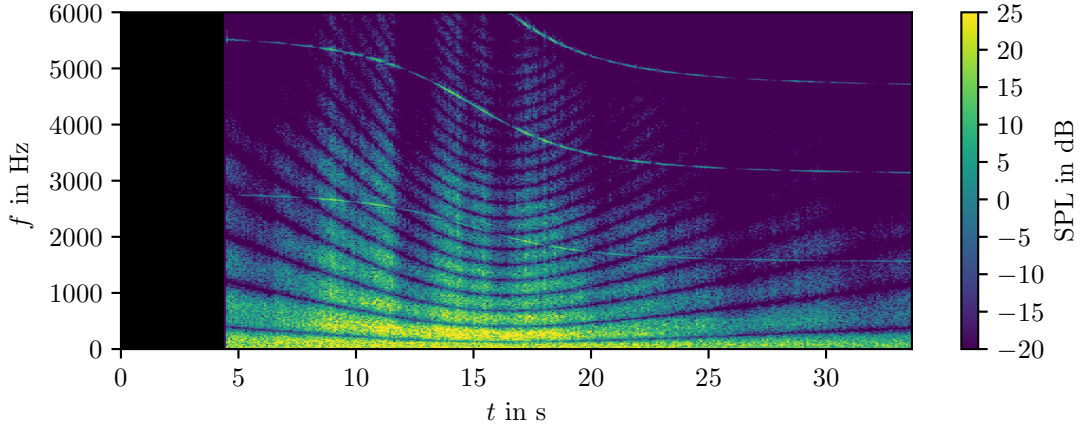

(b) 1×10^{-6}

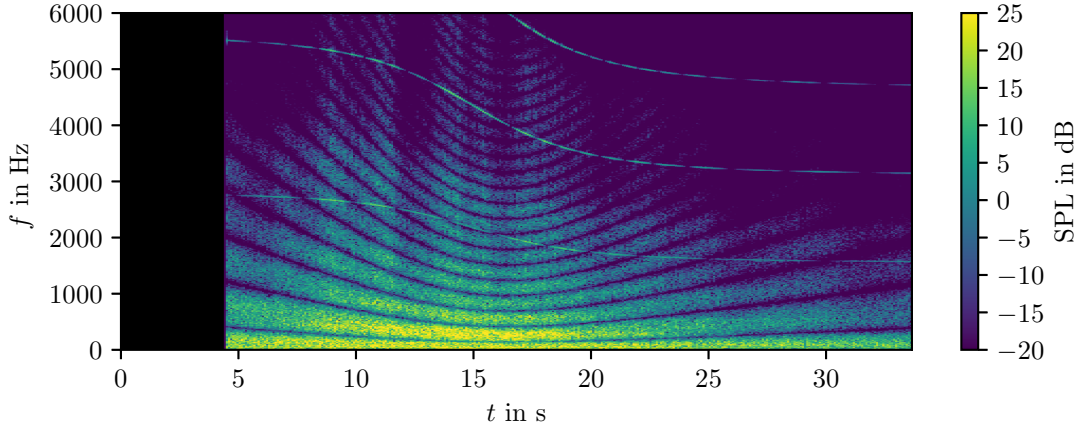

(c) 1×10^{-7}

Figure 5.11: The influence of the variance of the dynamic refractive-index σ_μ^2. The correlation length is fixed at 1 m. A higher variance results in stronger fluctuations.

5.5 Conclusion

Fluctuations in the refractive-index field due to variations in temperature and wind affects sound propagation, and this causes audible modulations. A method was presented for generating sequences of modulations and applying these to monochromatic as well as broadband signals.

A Rytov approximation to first-order refractive-index fluctuations results in a complex phase ψ, which we can write as a log-amplitude χ fluctuation, and a phase S fluctuation. The propagating sound is modelled as a time-varying channel where we consider two sequences, one for the log-amplitude fluctuations, and another for the phase fluctuations.

The fluctuations are frequency-dependent and therefore a filter was designed to take that into account. A Gaussian turbulence spectrum was considered, but the general method can be used with other turbulence spectra as well. The Von Karman spectrum describes real turbulence spectra typically better than the Gaussian spectrum, however, the Von Karman spectrum is computationally much more demanding.

Examples are shown where the method is applied to a tone and to an aircraft auralisation. The aircraft auralisation spectrogram shows several spikes corresponding to amplitude modulations as well as an increase in the amount of decorrelation. Furthermore the transverse velocity dependence on the frequency content of the modulations is demonstrated.

According to the author the method results in more plausible sounding auralisations, but this has not been validated yet with listening tests.

Chapter 6

Conclusions and future work

6.1 Conclusions

Aircraft noise has a negative impact on humans. To further study its impact on humans a tool was developed to simulate the audible sound caused by fly-overs of airplanes. The goal was to develop a tool that can create auralisations of the current fleet of aircraft that sound plausible.

The auralisation tool consists of an emission synthesiser and a propagation model based on geometrical acoustics. The emission synthesiser used spectral modelling synthesis as synthesis strategy and used features extracted from recordings as input. These features were automatically extracted from a signal that was obtained after applying an inverse propagation model to a recording. To verify whether the auralisations sound similar to recordings of the respective airplane types, a listening test was conducted.

In a listening test participants were presented with two stimuli at a time and were asked to rate on a categorical scale the similarity of the two stimuli, where the two stimuli could be recordings, auralisations, or one of each. The hypothesis was that *recordings and auralisations of aircraft of the same type and under similar conditions are samples of the same group*. This hypothesis would be true, if the distribution of the group with comparisons between recordings and auralisations would be the same as the other two distributions.

There were clear differences in the distributions, implying the hypothesis is not true. In case of the recordings, the participants were clearly discriminating between the two different aircraft types that were considered. With the auralisations this was not as clear, however, and it would appear that the auralisations sound more as different aircraft types.

An incorrect reproduction of the blade passing frequency and its harmonics is the likely cause of the dissimilarity between the auralisations and recordings. The feature-extraction algorithm was tuned for the relatively small bandwidth of the Buzz-Saw tones and is therefore underestimating the power and bandwidth of the blade-passing frequency and harmonics.

Section 1.1.5 listed several auralisation use cases. The relevance of audible differences between auralisations and recordings may depend on the application of

the auralisations and the precision it requires. Consider e.g. the Lelystad Airport example that was given in section 1.1.5. For that purpose, what is needed is auralisations of aircraft of a certain class, but not necessarily a specific aircraft type. Perception-influenced design of aircraft may require a higher precision. However, while a minimum error between auralisations and recordings is desirable, what is perhaps more important is that the auralisation tool behaves correctly when adjusting certain parameters.

To improve the plausibility of the auralisations a method was developed to simulate modulations due to weak atmospheric turbulence. Spatial and temporal variations in temperature cause variations in the soundspeed field. As sound propagates through a turbulent atmosphere, the variations will cause multiple scattering and result in audible modulations, known as scintillations. A method was presented for generating sequences of modulations and applying these to both monochromatic and broadband signals.

Starting with a Helmholtz equation for the sound pressure and a random soundspeed field, a Rytov approximation to first-order refractive-index fluctuations was done yielding the sound pressure as a sum of complex phases with increasing order. The zeroth order represents the unperturbed field and the first-order represents first-order perturbations of log-amplitude χ and phase S. Sound that is propagated is modelled as a time-varying channel and the perturbations are represented by two random sequences, one for the log-amplitude fluctuations, and another for the phase fluctuations.

The random fluctuations have a Gaussian statistical distribution and a spectrum. The spectrum is the Fourier transformation of the covariance of the random temporal fluctuations. To approximate the spectrum of the turbulence a Gaussian model was used. While other turbulence models are available and could be used, the Gaussian model was chosen for its simplicity and because its computationally least demanding. In the Gaussian model the correlation depends on the correlation length L of the turbulence and the transverse speed $v_\perp$, and the variance on distance d, correlation length L, wavenumber k and variance of the dynamic refractive-index field. Because of the frequency-dependency, the fluctuations or modulations were implemented as a time-variant filter. Furthermore, saturation of the log-amplitude was accounted for.

Examples were shown where the method is applied to a pure tone and to airplane auralisations. The log-amplitude fluctuations cause clearly audible modulations, and the phase fluctuations result in spectral broadening. The spectrograms of the airplane auralisations show spikes corresponding to amplitude modulations. They also show an increase in the amount of decorrelation. Furthermore, the impact of the transverse velocity on the frequency content of the modulations was demonstrated. While not validated with listening tests, it is the author's opinion that the method does seem to result in more plausible sounding auralisations.

6.2 Future work

In this section a list of possible future steps is given. The research that was presented spanned several topics, and therefore the suggested future steps are quite broad as well. Furthermore, future steps may also depend on the purpose of e.g. the auralisations as was explained in the introduction.

Investigate human response to aircraft sound

If one wants to study humans' response to aircraft sound, then the next step is to test whether auralisations of aircraft are sufficiently similar to the actual sound of aircraft, with respect to the parameter that is being investigated. For example, if one is interested in perceived annoyance, then the test should compare annoyance ratings of the recordings and auralisations. If the conclusion is that auralisations and recordings give sufficiently similar results, then that would imply the auralisation method can be used to further study that aspect of human response within the domain that was considered. If significant differences would still be found, it would have to be tested what is causing the differences.

Improve estimation and synthesis of blade passing frequency

From the study that was conducted and presented, it followed that participants did indeed notice differences between the auralisations and the recordings. A probable cause of these differences is the estimation of the power and bandwidth of the blade passing frequency and harmonics. Therefore, a possible improvement would be to enhance the feature-extraction algorithm to better estimate these properties. If the amount of fan blades is known, then that could be used as input to change the behaviour of the algorithm at the blade passing frequency and its harmonics.

Develop generic aircraft emission model

The emission synthesiser uses features determined from one specific event. The chosen emission synthesis strategy (spectral modelling synthesis with extracted features) produced auralisations that sound plausible. Therefore, a future step is to construct an emission model that produces these features as function of input parameters (e.g. thrust settings).

Subjective validation of scintillations model

The scintillations model is based on an existing statistical model. While the Gaussian model does not describe the whole turbulence spectrum, it may produce correct results within a limited domain of the spectrum. In this work the assumption was made the Gaussian model is sufficient along with other assumptions (e.g. that the correlation length is much smaller than the Fresnel zone). A possible future step would be a subjective validation to verify whether auralisations that use the model sound as realistic as recordings. An open question is how to conduct such a test,

because due the statistical nature of the turbulence the auralisations and recordings there is a limitation to how similar they may sound.

Correlation length not much smaller than Fresnel zone

As explained in 2.4.4 the variance of the fluctuations is a function of the correlation length and Fresnel zone size. The assumption was made that $L \ll \sqrt{\lambda d}$. A future step would be to account for situations where the correlation length is about the same size as the Fresnel zone or even larger.

Different model for describing turbulence spectrum

As mentioned in the text the basic method for generating scintillations should also work with other models, like the Von Karman spectrum. The Gaussian model was chosen for performance reasons, as its simplest, but also because it allowed certain optimisations. Future work could be to develop an algorithm that utilises other spectra like e.g. the Von Karman spectrum with the use of expressions given in [93].

Non-isotropic and non-homogeneous atmosphere for the scintillations model

The current model assumes an isotropic and homogeneous atmosphere. In practice, the atmosphere is neither and parameters like the correlation length L and the variance of the refractive-index fluctuations $\langle \mu^2 \rangle$ are height-dependent [97]. Ostashev et al. gave formulas for plane [98] and spherical [99] waves propagating through an anisotropic atmosphere and studies numerically the variances and correlation functions of the log-amplitude and phase fluctuations [100]. A future step would be to enhance the scintillations model to take into account an anisotropic atmosphere.

Appendix A

Audio files

This thesis discusses auralisations and recordings, and throughout the text figures of certain attributes of these sounds were shown. The table on the next page lists the available sound files. An archive with the audio files can be found online [56].

Table A.1: Table with audio files.

Figure	Description	Filename
2.2a	Reflection on hard surface	`2-2a.wav`
2.2b	Reflection on soft surface	`2-2b.wav`
2.4a	Linear interpolation	`2-4a.wav`
2.4b	Lanczos interpolation, $\alpha = 2$	`2-4b.wav`
2.4c	Lanczos interpolation, $\alpha = 10$	`2-4c.wav`
3.3	Emission	`3-3.wav`
3.4	Spreading	`3-4.wav`
3.5	Doppler	`3-5.wav`
3.6	Attenuation	`3-6.wav`
3.7	Reflection	`3-7.wav`
3.11	Recording	`3-11.wav`
3.12	Backpropagation	`3-12.wav`
3.13	Emission synthesis	`3-13.wav`
3.14	Auralisation	`3-14.wav`
4.1	Recording, approach	`4-1a.wav`
4.1	Recording, flyover	`4-1b.wav`
4.1	Recording, distancing	`4-1c.wav`
4.2	Auralisation, approach	`4-2a.wav`
4.2	Auralisation, flyover	`4-2b.wav`
4.2	Auralisation, distancing	`4-2c.wav`
5.4	Tone	`5-4a.wav`
5.4	Modulated tone	`5-4b.wav`
5.6	Modulated tone, $v_\perp = 1$	`5-6a.wav`
5.6	Modulated tone, $v_\perp = 10$	`5-6b.wav`
5.6	Modulated tone, $v_\perp = 20$	`5-6c.wav`
5.6	Modulated tone, $v_\perp = 100$	`5-6d.wav`
5.6	Modulated tone, $v_\perp = 110$	`5-6e.wav`
5.10	Parameters, $L = 1$, $\sigma_\mu^2 = 1e-5$	`5-10a.wav`
5.10	Parameters, $L = 4$, $\sigma_\mu^2 = 1e-5$	`5-10b.wav`
5.10	Parameters, $L = 16$, $\sigma_\mu^2 = 1e-5$	`5-10c.wav`
5.11	Parameters, $L = 1$, $\sigma_\mu^2 = 1e-5$	`5-11a.wav`
5.11	Parameters, $L = 1$, $\sigma_\mu^2 = 1e-6$	`5-11b.wav`
5.11	Parameters, $L = 1$, $\sigma_\mu^2 = 1e-7$	`5-11c.wav`

Bibliography

[1] United Nations. *World Urbanization Prospects: The 2014 Revision, Highlights (ST/ESA/SER.A/352)*. 2014, p. 32. ISBN: 9789211515176. DOI: 10.4054/DemRes.2005.12.9. arXiv: arXiv:1011.1669v3. URL: http://esa.un.org/unpd/wup/Highlights/WUP2014-Highlights.pdf.

[2] C. European. "Climate change : Commission proposes bringing air transport into EU Emissions Trading Scheme". In: *Press Release IP/06/1862* December 2006 (2006), p. 2. ISSN: 09505849. DOI: 10.1016/j.infsof.2008.09.005. arXiv: 0402594v3 [arXiv:cond-mat].

[3] O. Zaporozhets, V. Tokarev, and K. Attenborough. *Aircraft Noise: Assessment, prediction and Control*. Spon Press (Taylor and Francis), 2011. ISBN: 9780203888827. URL: http://oro.open.ac.uk/32193/.

[4] MPD Group Limited. "Study of aicraft noise exposure at and around community airports : evaluation of the effect of measures to reduce noise. Final Report". In: October (2007), p. 179. URL: http://ec.europa.eu/transport/modes/air/studies/doc/environment/2007%7B%5C_%7D10%7B%5C_%7Daircraft%7B%5C_%7Dnoise%7B%5C_%7Dexposure%7B%5C_%7Den.pdf.

[5] I. Kirk and K. Micha. "Noise Pollution in Switzerland:Results of the SonBase National noise Monitoring Programme". In: (2009), p. 61.

[6] B. Schäffer, S. Plüss, and G. Thomann. "Estimating the model-specific uncertainty of aircraft noise calculations". In: *Applied Acoustics* 84 (Oct. 2014), pp. 58–72. ISSN: 0003682X. URL: http://www.sciencedirect.com/science/article/pii/S0003682X14000280.

[7] R. Freestone and D. Baker. "Challenges in land use planning around Australian airports". In: *Journal of Air Transport Management* 16.5 (2010), pp. 264–271. ISSN: 09696997. DOI: 10.1016/j.jairtraman.2010.03.001. URL: http://dx.doi.org/10.1016/j.jairtraman.2010.03.001.

[8] M. Theebe. "Planes, Trains, and Automobiles: The Impact of Traffic Noise on House Prices". In: *the Journal of Real Estate Finance and Economics* 38.2 (2004), pp. 35–37. ISSN: 02583127. DOI: 10.1023/B. arXiv: arXiv:1112.2903v1.

[9] T. Bjørnskau. "Road traffic change: a catalyst for segregation?" In: *Urban Studies (Routledge)* 42.1 (2005), pp. 69–89. ISSN: 00420980. DOI: 10.1080/0042098042000309702. URL: http://10.0.4.56/0042098042000309702%7B%5C%%7D5Cnhttps://search.ebscohost.com/login.aspx?direct=true%7B%5C&%7Ddb=bth%7B%5C&%7DAN=16111099%7B%5C&%7Dsite=ehost-live.

[10] R. Guski, U. Felscher-Suhr, and R. Schuemer. "The Concept of Noise Annoyance: How International Experts See It". In: *Journal of Sound and Vibration* 223.4 (1999), pp. 513–527. ISSN: 0022460X. DOI: 10.1006/jsvi.1998.2173. URL: http://linkinghub.elsevier.com/retrieve/pii/S0022460X98921733.

[11] W. Babisch et al. "Annoyance due to aircraft noise has increased over the years - Results of the HYENA study". In: *Environment International* 35.8 (2009), pp. 1169–1176. ISSN: 01604120. DOI: 10.1016/j.envint.2009.07.012. URL: http://dx.doi.org/10.1016/j.envint.2009.07.012.

[12] D. S. Michaud et al. "Review of field studies of aircraft noise-induced sleep disturbance". In: *The Journal of the Acoustical Society of America* 121.1 (2007), pp. 32–41. ISSN: 0001-4966. DOI: 10.1121/1.2400613. URL: http://asa.scitation.org/doi/10.1121/1.2400613.

[13] *International Civil Aviation Organization*. URL: https://www.icao.int/Pages/default.aspx (visited on 06/13/2017).

[14] *ICAO Doc 9501 Volume 1: Procedures for the Noise Certification of Aircraft*. Tech. rep. URL: https://www.icao.int/environmental-protection/Documents/Publications/Doc%7B%5C_%7D9501%7B%5C_%7DVolume%7B%5C_%7DI.pdf.

[15] *European Civil Aviation Conference*. URL: https://www.ecac-ceac.org/ (visited on 06/13/2017).

[16] *ECAC.CEAC Doc 29, 4th edition*. Tech. rep. 2016.

[17] "DIRECTIVE 2002/49/EC OF THE EUROPEAN PARLIAMENT AND OF THE COUNCIL of 25 June 2002 relating to the assessment and management of environmental noise". In: *Official Journal of the European Communities* L189 (2002), pp. 12–25. ISSN: 0959-6526. DOI: 10.1016/j.jclepro.2010.02.014. URL: http://eur-lex.europa.eu/legal-content/EN/TXT/PDF/?uri=CELEX:32002L0049%7B%5C&%7Dfrom=EN%7B%5C%%7D0Ahttp://eur-lex.europa.eu/legal-content/EN/TXT/?uri=celex:32002L0049.

[18] B. Schäffer et al. "Zurich Aircraft Noise Index: An Index for the Assessment and Analysis of the Effects of Aircraft Noise on the Population". In: *Acta Acustica united with Acustica* 98.3 (May 2012), pp. 505–519. ISSN: 16101928. DOI: 10.3813/AAA.918533. URL: http://openurl.ingenta.com/content/xref?genre=article%7B%5C&%7Dissn=1610-1928%7B%5C&%7Dvolume=98%7B%5C&%7Dissue=3%7B%5C&%7Dspage=505%20http://id22079462.library.ingentaconnect.com/content/dav/aaua/2012/00000098/00000003/art00014?token=004c19a1ab503aae9573d257025702c492b462d3144425547637c4e754.

[19] A. Sahai et al. "Interactive simulation of aircraft noise in aural and visual virtual environments". In: *Applied Acoustics* 101 (2016), pp. 24–38. ISSN: 0003682X. DOI: 10.1016/j.apacoust.2015.08.002. URL: http://www.sciencedirect.com/science/article/pii/S0003682X15002169.

[20] A. K. Sahai and E. Stumpf. "Incorporating and minimizing aircraft noise annoyance during conceptual aircraft design". In: *20th AIAA/CEAS aeroacoustics conference Part of AVIATION forum*. 2014.

[21] M. D. Moore. *Distributed Electric Propulsion (DEP) Aircraft*. 2012. URL: http://aero.larc.nasa.gov/files/2012/11/Distributed-Electric-Propulsion-Aircraft.pdf.

[22] A. Beutel. "NASA Electric Research Plane Gets X Number, New Name". In: (2016). URL: https://www.nasa.gov/press-release/nasa-electric-research-plane-gets-x-number-new-name.

[23] S. A. Rizzi and D. Palumbo. "Advances in Distributed Propulsor Acoustic Modeling". In: *2015 Transformative Vertical Flight Workshop* August (2015).

[24] M. Kleiner, B.-I. Dalenbäck, and P. Svensson. "Auralization - An Overview". In: *Journal of the Audio Engineering Society* 41.11 (1993), pp. 861–875.

[25] M. Vorländer and M. Vörlander. *Auralization*. RWTHedition. Berlin, Heidelberg: Springer Berlin Heidelberg, 2008, p. 335. ISBN: 9783540488293. DOI: 10.1007/978-3-540-48830-9. URL: http://adsabs.harvard.edu/abs/2008aura.book.....V%20http://link.springer.com/10.1007/978-3-540-48830-9.

[26] J. Forssén et al. "Auralization of traffic noise within the LISTEN project Preliminary results for passenger car pass-by". In: *Euronoise*. 2009.

[27] J. Jagla, J. Maillard, and N. Martin. "Sample-based engine noise synthesis using an enhanced pitch-synchronous overlap-and-add method". In: *The Journal of the Acoustical Society of America* 132.5 (Nov. 2012), pp. 3098–3108. ISSN: 0001-4966. DOI: 10.1121/1.4754663. URL: http://asa.scitation.org/doi/10.1121/1.4754663.

[28] R. Pieren, T. Bütler, and K. Heutschi. "Auralization of Accelerating Passenger Cars Using Spectral Modeling Synthesis". In: *Applied Sciences* 6.1 (2015), p. 5. ISSN: 2076-3417. DOI: 10.3390/app6010005. URL: http://www.mdpi.com/2076-3417/6/1/5/htm.

[29] A. Hoffmann. "Auralization, perception and detection of tyre-road noise". PhD thesis. Chalmers University of Technology, 2016. ISBN: 9789175974699.

[30] A. Hoffmann, P. Bergman, and W. Kropp. "Perception of tyre noise: Can tyre noise be differentiated and characterized by the perception of a listener outside the car?" In: *Acta Acustica united with Acustica* 102.6 (2016), pp. 992–998. ISSN: 16101928. DOI: 10.3813/AAA.919014.

[31] R. Pieren et al. "Auralisation of Railway Noise: A Concept for the Emission Synthesis of Rolling and Impact Noise". In: *InterNoise 2016*. Hamburg, 2016.

[32] R. Pieren et al. "Auralization of Wind Turbine Noise: Emission Synthesis". In: *Acta Acustica united with Acustica* 100.1 (Jan. 2014), pp. 25–33. ISSN: 16101928. DOI: 10.3813/AAA.918683. URL: http://openurl.ingenta.com/content/xref?genre=article%7B%5C&%7Dissn=1610-1928%7B%5C&%7Dvolume=100%7B%5C&%7Dissue=1%7B%5C&%7Dspage=25.

[33] K. Heutschi et al. "Auralization of Wind Turbine Noise: Propagation Filtering and Vegetation Noise Synthesis". In: *Acta Acustica united with Acustica* 100.1 (2014), pp. 13–24. ISSN: 16101928. DOI: 10.3813/AAA.918682. URL: http://openurl.ingenta.com/content/xref?genre=article%7B%5C&%7Dissn=1610-1928%7B%5C&%7Dvolume=100%7B%5C&%7Dissue=1%7B%5C&%7Dspage=13.

[34] I. García Merino and K. Larsson. "Auralization of outdoor fan noise in shielded areas". In: (2016), pp. 2939–2949. URL: http://ri.diva-portal.org/smash/record.jsf?pid=diva2%7B%5C%%7D3A1059676%7B%5C&%7Ddswid=-1026.

[35] M. Arntzen. *Aircraft noise calculation and synthesis in a non-standard atmosphere*. TU Delft, Delft University of Technology, 2014. ISBN: urn:isbn:9789462594647. DOI: 10.4233/uuid:c56e213c-82db-423d-a5bd-503554653413. URL: http://repository.tudelft.nl/view/ir/uuid:c56e213c-82db-423d-a5bd-503554653413/.

[36] S. A. Rizzi. "Toward Reduced Aircraft Community Noise Impact via a Perception-Influenced Design Approach". In: *InterNoise 2016*. Hamburg, 2016.

[37] S. A. Rizzi, C. L. Burley, and R. H. Thomas. "Auralization of NASA N+2 Aircraft Concepts from System Noise Predictions". In: *22nd AIAA/CEAS Aeroacoustics Conference*. Lyon, 2016.

[38] *VASTCON Technical Working Group*. URL: https://vastcon.wordpress.com/ (visited on 05/02/2017).

[39] M. Arntzen. "Auralization and visualization of future air traffic from Lelystad Airport". In: *Internoise 2015* July (2015).

[40] M. Hornikx. "Ten questions concerning computational urban acoustics". In: *Building and Environment* 106 (Sept. 2016), pp. 409–421. ISSN: 03601323. DOI: 10.1016/j.buildenv.2016.06.028. URL: http://linkinghub.elsevier.com/retrieve/pii/S0360132316302359.

[41] F. Georgiou and M. Hornikx. "Incorporating directivity in the Fourier pseudospectral time-domain method using spherical harmonics". In: *The Journal of the Acoustical Society of America* 140.2 (Aug. 2016), pp. 855–865. ISSN: 0001-4966. DOI: 10.1121/1.4960467. URL: http://asa.scitation.org/doi/10.1121/1.4960467.

[42] F. Georgiou and M. Hornikx. "Auralisation of car pass-by using simulated impulse responses". In: *Urban SOUND Planning-International Symposium*. Munich, 2016.

[43] S. Rizzi et al. "Auralization of Hybrid Wing Body Aircraft Flyover Noise from System Noise Predictions". In: (2013), pp. 1–19. URL: http://arc.aiaa.org/doi/pdf/10.2514/6.2013-542.

[44] A. Paté et al. "Perceived Unpleasantness of Aircraft Flyover Noise: Influence of Temporal Parameters". In: *Acta Acustica united with Acustica* 103.1 (Jan. 2017), pp. 34–47. ISSN: 1610-1928. DOI: 10.3813/AAA.919031. URL: http://www.ingentaconnect.com/content/10.3813/AAA.919031.

[45] L. Bertsch, D. G. Simons, and M. Snellen. "Aircraft Noise: The major sources, modelling capabilities, and reduction possibilities". In: (2015). URL: http://elib.dlr.de/95939/.

[46] L. V. Lopes and C. L. Burley. "ANOPP2 User's Manual Version 1.2". In: (2016).

[47] B. Tuttle et al. "Flyover Noise Simulation Using NASA's Coupled Aircraft System Noise Prediction and Auralization Frameworks". In: *NOISE-CON*. Grand Rapids, 2017.

[48] A. R. Aumann et al. "The NASA Auralization Framework and plugin architecture". In: *INTER-NOISE 2015 - 44th International Congress and Exposition on Noise Control Engineering* (2015), ADC 40, Institute of Noise Control Engineering of.

[49] *ECAC.CEAC Doc 29, 3rd edition*. Tech. rep. 2005.

[50] C. Zellmann, J. M. Wunderli, and B. Schäffer. "SonAIR - Data acquisition for a next generation aircraft noise simulation model". In: *42nd International Congress and Exposition on Noise Control Engineering 2013, INTER-NOISE 2013: Noise Control for Quality of Life*. Vol. 1. OAL-Osterreichischer Arbeitsring fur Larmbekampfung, 2013, pp. 842–850. ISBN: 9781632662675. URL: http://www.scopus.com/inward/record.url?eid=2-s2.0-84904458708%7B%5C&%7DpartnerID=tZOtx3y1.

[51] C. Zellmann, J. M. Wunderli, and C. O. Paschereit. "The sonAIR sound source model: spectral three-dimensional directivity patterns in dependency of the flight condition". In: *Proceedings of the INTER-NOISE 2016 - 45th International Congress and Exposition on Noise Control Engineering: Towards a Quieter Future* (2016), pp. 786–794.

[52] Empa. "FLULA2 Ein Verfahren zur Berechnung und Darstellung der Fluglrmbelästung". In: (2010). URL: http://www.empa.ch/plugin/template/empa/*/37718.

[53] G. A. Daigle. "Effects of atmospheric turbulence on the interference of sound waves above a finite impedance boundary". In: *The Journal of the Acoustical Society of America* 65.1 (1979), p. 45. ISSN: 00014966. DOI: 10.1121/1.382265. URL: http://scitation.aip.org/content/asa/journal/jasa/65/1/10.1121/1.382265.

[54] H.-C. C. Shin, C. Hall, and D. Crichton. "Auralisation of turbofan engine noise components". en. In: *Collection of Technical Papers - 12th AIAA/CEAS Aeroacoustics Conference*. Vol. 5. 2006, pp. 2841–2854. ISBN: 1563478099. URL: http://arc.aiaa.org/doi/abs/10.2514/6.2006-2620%20http://www.scopus.com/inward/record.url?eid=2-s2.0-33845621935%7B%5C&%7DpartnerID=tZOtx3y1.

[55] M. Arntzen and D. G. Simons. "Ground reflection with turbulence induced coherence loss in flyover auralization". In: *International Journal of Aeroacoustics* 13.5-6 (2014), pp. 449–462. ISSN: 1475472X. DOI: 10.1260/1475-472X.13.5-6.449. URL: http://www.scopus.com/inward/record.url?eid=2-s2.0-84913619129%7B%5C&%7DpartnerID=40%7B%5C&%7Dmd5=7e7abbfff2b761722a31ac68b9b96fe1.

[56] F. Rietdijk. *Supplementary audio files for doctoral thesis*. 2017. DOI: 10.5281/zenodo.844811.

[57] S. Rienstra and A. Hirschberg. *An Introduction to Acoustics*. Eindhoven, 2017. URL: http://www.win.tue.nl/%7B~%7Dsjoerdr/papers/boek.pdf.

[58] "ISO 9613-1:1993 - Acoustics – Attenuation of sound during propagation outdoors – Part 1: Calculation of the absorption of sound by the atmosphere". In: (1993). URL: http://www.iso.org/iso/iso%7B%5C_%7Dcatalogue/catalogue%7B%5C_%7Dtc/catalogue%7B%5C_%7Ddetail.htm?csnumber=17426.

[59] K. Attenborough, I. Bashir, and S. Taherzadeh. "Outdoor ground impedance models." In: *The Journal of the Acoustical Society of America* 129.5 (May 2011), pp. 2806–2819. ISSN: 00014966. DOI: 10.1121/1.3569740. URL: http://scitation.aip.org.proxy.lib.chalmers.se/content/asa/journal/jasa/129/5/10.1121/1.3569740.

[60] M. J. Crocker. *Encyclopedia of acoustics*. Wiley, 1997. ISBN: 0471177679. URL: http://chans.lib.chalmers.se/record=b1015140.

[61] J. B. Allen and D. A. Berkley. "Image method for efficiently simulating small-room acoustics". In: *The Journal of the Acoustical Society of America* 65.4 (Apr. 1979), pp. 943–950. ISSN: 0001-4966. DOI: 10.1121/1.382599. URL: http://asa.scitation.org/doi/10.1121/1.382599.

[62] F. Mechel. *Room Acoustical Fields*. Springer, 2013, p. 595. ISBN: 9783642223556.

[63] A. Ishimaru. *Wave Propagation and Scattering in Random Media*. New York: Wiley-IEEE Press, 1997. ISBN: 0-7803-4717-X. URL: http://ieeexplore.ieee.org/xpl/bkabstractplus.jsp?bkn=5270963%20http://ieeexplore.ieee.org/xpl/bkabstractplus.jsp?reload=true%7B%5C&%7Dbkn=5270963%20https://books.google.ch/books/about/Wave%7B%5C_%7DPropagation%7B%5C_%7Dand%7B%5C_%7DScattering%7B%5C_%7Din%7B%5C_%7DRando.html?id=wAZnuHdEKL0C%7B%5C&%7Dpgis=1.

[64] A. Jurado-navas et al. "Numerical Simulation of Physical and Engineering Processes". In: 2011. Chap. 7, p. 612. ISBN: 9789533076201. DOI: 10.5772/1828. URL: http://www.intechopen.com/subjects/numerical-analysis-and-scientific-computing.

[65] V. Tatarskii. *The effects of the turbulent atmosphere on wave propagation*. 1971, p. 472. ISBN: 0 7065 0680 4.

[66] E. M. Salomons. *Computational Atmospheric Acoustics*. 2001. ISBN: 9781402003905. URL: http://books.google.ch/books/about/Computational%7B%5C_%7DAtmospheric%7B%5C_%7DAcoustics.html?id=Lo-tMmH6EqMC%7B%5C&%7Dpgis=1.

[67] G. A. Daigle, J. E. Piercy, and T. F. W. Embleton. "Line-of-sight propagation through atmospheric turbulence near the ground". In: *Journal of the Acoustical Society of America* 74.5 (1983), pp. 1505–1513. ISSN: 00014966. URL: http://www.scopus.com/inward/record.url?eid=2-s2.0-0020850406%7B%5C&%7DpartnerID=tZOtx3y1.

[68] *Max Software Tools*. URL: https://cycling74.com/products/max/ (visited on 06/14/2017).

[69] *Pure Data Pd Community Site*. URL: http://puredata.info/ (visited on 06/14/2017).

[70] *SuperCollider*. URL: http://supercollider.github.io/ (visited on 06/14/2017).

[71] *Simulink - Simulation and Model-Based Design*. URL: https://www.mathworks.com/products/simulink.html (visited on 06/14/2017).

[72] *Faust Programming Language*. URL: http://faust.grame.fr/ (visited on 06/14/2017).

[73] G. van Rossum. *Python*. URL: https://www.python.org/ (visited on 05/09/2017).

[74] S. Behnel et al. "Cython: The Best of Both Worlds". In: *Computing in Science & Engineering* 13.2 (Mar. 2011), pp. 31–39. ISSN: 1521-9615. DOI: 10.1109/MCSE.2010.118. URL: http://ieeexplore.ieee.org/document/5582062/.

[75] *Cython*. URL: http://cython.org/.

[76] S. van der Walt, S. C. Colbert, and G. Varoquaux. "The NumPy Array: A Structure for Efficient Numerical Computation". In: *Computing in Science & Engineering* 13.2 (Mar. 2011), pp. 22–30. ISSN: 1521-9615. DOI: 10.1109/MCSE.2011.37. URL: http://ieeexplore.ieee.org/document/5725236/.

[77] *Numpy*. URL: http://www.numpy.org/.

[78] *Scipy*. URL: https://www.scipy.org/.

[79] W. McKinney. "Data Structures for Statistical Computing in Python". In: *Proceedings of the 9th Python in Science Conference*. 2010, pp. 51–56.

[80] F. Rietdijk. *auraliser*. 2017. DOI: 10.5281/ZENODO.573280. URL: https://zenodo.org/record/573280.

[81] F. Rietdijk, K. Heutschi, and C. Zellmann. "Determining an empirical emission model for the auralization of jet aircraft". In: *Proceedings of EuroNoise 2015*. Maastricht, The Netherlands, 2015, pp. 781–784. DOI: 10.5281/zenodo.15702.

[82] B. C. Tuttle and S. A. Rizzi. "Simulation of excess ground attenuation for aircraft flyover noise synthesis". In: *The Journal of the Acoustical Society of America* 136.4 (Oct. 2014), pp. 2287–2287. ISSN: 0001-4966. DOI: 10.1121/1.4900269. URL: http://asa.scitation.org/doi/10.1121/1.4900269.

[83] T. A. Lampert and S. E. O'Keefe. "A survey of spectrogram track detection algorithms". In: *Applied Acoustics* 71.2 (Feb. 2010), pp. 87–100. ISSN: 0003682X. DOI: 10.1016/j.apacoust.2009.08.007. URL: http://www.sciencedirect.com/science/article/pii/S0003682X09001959.

[84] *ISO 1996-2:2007 - Acoustics – Description, measurement and assessment of environmental noise – Part 2: Determination of environmental noise levels*. Tech. rep. 2007. URL: http://www.iso.org/iso/catalogue%7B%5C_%7Ddetail.htm?csnumber=41860.

[85] J. Maillard and J. Jagla. "Auralization of Urban Traffic Noise - Quantitative and Perceptual Validation Auralization system". In: *Cfa 2014* April (2014), pp. 1363–1368.

[86] A. Southern and D. Murphy. "Comparison of Road Tyre Noise Auralisation Methods". In: *InterNoise 2016*. Hamburg, 2016.

[87] F. Rietdijk. *Listening test stimuli and tests*. 2017. DOI: 10.5281/ZENODO.376263. URL: https://zenodo.org/record/376263.

[88] F. Rietdijk. *Listening Test Results*. 2017. DOI: 10.5281/ZENODO.376268. URL: https://zenodo.org/record/376268.

[89] A. Minard et al. "Sound synthesis and 3D sound rendering of aircraft flyovers with controllable parameters". In: *22nd AIAA/CEAS Aeroacoustics Conference*. Lyon, 2016. ISBN: 978-1-62410-386-5. DOI: 10.2514/6.2016-2908. URL: http://arc.aiaa.org/doi/10.2514/6.2016-2908.

[90] J. Forssén. "Calculation of Noise Barrier Performance in a Turbulent Atmosphere by Using Substitute Sources With Random Amplitudes". In: *Proc. 9th Long Range Acoustic Propagation Symposium*. Vol. 86. The Hague, The Netherlands, 2000, pp. 16–26.

[91] A. R. Aumann and S. A. Rizzi. "An atmospheric turbulence model plugin for the NASA auralization framework". In: *The Journal of the Acoustical Society of America* 141.5 (May 2017), pp. 3885–3886. ISSN: 0001-4966. DOI: 10.1121/1.4988710. URL: http://asa.scitation.org/doi/10.1121/1.4988710.

[92] S. F. Clifford and R. J. Lataitis. "Turbulence effects on acoustic wave propagation over a smooth surface". In: *Journal of the* 73.5 (May 1983), pp. 1545–1550. ISSN: 0001-4966. DOI: 10.1121/1.389416. URL: http://scitation.aip.org/content/asa/journal/jasa/73/5/10.1121/1.389416%20http://asa.scitation.org/doi/10.1121/1.389416.

[93] V. E. (E. Ostashev and D. K. Wilson. *Acoustics in moving inhomogeneous media*. 2nd ed. 2015, p. 541. ISBN: 9780415564168.

[94] A. R. Wenzel. "Saturation effects associated with sound propagation in a turbulent medium". en. In: *American Institute of Aeronautics and Astronautics* (1975). URL: http://adsabs.harvard.edu/abs/1975aiaa.confR....W%20http://arc.aiaa.org/doi/abs/10.2514/6.1975-546.

[95] V. E. Ostashev et al. "Spectral broadening of acoustic tones generated by unmanned aerial vehicles in a turbulent atmosphere". In: *Journal of the Acoustical Society of America* 140.4 (Oct. 2016), pp. 3119–3119. ISSN: 0001-4966. DOI: 10.1121/1.4969767. URL: http://scitation.aip.org/content/asa/journal/jasa/140/4/10.1121/1.4969767.

[96] D. K. Wilson, J. G. Brasseur, and K. E. Gilbert. "Acoustic scattering and the spectrum of atmospheric turbulence". In: *The Journal of the Acoustical Society of America* 105.1 (1999), pp. 30–34. ISSN: 00014966. DOI: 10.1121/1.424594. URL: http://scitation.aip.org/content/asa/journal/jasa/105/1/10.1121/1.424594.

[97] N. P. N. Krasnenko et al. "Outer Scales of Temperature Turbulence and Dynamic Turbulence from Results of Acoustic Sounding of the Atmosphere". In: *Russian Physics Journal* 56.6 (Oct. 2013), pp. 667–673. ISSN: 1064-8887. DOI: 10.1007/s11182-013-0083-8. URL: http://cat.inist.fr/?aModele=afficheN%7B%5C&%7Dcpsidt=27755226%20http://link.springer.com/10.1007/s11182-013-0083-8.

[98] V. E. Ostashev et al. "Propagation of sound in a turbulent medium. II. Spherical waves". In: *The Journal of the Acoustical Society of America* 102.2 (Nov. 1997), p. 2571. ISSN: 00014966. DOI: 10.1121/1.420312. URL: http://scitation.aip.org.proxy.lib.chalmers.se/content/asa/journal/jasa/102/5/10.1121/1.420312.

[99] V. E. Ostashev et al. "Propagation of sound in a turbulent medium. I. Plane waves". In: *The Journal of the Acoustical Society of America* 102.5 (1997), pp. 2561–2570. ISSN: 0001-4966. DOI: 10.1121/1.420311. URL: http://asa.scitation.org/doi/10.1121/1.420311.

[100] V. E. Ostashev, D. K. Wilson, and G. H. Goedecke. "Spherical wave propagation through inhomogeneous, anisotropic turbulence: Log-amplitude and phase correlations". In: *The Journal of the Acoustical Society of America* 115.1 (Dec. 2004), p. 120. ISSN: 00014966. DOI: 10.1121/1.1628680. URL: http://scitation.aip.org/content/asa/journal/jasa/115/1/10.1121/1.1628680.

[101] F. Rietdijk, J. Forssén, and K. Heutschi. "Generating sequences of acoustic scintillations". In: *Acta Acustica united with Acustica* 103.2 (2017).

[102] F. Rietdijk and K. Heutschi. "Auralisation of aircraft with a synthesised emission signal based on features determined from recordings". In: *To be submitted* ().

[103] F. Rietdijk and K. Heutschi. "Auralization of aircraft noise in an urban environment". In: *InterNoise 2016*. 2016, pp. 2877–2881. DOI: 10.5281/zenodo.12642.

[104] F. Rietdijk, K. Heutschi, and J. Forssén. "Modelling sound propagation in the presence of atmospheric turbulence for the auralisation of aircraft noise". In: *Forum Acusticum 2014*. Krakow, 2014.